Chronostratigraphy of the Cambrian Series 2-Miaolingian boundary, western Stansbury Basin, South Australia

By

Courtney Birksmith

School of Natural Sciences

Faculty of Science and Engineering

Macquarie University, Sydney, 2109, Australia

A thesis submitted in partial fulfillment of the requirements for the degree of Master of Research

25th November 2022

DECLARATION

I declare that this thesis, as a whole or in parts, has not been submitted for a higher degree to any other university or institution. To the best of my knowledge and belief, the thesis contains no material previously published or written by another person except where due reference is made in the thesis itself.

The planning, fieldwork, lab work, analyses, writing and conclusions are my own though I wish to acknowledge the following assistance with the research detailed in this thesis:

- Litholab of University of New England for cutting of thin sections
- Dr. Robert Klaebe and Dr. Tony Hall at the Mawson Laboratory, University of Adelaide for processing of Carbon and Oxygen isotopic data

No ethics approval was required for this project.

SIGN HERE

Courtney Birksmith Date: 25th November 2022

This thesis is formatted as a manuscript for submission to *Gondwana Research*, with some exceptions to meet the requirements of Macquarie University. This includes the requirement of an abstract of 200 words, 2cm margins, 1.5x line spacing, figures and tables embedded within the text.

TABLE OF CONTENTS

ACKNOWLEDGEMENTS

Firstly, I would like to thank my Primary Supervisor, Honorary Professor Glenn Brock. Even from a time well before this Master's, Glenn has provided immense support as well as incredibly insightful feedback. He has ensured this thesis has maintained it's course, progressing at the right pace and provided the necessary push to ensure my writing improved. I would also like to extend my thanks to both my co-supervisors. Dr. Zhiliang Zhang who showed me all the tips and tricks when working with the FESEM, how to create stunning fossil plates, and always making himself available if I had any questions. Dr. Marissa Betts who provided practical support with my methods, sample preparation, and data collection all while hosting me at University of New England, sharing her wide knowledge of Cambrian lithostratigraphy, interpretation and small shelly fossils. Their support and kindness were invaluable for the entirety of the project.

Thank you, Dr. James (Jimmy), Holmes for coming along to the Core Library and helping collect samples and offer support where needed. I am very appreciative for your wealth of information regarding the topic of this thesis, and for kindly allowing me to use some of your unpublished research as part of the Discussion.

Next, I would like to thank Sue Lindsay and Chao Shen from the MQU Microscopy Unit and Sean Murray and Josh Griffiths (Natural Sciences Technical Team). From maintaining lab spaces, teaching me to use resources and helping me whenever I needed access, all have offered their full support and guidance. I am extremely grateful to have been surrounded by such a supportive research community.

I would also like to thank everyone within the Macquarie University Palaeobiology Laboratory for making these past few years enjoyable. Specifically, I am thankful for Jack Jones for teaching me how to process samples through acid, drill powders for isotopes and being there as a support if I had any questions. Similarly, I am very thankful to Alyssa Fjeld for helping me if I had any questions and being a massive support, a person I could lean on when things became challenging. Thank you both for being awesome role models and friends that I could rely on.

Lastly, thank you to all of my friends, family, and my partner who have encouraged, supported, and held me together throughout this entire process. The amount of patience and kindness has meant the absolute world to me.

COVID STATEMENT

Dear Examiner,

Many of our HDR candidates have had to make changes to their research due to the impact of COVID-19. Below you will find a statement from the candidate, approved by their Supervisory Panel, that indicates how their original research plan has been affected by COVID-19 restrictions. Relevant ongoing restrictions in place caused by COVID-19 will also be detailed by the candidate.

Candidate's Statement

Though the collection of data from South Australia was not directly impacted by the effects of the COVID-19 global pandemic, various practical and lab related delays beyond my control impacted progress of the thesis.

Throughout 2022, access to on-campus labs and resources was periodically restricted. Although the restrictions varied in terms of their exact regulations, this project was dependent on the consistent use of on-campus laboratory equipment. Hence, the restrictions caused delays in sample processing especially in the Acid Leaching Facility.

Moreover, having fallen victim to COVID-19, not once, but twice this year caused further delays in the completion of sample processing and writing of the thesis. Due to COVID-19 and the restriction of not being allowed on campus for a week, procedures including acid processing, imaging, and use of key literary resources were interrupted and delayed. As a result, two extensions (total 2 weeks) for the submission of the thesis have been granted.

ABSTRACT

The GSSP of the Series 2–Miaolingian (= traditional lower–middle Cambrian) boundary was ratified in South China based on the first appearance of the trilobite *Orychtocephalus indicus* coincident with a major negative $\delta^{13}C$ excursion (Redlichiid–Olenellid Extinction Carbon isotope Excursion; ROECE). Unfortunately, *O. indicus* has not been recovered in Australian Cambrian successions and lack of isotopic data means definition of the Series 2–Miaolingian boundary has been problematic. This study integrates multiproxy data ($\delta^{13}C$ and $\delta^{18}O$ chemostratigraphy and biostratigraphy) along with lithostratigraphy to recognise the Series 2–Miaolingian boundary in the western Stansbury Basin, South Australia. Distinct faunal assemblages within drill cores CURD-9 and Port Julia-1A reveal range extensions of key taxa including *Pagetia* sp indet. within the Stansbury Limestone, below the interpreted ROECE event, which is consistent with occurrences in the GSSP. A -2.2 ‰ $\delta^{13}C$ peak in the Ramsay Limestone in CURD-9 and coeval Wirrealpa Limestone (Arrowie Basin) represent the Archaeocyathid Extinction Carbon isotope Excursion event. The -5.3 ‰ $\delta^{13}C$ peak in the Stansbury Limestone in CURD-9 and the ~ -2.7 ‰ $\delta^{13}C$ in Port Julia-1A, represents the global ROECE event. Similar lithologies observed within the Stansbury Limestone of both cores reveal the same ROECE event.

1. INTRODUCTION

The Cambrian Radiation records the most significant animal diversification event in Earth's history, especially the emergence of bilaterian animal groups. The rise of bilaterian animals led to the establishment of complex marine ecosystems that set the stage for modern biological communities (Peng et al. 2012; Zhao et al. 2019; Sundberg et al. 2020). Many Australian rock successions capture the Cambrian Radiation with exceptional clarity, serving as an archive for the evolution of many of the earliest animal phyla (Jago et al. 2006, 2012; Betts et al. 2018; Zhang et al. 2021). Resolving the Cambrian timescale using chronostratigraphic methods provides crucial temporal resolution required to chart key evolutionary events including the timing of the origin of animal phyla, key character traits across phyla, and the onset of animal radiations and extinctions. A high-resolution timescale also provides "ground truth" for the timing of lineage splits obtained from non-fossil estimates such as molecular clocks (Wray 2015; Erwin 2011, 2020). Definition of international chronostratigraphic boundaries that subdivide the Cambrian Period can be ratified with an integrated multiproxy approach founded on biostratigraphy and chemostratigraphy. This multiproxy approach has proven to be most effective for correlating Cambrian rock successions across regional and global scales (Betts et al. 2016, 2018; Zhao et al. 2019, Topper et al. 2022).

The Global Standard Stratotype-Section and Point (GSSP) for the Series 2–Miaolingian boundary (and conterminous Stage 4–Wuliuan Stage boundary) has recently been ratified based on the First Appearance of the trilobite *Oryctocephalus indicus* in the Wuliu-Zengjiayan section, South China (Zhao et al. 2019). Critically, the lack of this "index" species in Australia-Antarctica means correlation of the Series 2–Miaolingian (=lower–middle) Cambrian boundary in these areas is more problematic (Sundberg et al. 2016; Faggetter et al. 2017; Schmid 2017; Zhuravlev et al. 2018; Geyer 2019; Jago & Kruse 2020) and requires a detailed multiproxy approach using accessory fossils and chemostratigraphy.

The Series 2–Miaolingian boundary marks the transition from the initial pulse of the Cambrian Radiation in the early Cambrian to the global extinctions of biostratigraphically important groups such as the reef building archaeocyaths (associated with the Archaeocyathid Extinction Carbon isotope Excursion [AECE]) and some groups of small shelly fossils (SSFs) and trilobites (associated with the Redlichiid–Olenellid Extinction Carbon isotope Excursion Event [ROECE]; Zhuravlev et al. 2018, Zhao et al. 2019).

Lack of synchronous biostratigraphic and chemostratigraphic sampling has prevented the identification, and regional and global correlation of the Series 2–Miaolingian boundary in

Australia. Currently, the Series 2–Miaolingian Cambrian biostratigraphy in Australia is based predominantly on trilobites (Bengtson et al. 1990; Laurie 2004, 2006a, 2006b, 2012; Jago et al. 2006; Sundberg 2016, 2020; Geyer 2019). However, small shelly fossils (SSFs) are also now established as critically important biostratigraphic tools since they are widespread, readily preserved, and easily retrievable using acid leaching techniques (e.g., Steiner et al., 2004, 2007; Devaere et al., 2013, 2014; Betts et al. 2016, 2017, 2019). Multiproxy research using the stratigraphic ranges of SSFs and $\delta^{13}C$ and $\delta^{18}O$ isotopic data have successfully been applied to refine the lower Cambrian timescale in rock successions from South Australia (Betts et al. 2018). This has resulted in a new chronostratigraphic framework for carbonate-dominated lower Cambrian rock successions in the Arrowie Basin (Betts et al. 2016, 2017, 2018) and Stansbury Basin (Gravestock et al. 2001; Jacquet et al. 2017; Betts et al 2018) placing them within a regional and global timescale. However, although the chronostratigraphy of the lower Cambrian successions in the Stansbury and Arrowie basins have had much attention (Betts et al. 2016,2018), the multiproxy definition of the Series 2–Miaolingian (=lower–middle) Cambrian boundary in these basins is still very poorly understood.

Another important, but often neglected, aspect of chronostratigraphy is the description of the lithofacies and sedimentology to interpret depositional environments of the rock successions that hosts the multiproxy data being used to define boundaries. The original depositional environment not only directly determine faunal composition (biofacies), but post lithification history (diagenesis, thermal maturation, tectonism) also has the potential to greatly influence the isotopic signals. As such, recognition of key boundaries like the Series 2–Miaolingian boundary requires detailed lithostratigraphy to dovetail with the multiproxy chronostratigraphic data in order to better characterise rock successions that are suspected to cross this boundary.

Within Cambrian sedimentary basins of South Australia, the largely subsurface western Stansbury Basin has been suggested as perhaps the best candidate to capture the Series 2–Miaolingian boundary (Fig. 1; Gravestock et al. 2001; Jago & Kruse 2020). Drill cores CURD-9 and Port Julia-1A intersect a cyclic succession of marine carbonates and siliciclastic units in the subsurface of Yorke Peninsula in the western Stansbury Basin which has the most potential for resolving placement of the Series 2–Miaolingian boundary (Brock & Cooper 1993; Daily 1990; Gravestock et al. 2001; Jago & Kruse 2020). Although some lithostratigraphic data has been collected for Port Julia-1A (Gravestock et al. 2001; Jago & Kruse 2020), only observation of drill-core material was described, and no thin section analysis was completed.

Comprehensive analysis of thin section material from drill cores CURD-9 and Port Julia-1A will provide detailed understanding of the depositional environments and post-lithification history for

the drill cores which can be used to compare to regional basins. Occurrences of small shelly fossils from Port Julia-1A have been reported, however stratigraphic range data has not been adequately described, especially for important taxa that may define new biozones that help constrain the Series 2–Miaolingian boundary (Gravestock et al. 2001). Furthermore, there has been no chemostratigraphic data published for either Port Julia-1A or CURD-9. Hence, the new multiproxy results presented herein should greatly enhance correlation between successions from regional basins including the Arrowie, Amadeus, and Georgina Basins, will help facilitate better global correlation, and place the western Stansbury Basin firmly within the Cambrian Geological timescale for the first time.

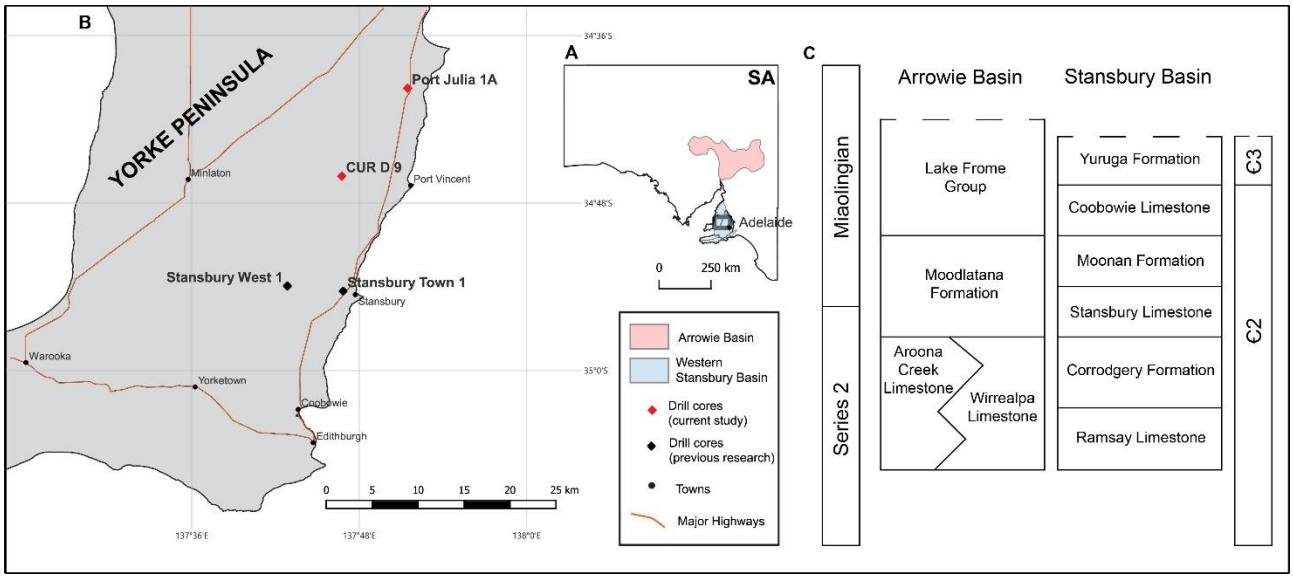

Figure 1. A. Geographical map of South Australia (SA) showing the relative position of the Arrowie Basin and the Western Stansbury Basin on Yorke Peninsula. B. Relevant drill hole on Yorke Peninsula locations marked; drill cores CURD9 and Port Julia-1A (red triangles; this study). Other related cores Stansbury West 1 and Stansbury Town 1 (black triangles; Brock & Cooper 1993; Gravestock et al 2001). C. Correlation chart for the Series 2-Miaolingian boundary in South Australia showing the stratigraphy and sequence sets (Є2 and Є3) for formations within the western Stansbury Basin, South Australia, and correlatives in the Arrowie Basin.

2. RESEARCH AIMS

The overarching goal of this research project is to apply multiproxy methods (biostratigraphy and chemostratigraphy), to define the position of the Series 2–Miaolingian Cambrian boundary in the western Stansbury Basin and establish the original depositional setting of the succession. This will help facilitate regional and global correlation. These goals will be achieved by integrating 3 independent Research Aims:

1. Construct high resolution biostratigraphy of small shelly fossils through the CURD-9 and Port Julia-1A drill cores in the western Stansbury Basin of South Australia.

2. Utilize $\delta^{13}C$ and $\delta^{18}O$ isotopes to reveal the chemostratigraphy of CURD-9 and Port Julia-1A drill cores establishing if the global negative ROECE (Redlichiid-Olenellid Extinction Carbon isotope Excursion) event, currently used to define the Series 2-Miaolingian Cambrian boundary, is present or absent in the western Stansbury Basin.
3. Utilize detailed thin section data to document the lithostratigraphy and original depositional environment of rock packages straddling the Series 2–Miaolingian Cambrian interval in the western Stansbury basin.

3. GEOLOGICAL SETTING

3.1. Western Stansbury Basin

Much of the Stansbury Basin consists of subsurface rock packages, with exposed outcrop only present along the Fleurieu Peninsula and Kangaroo Island. The western Stansbury Basin is characterised by Series 2–Miaolingian Cambrian marine carbonate and siliciclastic successions widespread across Yorke Peninsula. Outcrops are generally very patchy and consists of flat lying sedimentary rocks. Therefore, most knowledge of the western Stansbury Basin comes from drill-core data (Daily 1990; Brock & Cooper 1993; Gravestock & Gatehouse 1995; Gravestock et al. 2001; Jago & Kruse 2020). Formations within the western Stansbury Basin include (from oldest to youngest) the Winulta Formation, Kulpara Limestone, Parara Limestone (including the Koolywurtie Member), Minlaton Formation, Ramsay Limestone, Corrodgery Formation, Stansbury Limestone, Moonan Formation, Coobowie Limestone, and the Yuruga Formation. The current project focusses on the upper part of the succession including the Ramsay Limestone to Coobowie Limestone from drill cores CURD-9 and Port Julia-1A (Fig. 1).

Regional stratigraphy and correlation suggest that these formations span the Series 2–Miaolingian, ranging between Stage 4 to the recently termed Wuliuan Stage (Zhao et al. 2019; Jago & Kruse 2020). Previous work focused on building a lithostratigraphic and biostratigraphic framework for the western Stansbury Basin, from drill cores Stansbury West 1, Stansbury Town 1, and Port Julia-1A, describing key fossil taxa for regional correlations, particularly with the Arrowie Basin (Daily 1990; Brock & Cooper 1993; Gravestock et al. 2001).

3.2 Drill Core CURD-9

Drill core CURD-9 (434.8 m) was drilled by BHP Minerals Ltd. in 1981 to investigate lead and zinc minerals within Cambrian deposits, roughly 7.5 km west of Port Vincent (Fig. 1; Richards et al. 1986). CURD-9 intersected three main formations (from oldest to youngest): the Ramsay Limestone, Corrodgery Formation, and Stansbury Limestone. The lowest unit in the core (relevant

to this study) is the Ramsay Limestone which rests conformably over the older Minlaton Formation and is characterised by grey mottled limestone. The upper contact of the Ramsay and the overlying Corrodgery Formation appears conformable and transitions from carbonates into grey shales and siltstones with presence of pyrite and occasional calcite veins. The Corrodgery Formation has a conformable upper contact with the Stansbury Limestone comprising of grey mottled limestone with calcareous siltstone interbedded. The Stansbury Limestone has an unconformable upper contact with possible Permian units (Richards et al. 1986). No previous biostratigraphic or chemostratigraphic work has been completed for drill-core CURD-9.

3.3. Drill Core Port Julia-1A

Drill core Port Julia-1A (291 m) was drilled by BHP Minerals Ltd. in 1984 to investigate lead and zinc minerals within Cambrian deposits and lies within central Yorke Peninsula, 1.6 km west of Port Julia (Fig. 1; Richards et al. 1986; Ushatinskaya et al. 1995; Gravestock et al. 2001). Three formations were cored (from oldest to youngest): the Stansbury Limestone, Moonan Formation, and Coobowie Limestone. The Stansbury Limestone unconformably overlies Proterozoic basement (Oorlano Metasomatites) and consists of a nodular bedded ooidal/peloidal packstone with interbeds of lime-mudstone and brecciated limestone. The conformably overlying Moonan Formation comprises of dark grey to black shales with calcareous laminae grading upwards into siltstone and micaceous sandstones. Bioturbation has been recorded in the upper part of the formation (Gravestock et al. 2001). The conformable overlying Coobowie Limestone then transitions into a nodular lime-mudstone with ooidal to peloidal packstone and skeletal/peloidal wackestone. The upper boundary contact with the Coobowie Limestone is unconformably overlain by Cenozoic rocks.

4. CONTEXT AND PREVIOUS WORK

4.1. Lithostratigraphy

One of the first detailed lithostratigraphic frameworks of the Stansbury Basin was developed by Daily (1956, 1972, 1990) which established the foundations for the current Cambrian lithostratigraphic scheme (Gravestock et al. 2001). Cambrian units deposited within the Stansbury Basin were formed along a rifted continental platform, bounded by the Gawler Craton to the west (Gravestock & Gatehouse 1990). Three sequence sets Є1, Є2, and Є3 for Cambrian deposits within the Stansbury Basin were originally recognised (Gravestock & Gatehouse 1995). Set Є2 from the western Stansbury Basin captures a 400 m thick sequence incorporating (oldest to youngest) the Ramsay to Coobowie Limestone. The Ramsay Limestone is known to poorly outcrop (Crawford

1965; Holmes 2021), however, the remaining younger formation are only known from subsurface deposits. Based on previous observations (Daily 1990, Gravestock & Gatehouse 1995; Gravestock et al. 2001), the Ramsay Limestone is interpreted as a transgressive marine sequence that is largely fossiliferous, containing Faunal Assemblage 10 based on the 12 informal "assemblage zones" established by Daily (1956), which are comparable to the skeletal remains from the contemporaneous Wirrealpa and Aroona Creek Limestone in the Arrowie Basin (Fig. 1; Daily 1956; Brock & Cooper 1993). The base of the Ramsay Limestone has been described as consisting of bioclastic packstone/grainstone with oncolites transitioning into a black nodular, fossiliferous lime mudstone (Gravestock & Gatehouse 1995).

Compared to the Corrodgery Formation, the Moonan Formation is a non-calcareous, dark-grey shale succeeded by fine-grained, red, micaceous/glauconitic, bioturbated sandstone. Shelly fossils, acritarchs and bacterial filaments are all present within the Moonan Formation, hence, it is presumed to have a shallow marine setting (Gravestock et al. 2001). There is an abrupt lithological transition from the siliciclastic deposits of the Moonan Formation to the carbonates of the Coobowie Limestone linked to sea-level decreases (Gravestock & Gatehouse 1995). Pale grey, oolitic limestone interbedded with wavy bedded skeletal/peloidal wackestone comprise the Coobowie Limestone (Gravestock & Gatehouse 1995; Gravestock et al. 2001).

4.2. Biostratigraphy

The pioneering work of Daily (1956) first established 12 informal "assemblage zones" in South Australia from well preserved material within the Stansbury and Arrowie Basins. This preliminary scheme served as a way of correlating Cambrian rocks within regional Australia for decades, laying the foundations for establishing faunal assemblages of the Cambrian within South Australia (Brock & Cooper 1993; Gravestock & Gatehouse 1995; Gravestock et al. 2001; Betts et al 2016, 2017, 2018). However, the lack of detailed taxonomic description of faunas and imprecision of biostratigraphic ranges for taxa associated with all of Daily's (1956) Faunal Assemblages impeded precise regional and international correlation.

Utilising the stratigraphic ranges of fossils has provided a robust means of linking regional and global rock sequences based on shared faunal assemblages (Brock & Cooper 1993; Brock & Percival 2006; Steiner et al. 2007; Percival & Kruse 2014; Yang et al. 2014; Smith et al. 2015; Betts et al. 2018; Lin et al. 2019; Claybourn et al 2020; Skovsted et al. 2021; Zhang et al. 2021). Traditionally, trilobites and agnostoid arthropods have been used as key taxa for building biostratigraphic schemes for within the lower to middle Cambrian successions as these groups are

well studied, abundant, and have a wide geographic occurrence with short stratigraphic ranges (Laurie 2006, 2012; Betts et al. 2018; Geyer et al. 2019; Sundberg et al. 2016, 2020).

New research continues to build and improve this scheme using a variety of key non-trilobite fossil groups including, archaeocyaths (Zhuravlev & Gravestock 1994), molluscs, and especially Small Shelly Fossils (SSFs; Demidenko 1999; Betts et al 2016, 2017, 2018; Jacquet et al. 2017; Parkhaev 2019) to effectively construct high resolution stratigraphic range data to correlate lower and middle Cambrian rock successions (see also Jago et al. 2012, 2020; Kruse et al. 2009). Many authors are beginning to recognise the potential of SSFs in providing accurate biostratigraphic correlation, especially within Australian rock successions (Betts et al. 2016, 2017, 2019; Jacquet et al. 2019) or in rock successions where trilobites are absent (Sundberg et al. 2020). "Small shelly fossils" collectively refers to groups of small organophosphatic or calcareous fossils that are extremely variable in form and have a global distribution occurring across a wide range of facies (Skovsted et al. 2006; Butler 2015; Betts et al. 2018). They provide an extraordinary window into the palaeontological record of the Cambrian due to the timing of their appearance and their exceptional preservation potential (Butler 2015). Cambrian SSFs are diverse, globally distributed and readily preserved, and they have proven useful in accurately defining biozones within the lower Cambrian timescale (Betts et al. 2016). Newly established biozones in the Arrowie and Stansbury Basins provide robust regional and global correlation (Betts et al. 2017; Betts et al. 2018; Claybourn et al. 2020).

4.3. Chemostratigraphy

Carbon ($\delta^{13}C$) and oxygen ($\delta^{18}O$) chemostratigraphy is a reliable, robust, and commonly used correlation method for Cambrian strata (Brasier et al. 1992; Maloof et al. 2010; Ishikawa et al. 2014; Chang et al. 2017; Ren et al. 2017; Zhao et al. 2019; Skovsted et al. 2021). Oceans are typically very well mixed, so isotope values from seawater can be preserved contemporaneously in carbonate deposits around the world (Brasier 1993; Brand 2004; Frimmel et al. 2010). The inorganic $\delta^{13}C$ and $\delta^{18}O$ values obtained from bulk rock samples reveals changes in seawater chemistry over time and can therefore facilitate global correlation of key evolutionary and faunal transitions (Zhu et al. 2006; Geyer et al. 2019). Global extinction events are often marked by severe environmental changes that can be reconstructed through isotopic records in sedimentary deposits (Lin et al. 2019; Zhang et al. 2020). Accompanying this, significant increases in pyrite burial rates and decreases in strontium, nitrogen and carbon isotope signals are indicative of widespread anoxia in Cambrian oceans (Hough et al. 2006).

The most important limitation associated with bulk-rock stable isotope chemostratigraphy includes post-depositional alteration caused by recrystallisation of carbonates (Bradbury et al. 2015). Local impacts due to depositional environments, as seen in certain types of rift basins including the type of carbonate grains, composition of calcareous shells within the habitat as well as the effects of ambient water (Melezhik et al. 2001; Weissert et al. 2008; Wendler 2013), can make interpretations of $\delta^{13}C$ trends difficult (Weissert et al. 2008). However, $\delta^{13}C$ is generally considered a reliable chemostratigraphic tool because it is relatively resistant to diagenesis and reworking when potential sources are identified and addressed (Kaufmann & Knoll 1995; Maloof et al. 2010; Wendler 2013; Bradbury et al. 2015), for example through the use of thin section examination (e.g., Betts et al. 2018, see Methods and Results below). $\delta^{18}O$ data can show diagenetic influence of temperature and hence, is frequently compared directly with $\delta^{13}C$ data in isotopic cross-plots which can show co-variance related to diagenetic overprint (Brand 2004).

$\delta^{13}C$ and $\delta^{18}O$ data, as an independent chronostratigraphic proxy, can also circumvent limitations associated with the application of SSF to correlation (e.g., endemism, facies dependence, and diachronism), and can be a way of "calibrating" this method (Wendler 2013). Betts et al. (2018) established consistent and reliable relationships between SSF biozones and chemostratigraphic curves in the Arrowie Basin. The chemostratigraphic curves from the Arrowie Basin are also consistent with global curves, which allows for accurate correlations between the endemic fossil assemblages of the lower Cambrian in South Australia to contemporaneous faunas globally (Betts et al. 2018). Based on the calibrated age model for the global curve documented in Maloof et al. (2010) the correlation of the chemostratigraphic curve from South Australia aligns the base of the Series 2, Stage 3 boundary with the *Micrina etheridgei* and *Dailyatia odyssei* zones (Betts et al. 2018). The most recent radiometric dates for the age of the Series 2–Miaolingian (=Stage 4–Wuliuan Stage) boundary is 506.5 Ma reported from an ash bed just above the Tapeats Sandstone, Laurentia (Sundberg et al. 2020) which is ~3 Ma years younger than the estimated 509.01±0.22 Ma at the GSSP (Zhao et al. 2019; see also Montanez et al. 2000; Peng et al. 2012). Betts et al. (2018) report a CA-TIMS date of 511.87±0.14 Ma from the middle part of the Billy Creek Formation in the Arrowie Basin and based on the presence of ~200 metres of *Redlichia* bearing strata above this ash bed, the 506.5 Ma absolute date for the Stage 4–Wuliuan boundary could lie with the succeeding Lake Frome Group of the Arrowie Basin.

The base of the Miaolingian Series (= traditional middle Cambrian) in the GSSP (Zhao et al. 2019) and many other places around the globe (Guo et al. 2010; Schmid et al. 2017; Lin et al. 2019) is characterised by a large (and sharp) negative $\delta^{13}C$ excursion known as the Redlichiid-Olenellid Extinction Carbon Isotope Excursion (ROECE). This negative excursion was first reported from the

Kuonamka Formation in Siberia by Brasier & Sukhov (1998), later supported by Montanez et al. (2000) from the Great Basin, USA, in the Split Mountain and Echo Canyon sections. Their data exhibited high fluctuations of up to ≥ -4 ‰ for $\delta^{13}C$ values around the Series 2-Miaolingian boundary. This has since been subsequently recognised as ROECE (Fan et al. 2011) and has been shown to be a contemporaneous global event with similar negative excursions occurring in the Carrara Formation in Laurentia (Faggetter et al. 2017) and at the base of the Miaolingian at the GSSP in the Kaili Formation in South China (Zhao et al. 2019).

In Australia, the ROECE has only been recovered from the Chandler Formation in drill cores Dingo 2 and Alice 1, and in the Tempe Formation in drill core East Johnny's Creek 1 in the Amadeus Basin, Northern Territory (Schmid et al. 2017). In South Australia, the ROECE event has only previously been documented in an unpublished PhD thesis by Hall (2012) from the upper Ramsay Limestone-lower Corrodgery Formation in drill core Stansbury West 1 with a negative $\delta^{13}C$ peak of – 3.5 ‰.

5. MATERIALS AND METHODS

5.1. Sample Collection

Systematic sampling of Cambrian intervals of targeted drill cores CURD-9 (147.55 m) and Port Julia-1A (148.9 m) every ~2-3 m for both cores was undertaken at the South Australian Drill Core Reference Library, Tonsley, South Australia. All samples were transported back to Macquarie University. Quarter to half core samples 3.5–4.5 cm in width (CURD-9 and Port Julia-1A respectively) ranging from 6–30 cm in length were used for fossil recovery, isotope geochemistry, and thin sections. Key lithological textures were photographed and descriptions of lithologies were recorded, noting lithological changes, sedimentological structures, macrofossils, and potential boundaries between formations. A total of 140 samples were taken across both cores.

5.2. Thin Sections

A total of 29 oriented half core samples from both CURD-9 (10 thin sections) and Port Julia-1A (19 thin sections) were selected for petrological thin section analysis to investigate sedimentological structures and lithological features (Figs. 2-3). Stratigraphic horizons chosen for thin section analysis were chosen to maximise greatest variety of sedimentological features in hand specimens for both cores (including sampling of cyclical repetition of lithology). Blocks were cut using a diamond tipped saw at Macquarie University and the uncoverslipped, polished thin sections were made at the Litholabs, University of New England, Armidale, Australia. Thin sections were imaged in plane polarised and cross polarised light using a Nikon Axioscope 7 with Zeiss ZEN microscope

imaging software at the LithoLabs of University of New England. Thin section descriptions are based on Dunham's (1962) carbonate characteristics chart for classification of carbonate rocks, Mackenzie et al. (2017) for identification of siliciclastic material, Folk (1968) for grain size comparisons, and Flugel & Munnecke (2010) for relative frequency of grains.

5.3. Microfossil Extraction

A total of 66 samples were selected from CURD-9 and Port Julia-1A for processing (Figs. 4-5). Fossils were extracted from carbonates in the MQU Acid Leaching Facility (ALF) following the protocols described in Jeppsson et al. (1999). Samples were placed into 2 L plastic containers containing a 2 cm suspending mesh to keep the sample above the floor of the container to ensure maximum carbonate dissolution and microfossil yield. A 10% concentration of water and acetic acid was added to the container (1.5 L of water followed by 250 mL of 75% acetic acid). Samples were left in the solution for a week to dissolve, after which, insoluble residues were wet sieved into 250 µm (coarse) and 63 µm (fine) fractions and placed in aluminium containers that were oven dried at 45°C. Any undissolved rock was returned to the container with residual liquid to act as a buffer for the addition of new acid and water. This process was continued until the near-complete dissolution or extinction of samples.

5.4. Manual Picking

Coarse fraction samples were spread onto a grid tray and viewed using an Olympus SZ40 dissecting microscope to pick and isolate microfossils in a systematic fashion. Complete and well-preserved fossils were preferentially selected, however, any fragments that were identifiable were also picked out. All picked microfossils were placed into green plastic 3-well slides, covered with glass microscope slides and labelled with their specific stratigraphic location.

5.5. SEM imaging

Fossils were mounted on pin type stubs using double sided sticky tabs. Stubs were coated with a 20-micron layer of gold using a Zemitech K550 Gold Sputter Coater. Stubs were mounted and imaged using a JEOL JSM 7100F Field Emission Scanning Electron Microscope at an accelerating voltage of 5 kV at the Microscopy Unit of Macquarie University (Figs. 6-12).

5.6. Isotopic Analysis

A total of 144 samples were drilled using a Dremel rotary tool with a diamond bit attachment to produced 30 mg of carbonate powder (for each sample). Prior to drilling each sample, ethanol-

soaked Kim wipes were used to meticulously clean the drill bit and the surface of the core to prevent cross-contamination. Areas which were more homogenous in appearance with high carbonate content (characterised by lighter, more fine-grained areas) were selected to drill. This was done to ensure *in situ* lithology was sampled in order to achieve the most accurate primary $\delta^{13}C$ and $\delta^{18}O$ values. Formations which were largely siliciclastic were also sampled for $\delta^{13}C$ and $\delta^{18}O$ in the hope of retrieving enough carbonate for chemostratigraphic analysis. Powders were carefully placed into 5 mL Eppendorf tubes and sent to the Mawson Analytical Spectrometry Services facility in the University of Adelaide for analysis. Isotopic analysis was completed using a Fisons Isocarb carbonate preparation system as well as a Fisons Optima dual inlet isotope ratio mass spectrometer (IRMS). All replicate analysis of the standards were generally better than ± 0.1 for $\delta^{13}C$ and $\delta^{18}O$ with blanks run in each batch. Isotope values have been reported in per mil (‰) relative to the international standard VPDB. A cross-plot for $\delta^{13}C$ and $\delta^{18}O$ isotope data with all samples from both drill cores was built using RStudio to check for covariance. The chemostratigraphic logs (Figs. 13-14) were produced in RStudio and edited in Adobe Illustrator 2022.

6. RESULTS

6.1. CURD-9 Thin Sections

Drill core CURD-9 intersects (from top to bottom) Quaternary rocks (0.0–4.0 m) and possible Permian rocks (4.0–169.2 m) which overlie Cambrian units (169.2–434.8 m). The three Cambrian formations intersected by the core include (oldest to youngest) the Ramsay Limestone (317.2–261.56 m), Corrodgery Formation (261.56–187 m), and Stansbury Limestone (187–169.2 m).

6.1.1. Ramsay Limestone

In drill core CURD-9, the Ramsay Limestone is a 55.1 m-thick nodular limestone transitioning from a bioclastic packstone with occasional oncolites in the lower ~30 m (Fig. 2A–B) to a poorly sorted, extraclastic packstone in the upper ~25 m (Fig. 2C–E). Dissolution textures in the form of stylolites, as well as recrystallization of calcite and pyrite are present sporadically throughout the unit. Macrofossils are generally rare in the core, though trilobite fragments and echinoderm sclerites were observed in CUR-18 (301.014–300.99 m). Due to the fragmentary nature of the trilobites, identification to species level is impossible, however, due to their size (ranging up to 5 mm), the sclerites likely belong to polymeroid trilobites. The echinoderms are generally less than 1 mm in maximum dimension and are chaotically distributed amongst the other fossil material in CUR-18 (301.014–300.99 m; see Fig. 2A). There are very common sub-rounded to sub-angular sand sized

quartz and skeletal allochems but is classified as a packstone due to the presence of a dominant micritic matrix (Fig. 2A).

CUR-17 (292.27–292.218 m) is a packstone with oncolites. Oncolites are subspherical in shape with a recrystallized, lighter micritic mud cortex, often consisting of calcite and range from 1–9 mm in diameter, gradually increasing in size near the upper 3 cm of the section. The oncolites have an asymmetrical mottled micritic mud along the outer cortex. Other grains consist of rare sub-rounded, sand-sized quartz grains in a micritic mud matrix in the basal part of the thin section with peloids and trilobite fragments within a sparry limestone cement in the upper part of the thin section (Fig. 2B).

CUR-16 (283.934–283.909 m) is an extraclastic packstone with poorly sorted, sub-angular lithoclasts ranging from 0.1–5 mm. Lithoclasts compose of limestone fragments with occasional calcite veining. Fossils are absent (Fig. 2C).

CUR-14-15 (261.566–261.529 m) captures the lithological boundary between the coarse carbonate fabrics of the Ramsay Limestone and the fine-grained siliciclastic lithologies of the conformably overlying Corrodgery Formation. The poorly sorted, sub-rounded to sub-angular lithoclasts from the Ramsay Limestone with sparse fossil fragments in the basal part of the thin section are abruptly succeeded by fine grained, laminated, mud of the Corrodgery Formation (Fig. 2D–E).

6.1.2. Corrodgery Formation

The Corrodgery Formation is 74.56 m thick in the core, from the upper part of CUR-14-15 (261.56 m) to CUR-24 (187 m). The lithology is characterised by red, micaceous mudstones interbedded with red and grey fine, micaceous sandstones (Fig. 2F, 2G, 2I). Soft sediment deformation (e.g. flame structures) and potential bioturbation are present throughout the formation in addition to potential low angle crossbedding (Fig. 2F–G). Muddy rip up clasts within micaceous sandstone intervals occur in CUR-11 (221.19–221.164 m depth, Fig. 2H). Fossils were not observed throughout the entire formation. At CUR-24 (187 m) the siliciclastic Corrodgery Formation has a sharp, but presumably conformable contact with the overlying carbonate-dominated Stansbury Limestone.

6.1.3. Stansbury Limestone

The Stansbury Limestone consists of bioclastic grainstones interbedded with nodular bioclastic packstones (Fig. 2J–K). In CUR-21 (183.928–183.9 m), large asymmetrical (≥2 mm) oncolites are set within a sparry limestone cement (Fig. 2J). Skeletal grains consist of rare polymeroid trilobite fragments along with sub-rounded to sub-angular quartz and abundant peloids. Oncolites have a

recrystalized calcite centre coated by asymmetrical, darker mottled microbial micrite rinds (between 0.2-1 mm thickness; Fig. 2J). Bioclastic packstone nodules in CUR-9 (181.08–181.055 m) and intraclasts float within the micrite and are extremely fossil rich with fragmented trilobites, hyoliths and other SSFs (Fig. 2K). Dissolution textures in the form of stylolites are present throughout with evidence of calcite veins.

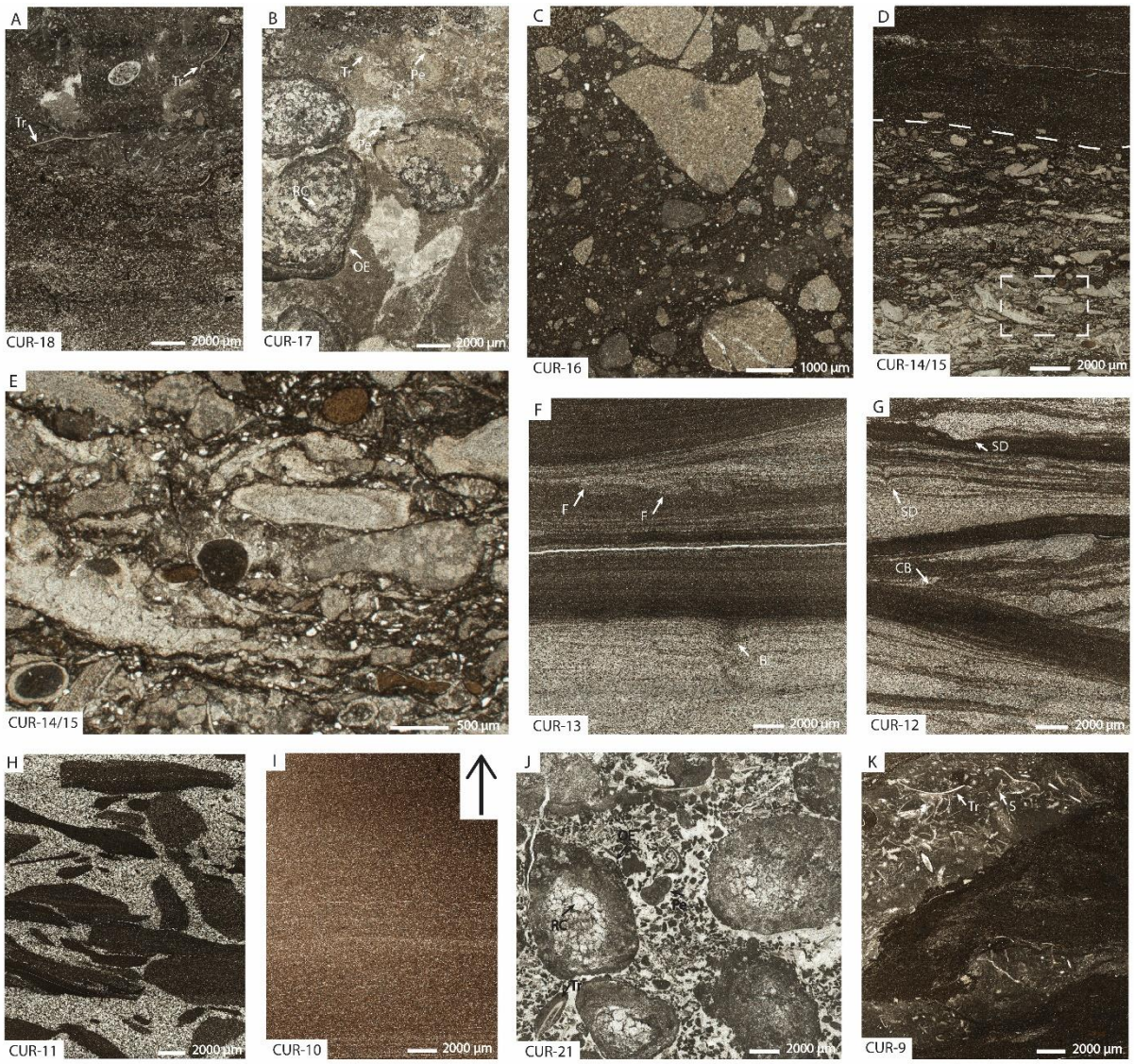

Figure 2. Thin section photomicrographs of fabrics and textures from CURD-9, Yorke Peninsula. All thin sections are positioned with the top up as illustrated by way up arrow. A: Ramsay Limestone; CUR-18 (301.014–300.99 m), bioclastic packstone with trilobite fragments. B: Ramsay Limestone; CUR-17 (292.27–292.218 m), basal packstone with oncolites. C: Ramsay Limestone, CUR-16 (283.934–283.909 m), extraclastic packstone. D: Ramsay Limestone, CUR-14-15 (261.266–261.529 m), boundary between packstone at base and upper micaceous mud. Dotted line indicates position of boundary. E: Ramsay Limestone, CUR-14-15 (261.266–261.529 m), magnification of dashed rectangle in D; poorly sorted lithoclasts. F, Corrodgery Formation, CUR-13 (235.426–235.394 m), micaceous mud/shale interbedded with micaceous sand with potential bioturbation and flame structures. G: Corrodgery Formation, CUR-12 (225.91–225.883 m), micaceous shale/fine mud interbedded with micaceous sand with soft sediment deformation and potential crossbedding. H: Corrodgery Formation, CUR-11 (221.19–221.164 m), micaceous

sandstone with muddy clasts. I: Corrodgery Formation, CUR-10 (189.765–189.741 m), uniform red micaceous mud. J: Stansbury Limestone, CUR-21 (183.928–183.9 m), bioclastic oncoidal limestone in a sparry cement. K: Stansbury Limestone, CUR-9 (181.08–181.055 m), bioclastic packstone and fine mud with dissolution textures. Way up arrow indicated in (I) for all samples. Abbreviations: Tr = Trilobite fragments; Pe = Peloids; OE = Oncolite Cortex; RC = Recrystalized nucleus of oncolite; F = Flame Structure; Bi = Bioturbation?; SD = Soft Sediment Deformation; CB = Crossbedding?; S = SSF fragments.

6.2. Port Julia-1A Thin Sections

Port Julia-1A intersects Tertiary rocks (0–59.53 m) which unconformably overlie Cambrian units (59.53–209.3 m) and the Oorlano Metasomatite basement (209.3–291 m). The three Cambrian formations intersected are (oldest to youngest): the Stansbury Limestone (209.3–162.2 m), Moonan Formation (162.2–98.7 m) and Coobowie Limestone (98.17–60.4 m; Richards et al. 1986).

6.2.1. Stansbury Limestone

The Stansbury Limestone rests unconformably on the Mesoproterozoic Oorlano Metasomatite (Cowley et al. 2003) with the lower part (see PJ1A-78 (210.11–210.07 m; Fig. 3A) showing major recrystallization, with detrital plagioclase and calcite. The Stansbury Limestone (47.1 m thick) transitions from recrystallized, sparry limestone with microbial textures at sample PJ1A-78 (210.11–210.07 m; Fig. 3A–B) to more micritic limestone with occasional grainstone intervals at PJ1A-76 (202.434–202.39 m; Fig. 3B–E). A micritic mud with a clear dissolution boundary between the fine grained micritic mud and grainstone with a sparry limestone cement and presence of lithoclasts and oncoids occurs in PJ1A-76. The oncoids range from 2 mm to 8 mm and are characterised by having a light micritic mud centre with darker mottled microbial micrite rinds. Macrofossils are relatively rare, consisting only of trilobite fragments in thin section (Fig. 3B). A poorly sorted, brecciated limestone occurs at PJ1A-75 (197.12–197.069 m). Clasts consisting of sub-angular limestone fragments range from 0.2–6 mm. Major calcite veining is evident in PJ1A-75 (197.12–197.069 m; Fig. 3C).

In PJ1A-47-74 (184.378–184.33 m), dissolution textures contact a bioclastic packstone. This bioclastic grainstone contains abundant peloids (0.05–0.1 mm), a large microsparite clast (10 mm), and polymeroid trilobite fragments (1–4 mm; Fig. 3D).

PJ1A-34-35 (170.024–169.997 m; Fig. 3E) is almost identical in lithological composition to the Stansbury Limestone fabrics in CUR-9 (Fig. 2K) with lighter micritic nodules surrounded by darker micrite. Fossils are absent in PJ1A-34-35 in contrast to the abundance of fossils observed in CUR9. At PJ1A-34-35 (170.024–169.997 m), major calcite veining cross-cuts poorly sorted, subangular

clasts (1–2 mm; Fig. 3E). The carbonate-dominant Stansbury Limestone is sharply overlain (with presumed conformity) by iron rich siliciclastics of the Moonan Formation.

6.2.2. Moonan Formation

The Moonan Formation is 63.5 m thick consisting of iron-rich micaceous sandstones interbedded with red mudstones (Fig. 3F–I). In PJ1A-72 (128.874–128.82 m), very fine micaceous sandstone consists of subrounded–subangular quartz grains that show very gradual fining up and potential crossbedding (Fig. 3F). High magnification of sample PJ1A-72 (128.874–128.82 m) reveals abundant mica throughout (Fig. 3G).

PJ1A-70 (105.985–105.952 m) shows a distinct coarsening upward, beginning immediately above a sharp boundary where red siltstone and mudstone with very rare, fine sand-sized, subangular quartz grains grade upwards into a fine red micaceous sand with abundant sand-sized, subangular quartz grains. Potential bioturbation is present as vertical burrowing at the top of thin section PJ1A-70 (105.985–105.952 m; Fig. 3H).

In PJ1A-67 (100.453–100.41 m), there is abundant 0.01–0.05 mm, rounded glauconite grains within a micaceous sandstone. Abundant, subangular quartz grains are also present (Fig. 3I). Fossils were not observed in the Moonan Formation. The siliciclastic Moonan Formation transitions with slowly increasing carbonate content into the Coobowie Limestone.

6.2.3. Coobowie Limestone

The Coobowie Limestone is 38.3 m thick and characterised by dolomitic, nodular limestone with major dissolution textures in the form of stylolites (Fig. 3J–L). The basal ~ 8 m of the Coobowie Limestone, from PJ1A-79 to PJ1A-65 (98.88–90.49 m), consists of interbedded sandstone and micritic mudstone. At PJ1A-63 (80.65–80.625 m) this transitions into recrystallized, dolomitic limestone that has overprinted a granular, micritic limestone (Fig. 3J). Micritic limestone persists throughout the remaining ~30 m of the formation becoming more bioclastic at PJ1A-66 (75.21–75.184 m; Fig. 3K-L). In PJ1A-66 (75.21–75.184 m), a recrystalised micritic packstone is cross-cut by a major stylolite with rare, sand-sized, subangular quartz grains. Fossils from PJ1A-66 include trilobite fragments and possible SSF material (Fig. 3K). In PJ1A-68 (61.941–61.889 m), an oncoidal packstone with a sparry limestone cement is bordered by minor stylolites with micrite transitioning into a mottled sparry limestone. Oncoids range between 0.1–0.5 mm with dark micritic rinds (Fig. 3L).

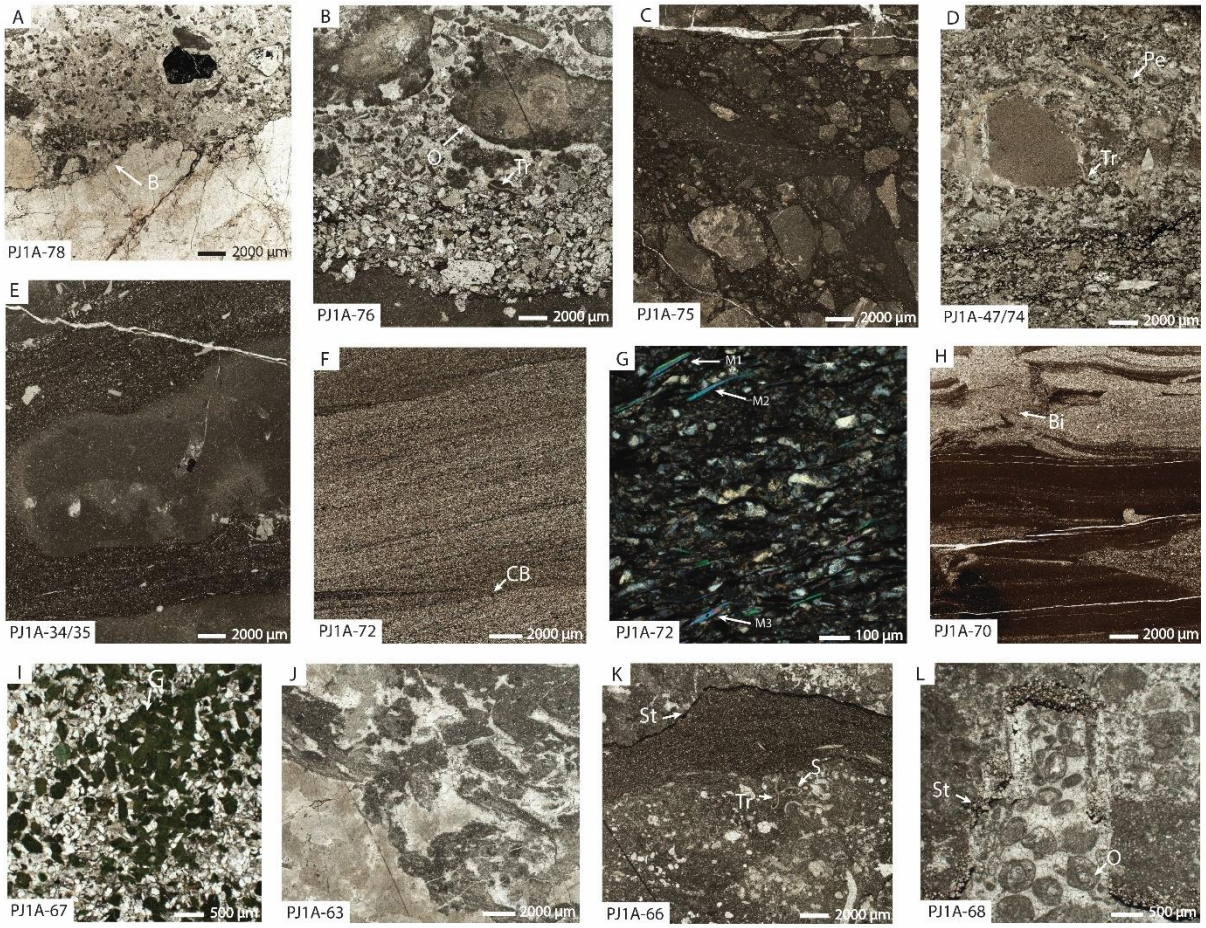

Figure 3. Thin section photomicrographs of fabrics and textures from Port Julia-1A, Yorke Peninsula. All thin sections are positioned with the top up as illustrated by way up arrow. A: Stansbury Limestone, PJ1A-78 (210.11–210.07 m), boundary between basement and significantly recrystallized limestone. B: Stansbury Limestone, PJ1A-76 (202.434-202.39 m), dissolution boundary between micritic mud and siliciclastic coarse sand. C: Stansbury Limestone, PJ1A-75 (197.12–197.069 m), poorly sorted clasts in brecciated limestone. D: Stansbury Limestone, PJ1A-47-74 (184.378–184.33 m), bioclastic packstone with dissolution textures. E: Stansbury Limestone, PJ1A-34-35 (170.024–169.997 m), granular micritic limestone. F: Moonan Formation, PJ1A-72 (128.874–128.82 m), micaceous sandstone with potential crossbedding. G: Moonan Formation, PJ1A-72, 10X cross polarised magnification of F; micaceous sandstone with mica highlighted (M 1–3). H: Moonan Formation, PJ1A-70 (105.985–105.952 m), potential bioturbated graded micaceous sand. I: Moonan Formation, PJ1A-67 (100.453–100.41 m), micaceous sand with abundant glauconite grains. J: Coobowie Limestone, PJ1A-63 (80.65–80.625 m), peloidal micritic limestone. K: Coobowie Limestone, PJ1A-66 (75.21–75.184 m), bioclastic limestone with dissolution textures. L: Coobowie Limestone, PJ1A-68 (61.941–61.889 m), dissolution boundary within oncolitic limestone. Abbreviations: B = Boundary; Tr = Trilobite fragments; Pe = Peloids; O = Oncolite; Bi = Bioturbation?; St = Stylolite; CB = Crossbedding?; G = Glauconite Grains; S = SSF fragments.

6.3. Fossil Fauna from CURD-9 and Port Julia-1A

A total of 20 fossil taxa have been recovered from drill-cores CURD-9 (Fig. 4) and Port Julia-1A (including seven taxa not previously reported; Fig. 5) in this study. The extracted faunal

assemblages from drill-cores CURD-9 (Fig. 4) and Port Julia-1A (Fig. 5) are similar to those described by Brock & Cooper (1993), Gravestock et al. (2001), and Jago & Kruse (2020). Since all taxa have been adequately described elsewhere (e.g., Bengtson et al. 1990; Brock & Cooper 1993; Gravestock et al. 2001; Smith et al. 2015, 2016), the fossils are not formally described herein but high-resolution images of taxa are provided. Organosphosphatic (lingulid and acrotretoid) brachiopods dominate the assemblages. Other biostratigraphically important (though rare) taxa include the eodiscid trilobite *Pagetia* sp. indet., the palaeoscolecid worm *Kaimenella* sp. aff. *K. reticulata*, the enigmatic SSF *Chalasiocranos exquisitum* Brock & Cooper, 1993, along with long ranging helcionelloid molluscs, hyoliths, hyolithelminthids, echinoderm sclerites and various types of spicules.

6.3.1. Trilobites

Identifiable trilobites are remarkably scarce from both cores. Large fragments from polymeroid trilobites were observed in thin section especially in the Stansbury Limestone (Fig. 2A-B, 2J-K, 3B, 3D, 3K), but these were not identifiable. Two fragmentary internal moulds of a partial cranidum (CUR-27, 183.12–183.19 m; see Fig. 6.1) and axial rings and spine of a pygidium (CUR7-8, 178.65–178.92 m; see Fig. 6.2) belong to an indeterminate species of the biostratigraphically important eodiscid genus *Pagetia*. Importantly, the discovery of *Pagetia* sp. indet. from two horizons (CUR-27, 183.12–183.19 m and CUR-7-8, 178.65–178.92 m) in the Stansbury Limestone in drill core CURD-9 greatly extends the range of this genus (see Fig. 4–5, 16) from the previously documented occurrence of *Pagetia* sp. within the stratigraphically younger Coobowie Limestone in Port Julia-1A (86.15 m; see Ushatinskaya et al. 1995; Gravestock et al. 2001; Jago & Kruse 2020). Re-sampling of Port Julia-1A as part of this study found no further specimens of *Pagetia* sp. in the Coobowie Limestone. The first occurrence (FO) of *Pagetia* sp. can thus confidently be placed in the Stansbury Limestone immediately below the significant negative $\delta^{13}C$ spike recorded in both cores (Fig. 13–14; see Chemostratigraphy Results below).

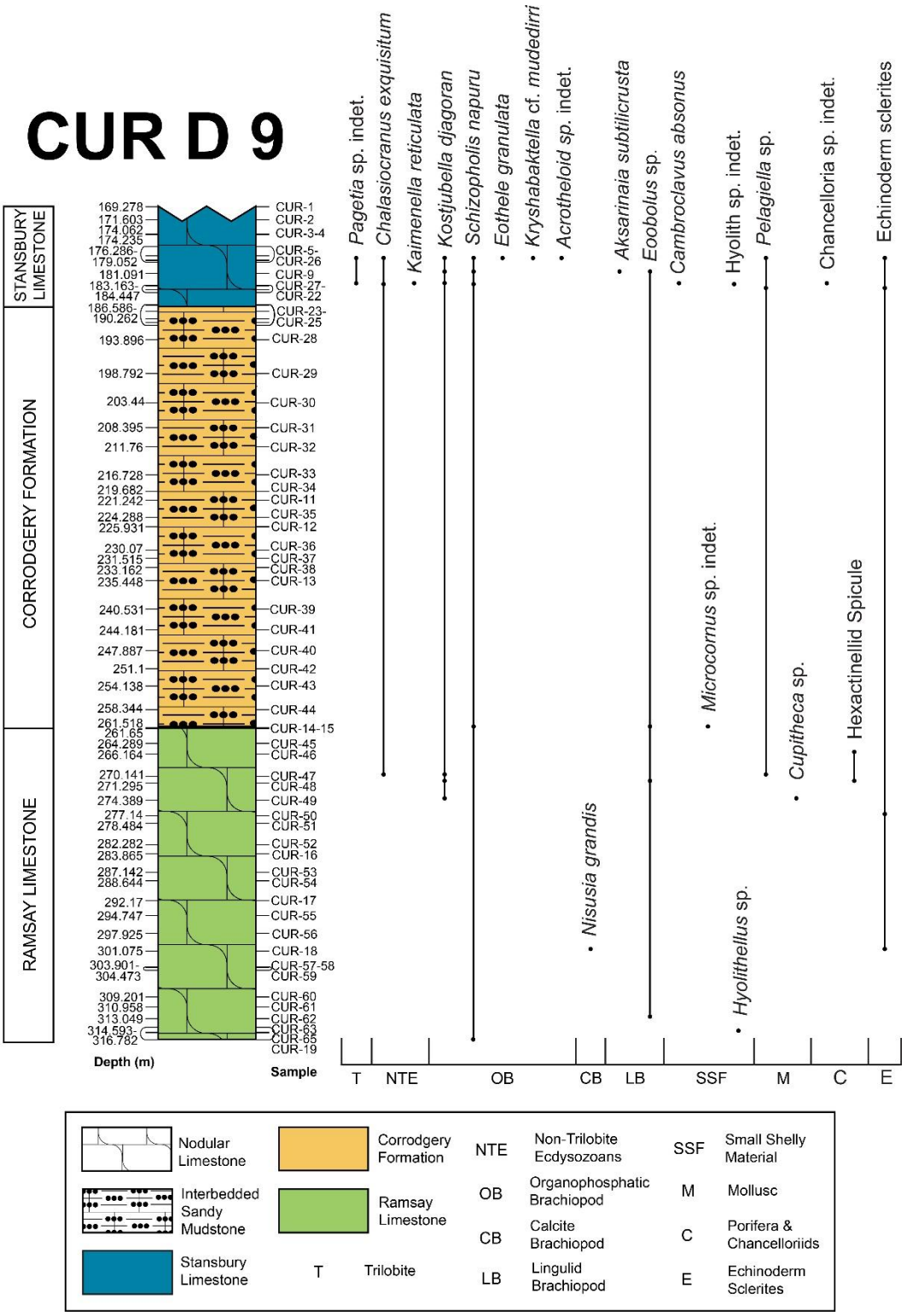

Figure 4. New stratigraphic ranges of fossil fauna from CURD-9 from the western Stansbury Basin. Stratigraphic depths (m) and their corresponding sample numbers illustrated to the left and right of the stratigraphic column (respectively).

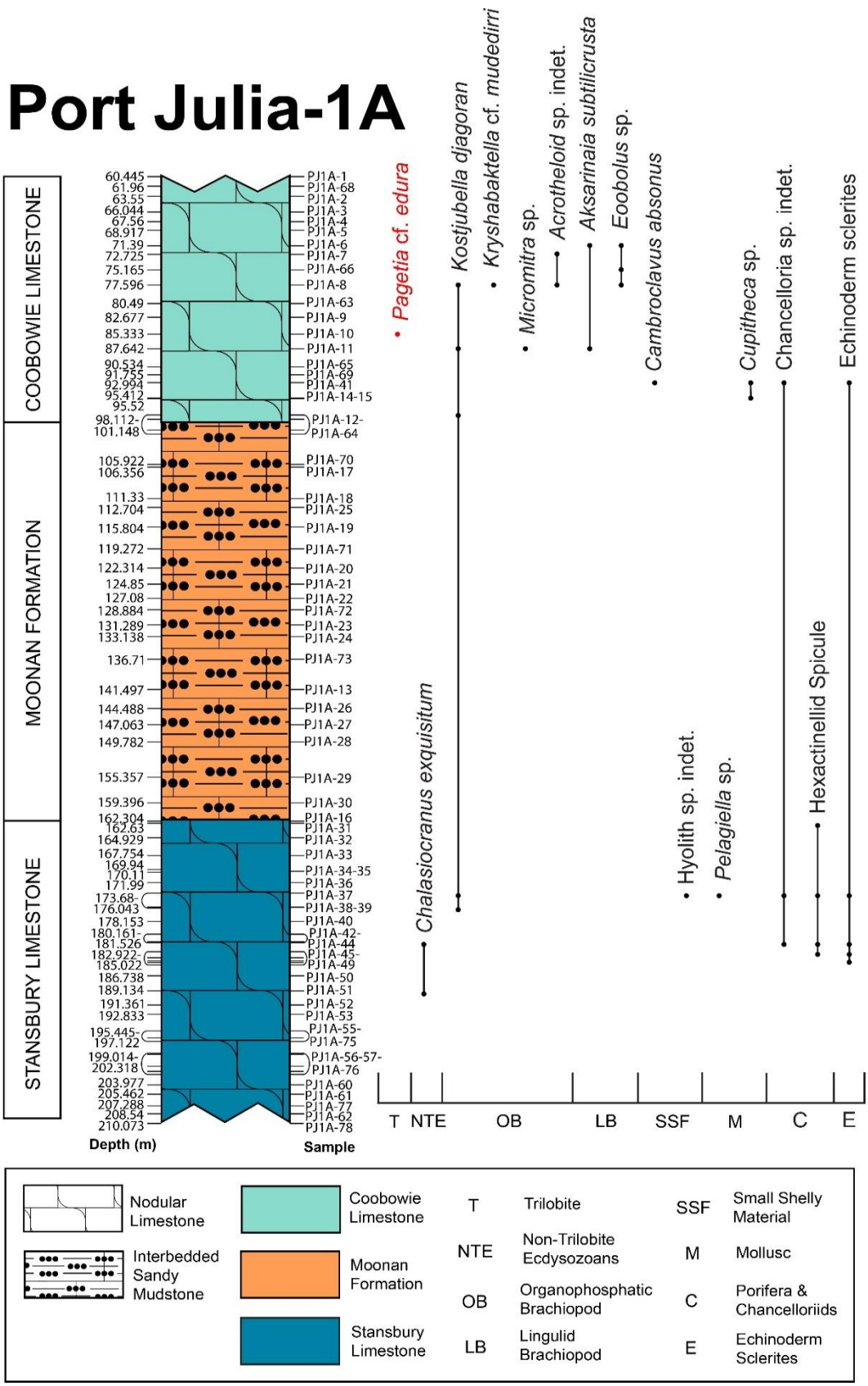

Figure 5. New stratigraphic ranges of fossil fauna from Port Julia-1A from the western Stansbury Basin. Red dot for *Pagetia* sp. included from Ushatinskaya et al. (1995) and Jago & Kruse (2020). Stratigraphic depths (m) and their corresponding sample numbers illustrated to the left and right of the stratigraphic column (respectively).

6.3.2. Non-Trilobite ecdysozoans

Two species of non-trilobite ecdysozoans were recovered from drill-cores CURD-9 and Port Julia-1A, the enigmatic SFF *Chalasiocranos exquisitum* Brock and Cooper, 1993 (Figs. 6.3–8) and the palaeoscolecid priapulid *Kaimenella sp. aff. K. reticulata* (Fig. 6.9). *Chalasiocranos exquisitum* has a FO in the upper Ramsay Limestone (CUR-47, 270.04–270.20 m) in drill core CURD-9 and ranges through to a last occurrence (LO) in the upper Stansbury Limestone (PJ1A-43, 181.26–181.5 m) in drill core Port Julia-1A (Fig. 4–5). The revised range data presented here extends the current range of *C. exquisitum* from the Ramsay Limestone into the upper Stansbury Limestone.

A single partial phosphatized scleritome of *Kaimenella* sp. aff. *K. reticulata* was recovered from a single stratigraphic horizon in the Stansbury Limestone (CUR-27, 183.12–183.19 m; Fig. 6.9) from drill core CURD-9. The new occurrence of *Kaimenella* sp. aff. *K. reticulata* within drill core CURD-9 extends the range of this taxon into the Stansbury Limestone.

6.3.3. Linguliformean brachiopods

Organophosphatic brachiopods are the most diverse and abundant faunal elements in both cores. The most abundant brachiopod in drill cores CURD-9 and Port Julia-1A is the acrotretid *Kostjubella djagoran* (Fig. 7) which has a FO in the upper Ramsay Limestone in CURD-9 (CUR-49, 274.36–274.56 m) ranging through to its LO in the Coobowie Limestone in Port Julia-1A (PJ1A-8 at 75.55–77.68 m).

Schizopholis napuru (Fig. 8.1–5) has a FO in the lower Ramsay Limestone (CUR-19, 316.62–316.84 m) and ranges through to the Stansbury Limestone (CUR-7-8, 178.65–178.92 m; Fig, 4). The LO of *S. napuru* at CUR-7-8 (178.65–178.92 m) also represents the FO of *Eothele granulata* (Fig. 8.6) in the Stansbury Limestone of Port Julia-1A (PJ1A-37, 173.56–173.75 m).

Kyrshabaktella cf. *mudedirri* (Fig. 9.1-4) has a FO in the Stansbury Limestone (CUR-7-8, 178.65–178.92 m) in drill core CURD-9 and ranges through to a LO in the Coobowie Limestone in drill core Port Julia-1A (PJ1A-8, 75.55–77.68 m).

A single steinkern of a specimen of *Micromitra* sp. with an enlarged arched homeodeltidium (Fig. 9.8) was also recovered from one stratigraphic horizon in the Coobowie Limestone (PJ1A-11, 87.57–87.69 m) from drill core Port Julia-1A. This taxon has not previously been documented within the Ramsay Limestone through to the Coobowie Limestone.

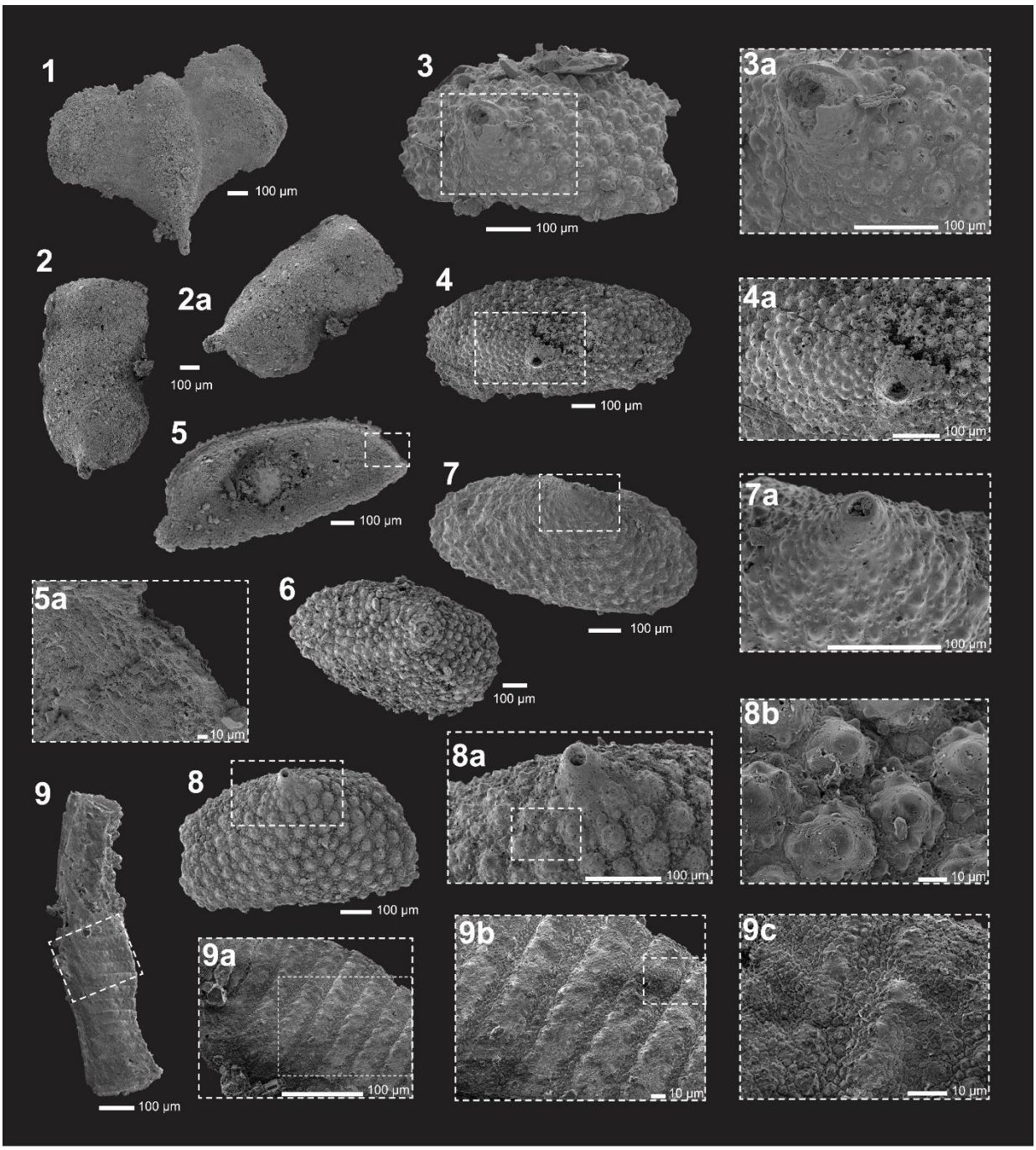

Figure 6. SEM Images of Trilobite and Non-Trilobite Ecdysozoans from drill cores CURD-9 and Port Julia-1A. **1-2.** *Pagetia* sp. indet.; 1: partial cranidum, MPAL0927 from CUR-27 (183.12–183.19 m), Stansbury Limestone. 2: axial rings and spine of pygidium, MPAL0928 from CUR-7-8 (178.65–178.92 m), Stansbury Limestone. 2a: oblique view of axial rings and spine of pygidium, MPAL0928 from CUR-7-8 (178.65–178.92m), Stansbury Limestone. **3-8.** *Chalasiocranos exquisitum*; 3. apical view of MPAL0929 from PJ1A-43 (181.26–181.5 m), Stansbury Limestone. 3a. magnification of apical view of MPAL0929 from PJ1A-43 (181.26–181.5 m), Stansbury Limestone. 4. apical view of MPAL0930 from PJ1A-51 (189.04–189.19 m), Stansbury Limestone. 4a. magnification of apical view of MPAL0930 from PJ1A-51 (189.04–189.19 m), Stansbury Limestone. 5. oblique abapical view of inner surface structure of MPAL0930 from PJ1A-51 (189.04–189.19 m), Stansbury Limestone. 5a. magnification of abapical view of inner surface structure of MPAL0930 from PJ1A-51 (189.04–189.19 m), Stansbury Limestone. 6. apical view of MPAL0931 from PJ1A-51 (189.04–189.19 m), Stansbury Limestone. 7. oblique apical view of

MPAL0932 from CUR-7-8 (178.65–178.92 m), Stansbury Limestone. 7a. magnification of oblique apical view of MPAL0932 from CUR-7-8 (178.65–178.92 m), Stansbury Limestone. 8. oblique apical view of MPAL0933 from CUR-20 (183.19–183.38 m), Stansbury Limestone. 8a. magnification of oblique apical view of MPAL0933 from CUR-20 (183.19–183.38 m), Stansbury Limestone. 8b. magnification of detail of surface ornament showing larger primary tubercles surrounded by small secondary tubercles of MPAL0933 from CUR-20 (183.19–183.38 m), Stansbury Limestone. **9.** *Kaimenella* sp. aff. *K. reticulata*; external surface of MPAL0934 from CUR-27 (183.12–183.19 m), Stansbury Limestone. 9a. magnification of external surface of MPAL0934 from CUR-27 (183.12–183.19 m), Stansbury Limestone. 9b. magnification of external surface of MPAL0934 from CUR-27 (183.12–183.19 m), Stansbury Limestone. 9c. magnification of external surface of MPAL0934 from CUR-27 (183.12–183.19 m), Stansbury Limestone.

Large, mostly fragmentary shells referred to Acrotheloid sp. indet. (Fig. 9.5–7) has a FO in the Stansbury Limestone (CUR-7-8, 178.65–178.92 m) in drill core CURD-9 and ranges through to a LO in the Coobowie Limestone in drill core Port Julia-1A (PJ1A-8, 75.55–77.68 m).

The lingulid brachiopod, *Aksarinaia subtilicrusta* (Fig. 10.1–3), ranges from the Stansbury Limestone (CUR-9, 181.02–181.15 m) through to the Coobowie Limestone (PJ1A-11, 87.57–87.69 m) within drill cores CURD-9 and Port Julia-1A. *A. subtilicrusta* has not been previously documented within the western Stansbury Basin.

The most abundant lingulid species found within drill cores CURD-9 and Port Julia-1A, *Eoobolus* sp. (Fig. 10.4–11), ranges from the lower Ramsay Limestone (CUR-62, 313.01–313.22 m) in CURD-9 through to the Coobowie Limestone (PJ1A-6, 71.33–71.5 m) in Port Julia-1A. *Eoobolus* sp. has not been previously documented within these cores in the western Stansbury Basin, thus, the range of *Eoobolus* sp. now extends from the upper Wilkawillina Limestone (MOG section) and lower Mernmerna Formation (MMT section) of the *Parabadiella huoi* Zone in the Arrowie Basin (currently correlated to late Stage 2–Early Stage 3; Betts et al. 2018) to the Coobowie Limestone in Port Julia-1A.

6.3.4. Calciate brachiopods

A single ventral valve of *Nisusia grandis* (Fig. 9.9-10) was found in one stratigraphic horizon in the lower Ramsay Limestone (CUR-18, 300.97–301.13 m) from drill core CURD-9. *N. grandis* has not previously been documented elsewhere within the western Stansbury Basin.

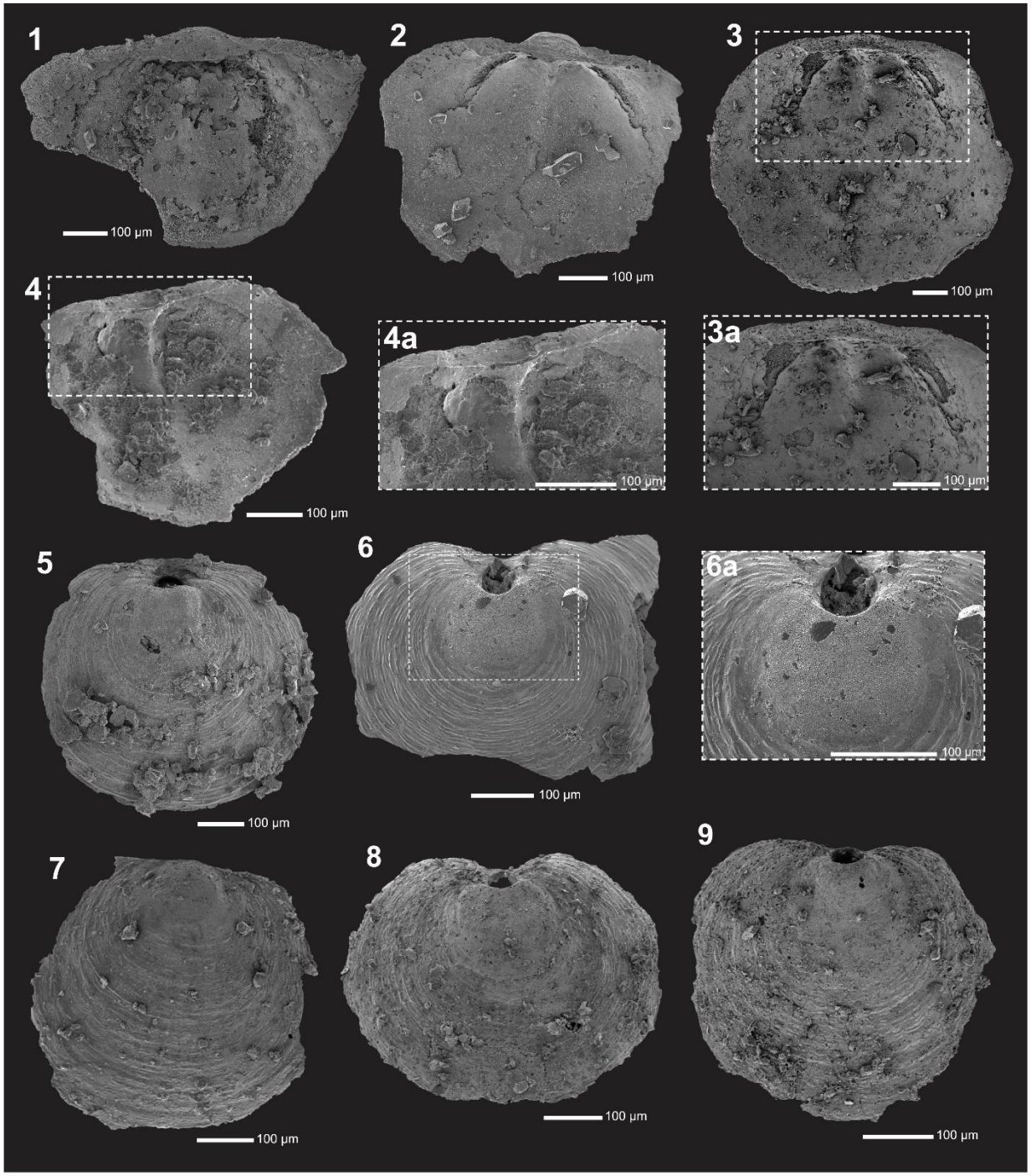

Figure 7. **1-9.** SEM Images of *Kostjubella djagoran* from drill cores CURD-9 and Port Julia-1A. 1: dorsal valve, interior view, MPAL0935 from PJ1A-8 (75.55–77.68 m), Coobowie Limestone. 2: dorsal valve, interior view, MPAL0936 from PJ1A-11 (87.57–87.69 m), Coobowie Limestone. 3: dorsal valve, oblique interior view, MPAL0937 from PJ1A-11 (87.57–87.69 m), Coobowie Limestone. 3a: magnification of dorsal valve, oblique interior view, MPAL0937 from PJ1A-11 (87.57–87.69 m), Coobowie Limestone. 4: dorsal valve, interior view, MPAL0938 from CUR-49 (274.36–274.56 m), Ramsay Limestone. 4a: magnification of dorsal valve, interior view, MPAL0938 from CUR-49 (274.36–274.56 m), Ramsay Limestone. 5: dorsal valve, exterior view, MPAL0939 from CUR-48 (271.26–271.47 m), Ramsay Limestone. 6: ventral valve, exterior view, MPAL0940 from PJ1A-11 (87.57–87.69 m), Coobowie Limestone. 6a: magnification of ventral valve, exterior view, MPAL0940 from PJ1A-11 (87.57–87.69 m), Coobowie Limestone. 7: ventral

valve, exterior view, MPAL0941 from PJ1A-11 (87.57–87.69 m), Coobowie Limestone. 8: ventral valve, exterior view, MPAL0942 from CUR-47 (270.04–270.2 m), Ramsay Limestone. 9. Ventral valve, exterior view, MPAL0943 from CUR-47 (270.04–270.2 m), Ramsay Limestone.

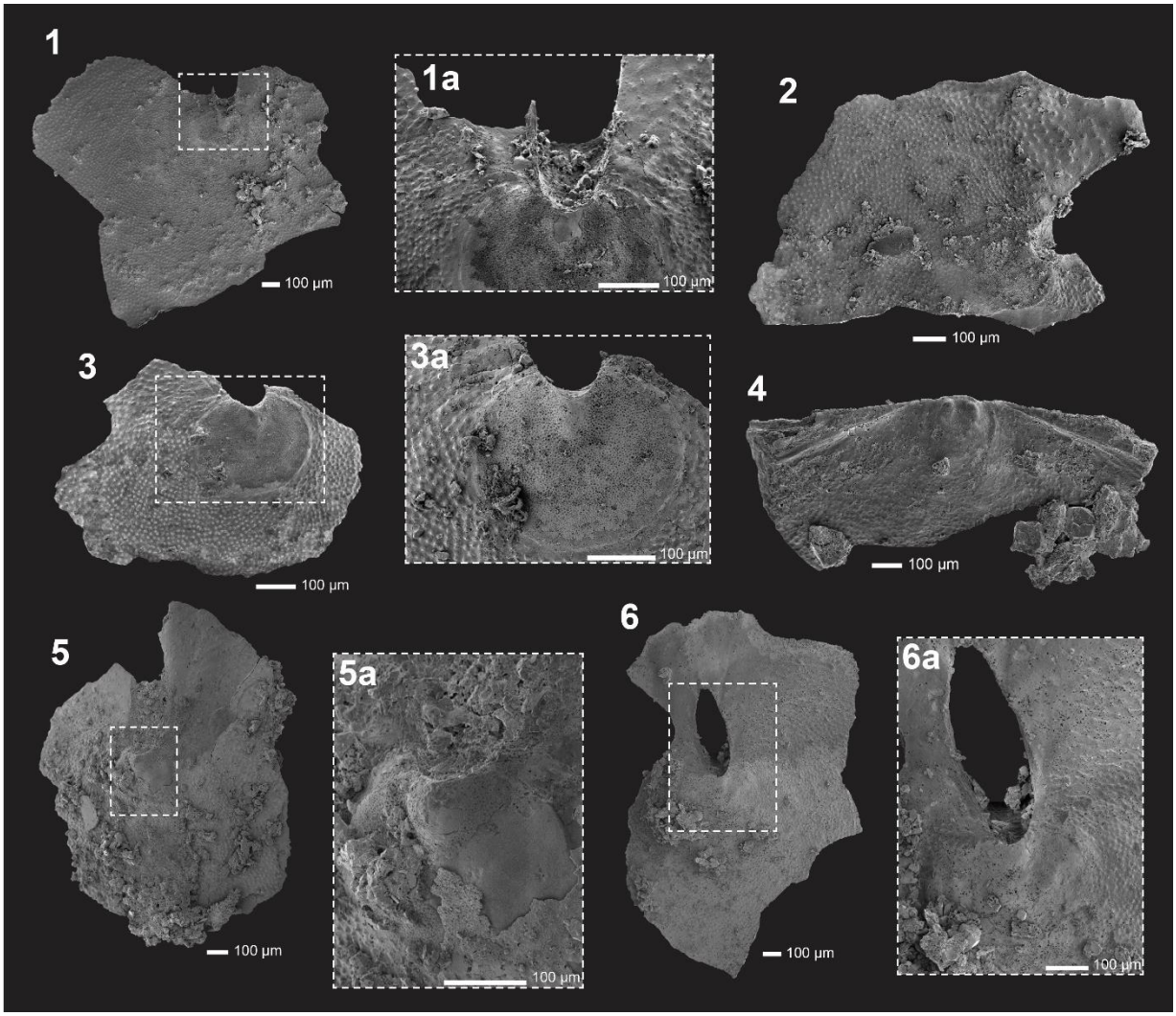

Figure 8. SEM Images of *Schizopholis napuru* and *Eothele granulata* from drill cores CURD-9 and Port Julia-1A. **1-5.** *Schizopholis napuru;* 1. ventral valve, exterior view, MPAL0944 from CUR-9 (181.02–181.15 m), Stansbury Limestone. 1a: magnification of ventral valve, interior view, MPAL0944 from CUR-9 (181.02–181.15 m), Stansbury Limestone. 2: ventral valve, exterior view, MPAL0945 from CUR-9 (181.02–181.15 m), Stansbury Limestone. 3: ventral valve, exterior view, MPAL0946 from CUR-9 (181.02–181.15 m), Stansbury Limestone. 3a: magnification of ventral valve, exterior view, MPAL0946 from CUR-9 (181.02–181.15 m), Stansbury Limestone. 4: dorsal valve, interior view, MPAL0947 from CUR-20 (183.19–183.38 m), Stansbury Limestone. 5: ventral valve, exterior view, MPAL0948 from CUR-7-8 (178.65–178.92 m), Stansbury Limestone. 5a: magnification of ventral valve, interior view, MPAL0948 from CUR-7-8 (178.65–178.92 m), Stansbury Limestone. **6.** *Eothele granulata*; ventral valve, exterior view, MPAL0949 from CUR-7-8 (178.65–178.92 m), Stansbury Limestone. 6a: magnification of ventral valve, interior view, MPAL0949 from CUR-7-8 (178.65–178.92 m), Stansbury Limestone.

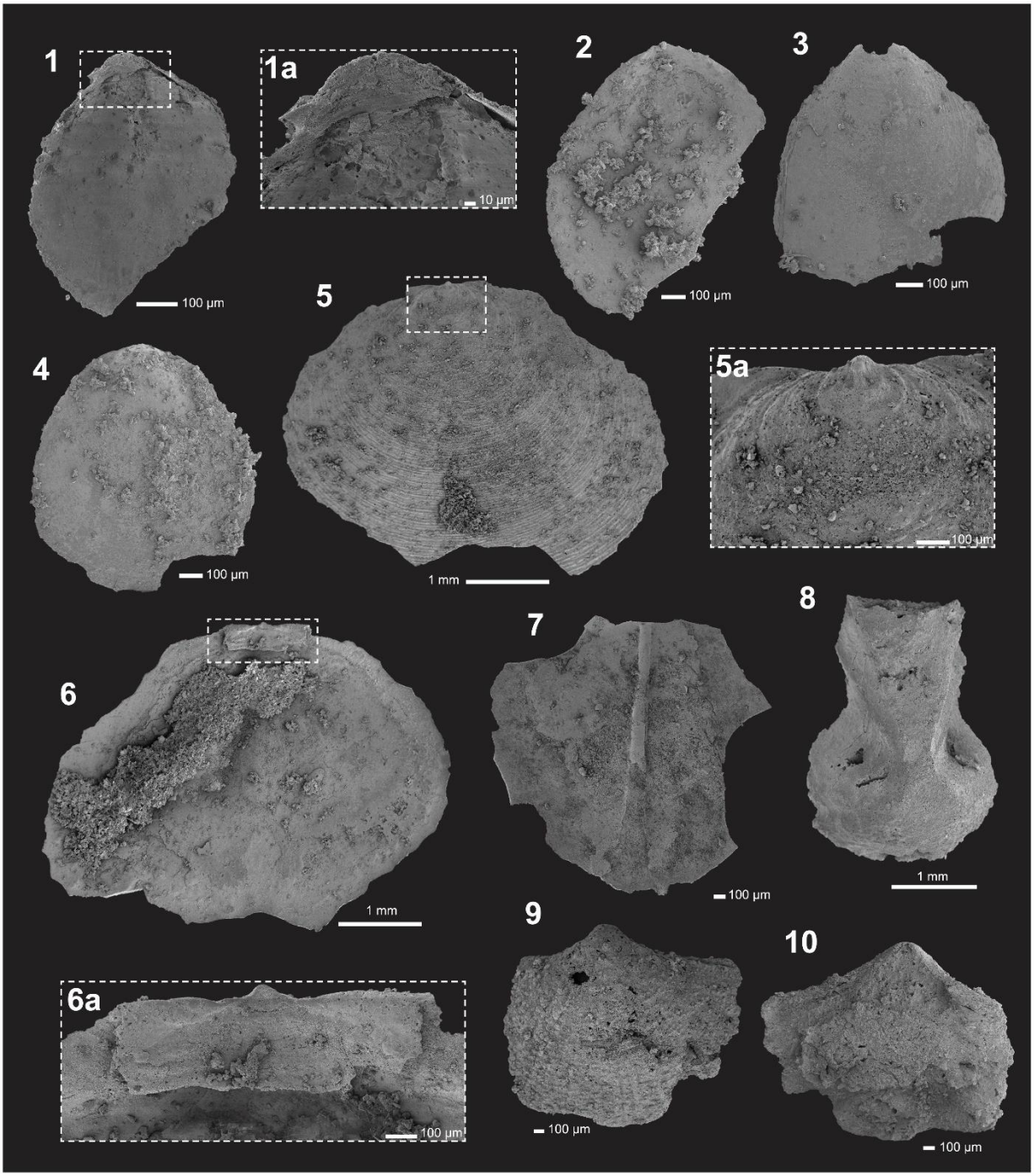

Figure 9. SEM Images of *Kyrshabaktella* cf. *mudedirri*, Acrotheloid sp. Indet, *Micromitra* sp., and *Nisusia grandis* from drill cores CURD-9 and Port Julia-1A. **1-4.** *Kyrshabaktella* cf. *mudedirri;* 1: ventral valve, interior view, MPAL0950 from PJ1A-8 (75.55–77.68 m), Coobowie Limestone. 1a: magnification of ventral valve, interior view, MPAL0950 from PJ1A-8 (75.55–77.68 m), Coobowie Limestone. 2: dorsal valve, interior view, MPAL0951 from CUR-7-8 (178.65–178.92 m), Stansbury Limestone. 3: dorsal valve, exterior view, MPAL0952 from CUR-7-8 (178.65–178.92 m), Stansbury Limestone. 4: dorsal valve, exterior view, MPAL0953 from CUR-7-8 (178.65–178.92 m), Stansbury Limestone. **5-7.** Acrotheloid sp. indet.; 5: ventral valve, exterior view, MPAL0954 from CUR-7-8 (178.65–178.92 m), Stansbury Limestone. 5a. magnification of ventral valve, exterior view, MPAL0954 from CUR-7-8 (178.65–178.92 m), Stansbury Limestone. 6: ventral valve, interior view, MPAL0954 from CUR-7-8 (178.65–178.92 m), Stansbury Limestone. 6a. magnification of ventral valve, interior view, MPAL0954 from CUR-7-8 (178.65–178.92 m),

Stansbury Limestone. 7: ventral valve, interior view, MPAL0955 from PJ1A-8 (75.55–77.68 m), Coobowie Limestone. **8.** *Micromitra* sp.; Phosphatised steinkern of MPAL0956 from PJ1A-11 (87.57–87.69 m), Coobowie Limestone. **9-10.** *Nisusia grandis*; 9. internal mould, ventral valve exterior, MPAL0957 from CUR-18 (300.97–301.13 m), Ramsay Limestone. 10. internal mould, interior view ventral valve, MPAL0957 from CUR-18 (300.97–301.13 m), Ramsay Limestone.

6.3.5. Molluscs

Steinkerns of *Pelagiella* sp. (Fig. 11.1–11) ranges from the upper Ramsay Limestone in drill core CURD-9 (CUR-47, 270.04–270.20 m) to the upper Stansbury Limestone in drill core Port Julia-1A (PJ1A-37, 173.56–173.75 m). *Figurina* sp. (Fig. 11.12) ranges from the lower Ramsay Limestone in drill core CURD9 (CUR-63, 314.51–314.69 m) through to the Stansbury Limestone in drill core CURD9 (CUR-21, 183.85–184 m). Although various species were identified by Brock & Cooper (1993), Gravestock et al. (2001), and Jago & Kruse (2020), the poor preservation and difficulties associated with identification of steinkerns of univalved molluscs (see Jacquet & Brock 2015 for discussion), species level identification is left in open nomenclature in the current study material.

Cupitheca sp., (Fig. 11.13-14) ranges from the upper Ramsay Limestone (CUR-49, 274.36–274.56 m) to the lower Coobowie Limestone (PJ1A-41, 92.88–93.05 m).

6.3.6. Porifera and Chancelloriids

Isolated rays of *Chancelloria* spp., *Allonia* sp. and hexactinellid spicules (Fig. 12.1-10) are common through the units in both cores, however these are not useful for biostratigraphy given that they range down into Fortunian aged rocks. It is therefore not surprising to find these taxa throughout all formations for drill cores CURD-9 and Port Julia-1A from the lower Ramsay Limestone in CURD-9 (CUR-62, 313.01–313.22 m) to the Coobowie Limestone in Port Julia-1A (PJ1A-41, 92.88–93.05 m). *Chancelloria* spp., and *Allonia* sp. range from the Stansbury Limestone to the Coobowie Limestone from drill core Port Julia-1A (86–184 m; Gravetsock et al. 2001; Jago & Kruse 2020) as well as the Ramsay Limestone from drill core Stansbury West 1 (Core 5, 761.4 m) and Stansbury Town 1 (Core 10, 981.5–984.5 m) in Brock & Cooper (1993) also support the current range.

6.3.7. Echinoderms

Isolated echinoderm sclerites (Fig. 12.11-16) range from the lower Ramsay Limestone in CURD-9 (CUR-62, 313.01–313.22 m) through to the upper Stansbury Limestone in Port Julia-1A (PJ1A-31, 162.6–162.65 m).

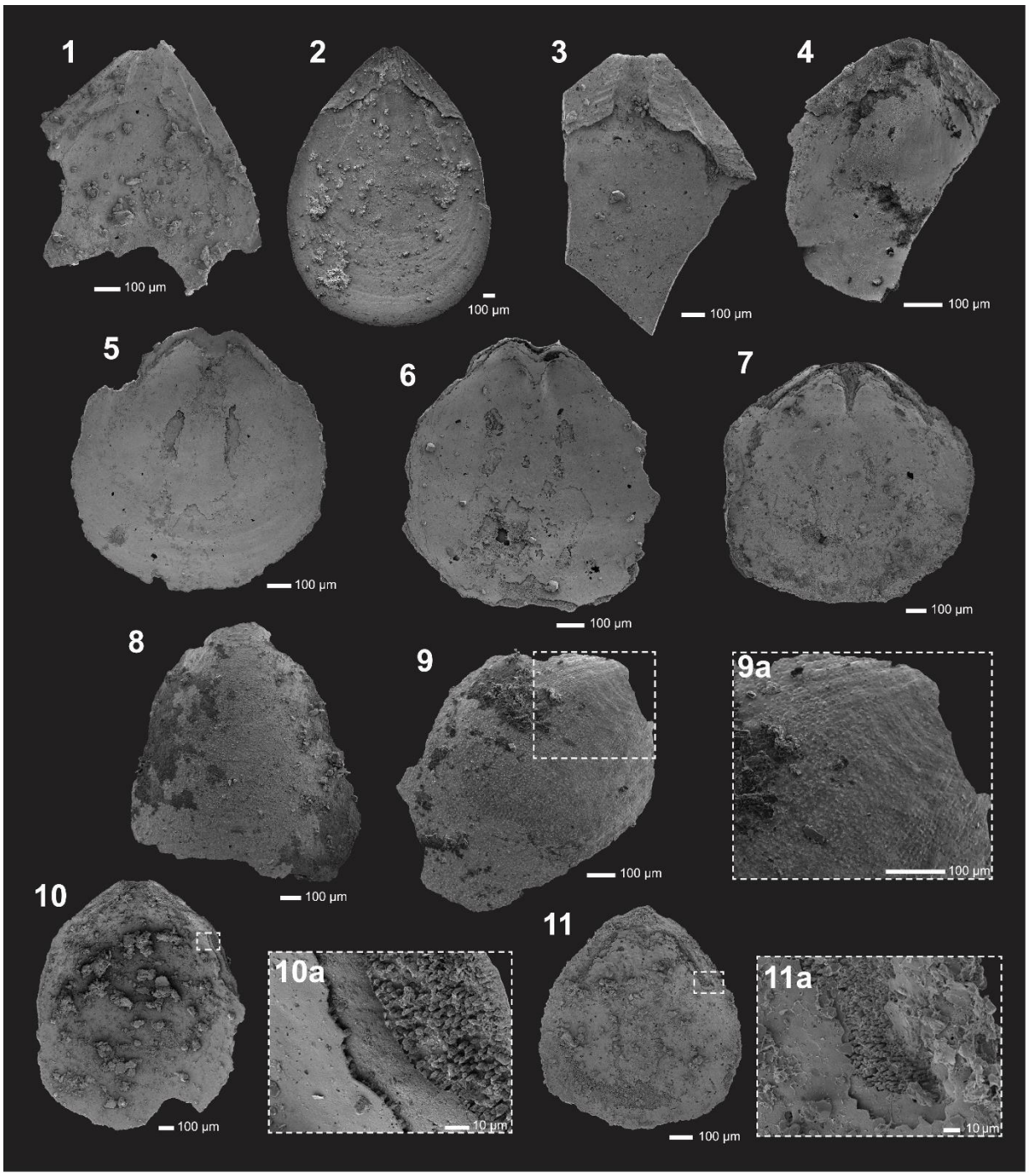

Figure 10. SEM Images of lingulid brachiopods from drill cores CURD-9 and Port Julia-1A. **1-3.** *Aksarinaia subtilicrusta*; 1: ventral valve, interior view, MPAL0958 from PJ1A-11 (87.57–87.69 m), Coobowie Limestone. 2: ventral valve, interior view, MPAL0959 from CUR-9 (181.02–181.15 m), Stansbury Limestone. 3: ventral valve, oblique interior view, MPAL0960 from PJ1A-6 (71.33–71.5 m), Coobowie Limestone. **4-11.** *Eoobolus* sp.; 4: ventral valve, interior view, MPAL0961 from PJ1A-66 (75.11–75.24 m), Coobowie Limestone. 5: dorsal valve, interior view, MPAL0962 from PJ1A-66 (75.11–75.24 m), Coobowie Limestone. 6: dorsal valve, interior view, MPAL0963 from PJ1A-6 (71.33–71.5 m), Coobowie Limestone. 7: dorsal valve, interior view, MPAL0964 from PJ1A-8 (75.55–77.68 m), Coobowie Limestone. 8: dorsal valve, exterior view, MPAL0965 from CUR-9 (181.02–181.15 m), Stansbury Limestone. 9. dorsal valve, exterior view, MPAL0966 from CUR-9 (181.02–181.15 m), Stansbury Limestone. 9a. magnification of dorsal valve, exterior view, MPAL0966 from CUR-9 (181.02–181.15 m), Stansbury Limestone. 10. ventral valve, interior view,

MPAL0967 from CUR-14-15 (261.5–261.66 m), Ramsay Limestone. 10a. magnification of ventral valve, interior view, MPAL0967 from CUR-14-15 (261.5–261.66 m), Ramsay Limestone. 11. ventral valve, interior view, MPAL0968 from CUR-62 (313.01–313.22 m), Ramsay Limestone. 11a. magnification of ventral valve, interior view, MPAL0968 from CUR-62 (313.01–313.22 m), Ramsay Limestone.

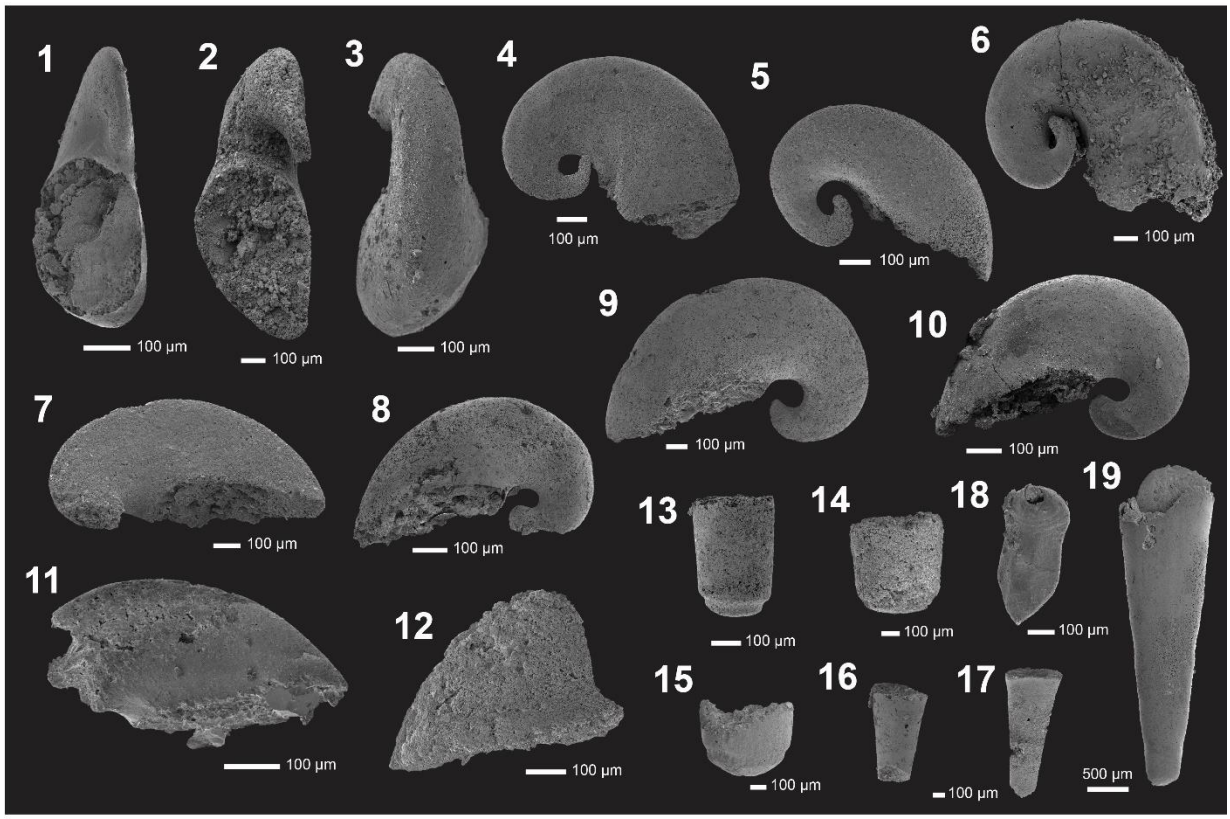

Figure 11. SEM Images of molluscs and other shelly fossil material from drill cores CURD-9 and Port Julia-1A. **1-11**. *Pelagiella* sp.; 1. apertural view, MPAL0969 from PJ1A-37 (173.56–173.75 m), Stansbury Limestone. 2. apertural view from MPAL0970, PJ1A-37 (173.56–173.75 m), Stansbury Limestone. 3. plan view, MPAL0971 from PJ1A-37 (173.56–173.75 m). 4. lateral view, MPAL0972 from PJ1A-37 (173.56-173.75 m), Stansbury Limestone. 5. lateral view, MPAL0973 from PJ1A-37 (173.56–173.75 m), Stansbury Limestone. 6. lateral view, MPAL0974 from PJ1A-37 (173.56–173.75 m), Stansbury Limestone. 7. lateral view, MPAL0975 from CUR-21 (183.85–184 m), Stansbury Limestone. 8. lateral view, MPAL0976 from CUR-7-8 (178.65–178.92 m), Stansbury Limestone. 9. lateral view, MPAL0977 from PJ1A-37 (173.56–173.75 m), Stansbury Limestone. 10. lateral view, MPAL0978 from PJ1A-37 (173.56–173.75 m), Stansbury Limestone. 11. lateral view, MPAL0979 from CUR-21 (183.85–184 m), Stansbury Limestone. **12.** *Figurina* sp.; lateral view, MPAL0980 from CUR-63 (314.51–314.69 m), Ramsay Limestone. **13-15.** *Cupitheca* sp.; lateral view, MPAL0981 from CUR-49 (274.36–274.56 m), Ramsay Limestone. 14. lateral view, MPAL0982 from PJ1A-41 (244.15–244.27 m), Coobowie Limestone. 15. lateral view, MPAL0983 from PJ1A-41 (244.15–244.27 m), Coobowie Limestone. **16-17.** Hyolith sp. indet.; lateral view, MPAL0984 from CUR-20 (183.19–183.38 m), Stansbury Limestone. 17. lateral view, MPAL0985 from CUR-20 (183.19–183.38 m), Stansbury Limestone. **18.** *Cambroclavus absonus.*; plan view, MPAL0986 from CUR-27 (183.12–183.19 m), Stansbury Limestone. **19.** *Microcornus* sp.; lateral view, MPAL0987 from CUR-14-15 (261.5–261.66 m), Ramsay Limestone.

6.3.8. Other shell fossil material

Cambroclavus absonus (Fig. 11.18) is a widespread, though enigmatic SFF, that was recovered from one stratigraphic horizon in the Stansbury Limestone (CUR-27, 183.12–183.19 m) from drill core CURD-9. There have been no previous recordings of *C. absonus* within the western Stansbury Basin for the Ramsay to Coobowie limestones.

Hyolith conchs (Fig. 11.19) mainly represented as steinkerns probably belong to *Microcornus* sp. indet. (Fig. 11.16-17) range from the upper Ramsay Limestone in CURD-9 (CUR-14-15, 261.5–261.66 m) to the upper Stansbury Limestone in Port Julia-1A (PJ1A-37, 173.56–173.75 m).

The hyolithelminthid taxon *Hyolithellus* sp. (Fig. 12.17) was recovered in one stratigraphic horizon in the lower Ramsay Limestone (CUR-65, 315.47–315.62 m) from drill core CURD-9. There have been no previous recordings of *Hyolithellus* sp. within the western Stansbury Basin for the Ramsay Limestone to Coobowie Limestone units, but it is well known in older Cambrian strata in South Australia (Bengtson et al. 1990) and around the world (e.g., Skovsted & Peel, 2010).

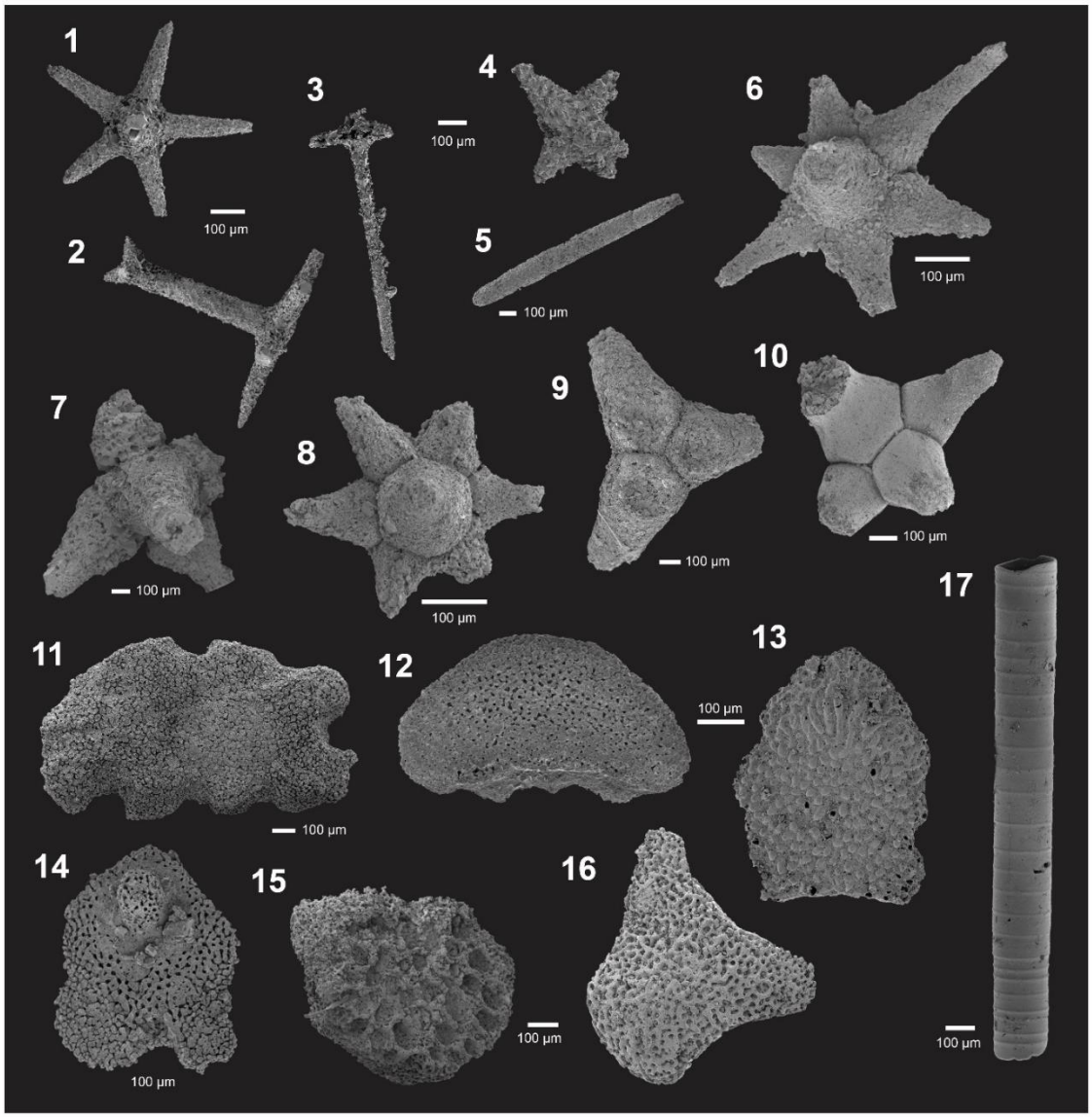

Figure 12. SEM Images of spicules, chancelloriids, tubes and echinoderm sclerites from drill cores CURD-9 and Port Julia-1A. **1-5.** hexactinellid spicules, 1. axial view of pentact, MPAL0988 from CUR-48 (271.26–271.47 m), Ramsay Limestone. 2. oblique view, MPAL0989 from CUR-48 (271.26–271.47 m), Ramsay Limestone. 3. lateral view, MPAL0990 from CUR-48 (271.26–271.47 m), Ramsay Limestone. 4. basal view, MPAL0991 from CUR-46 (266.1–266.23 m), Ramsay Limestone. 5. lateral view, MPAL0992 from PJ1A-45 (182.84–183.01 m), Stansbury Limestone. **6-10.** *Chancelloria* spp., *Allonia* sp., 6. MPAL0993 from PJ1A-51 (189.04–189.19 m), Stansbury Limestone. 7. MPAL0994 from PJ1A-43 (181.26–181.5 m), Stansbury Limestone. 8. MPAL0995 from PJ1A-51 (189.04–189.19 m), Stansbury Limestone. 9. MPAL0996 from PJ1A-51 (189.04–189.19 m), Stansbury Limestone. 10. MPAL0997 from PJ1A-51 (189.04–189.19 m), Stansbury Limestone. **11-16.** Echinoderm sclerites, 11. MPAL0998 from PJ1A-37 (173.56–173.75 m), Stansbury Limestone. 12. MPAL0999 from CUR-21 (183.85–184 m), Stansbury Limestone. 13. MPAL1000 from CUR-18 (300.97–301.13 m), Ramsay Limestone. 14. MPAL1001 from CUR-18 (300.97–301.13 m), Ramsay Limestone. 15. MPAL1002 from CUR-7-8 (178.65–178.92 m), Stansbury Limestone. 16. MPAL1003 from CUR-7-8 (178.65–178.92 m), Stansbury Limestone. **17.** *Hyolithellus* sp., MPAL1004 from CUR-65 (315.47–315.62 m), Ramsay Limestone.

6.4. Chemostratigraphy of the Western Stansbury Basin

6.4.1. CURD-9 Stable Isotope Chemostratigraphy

Figure 13. shows the $\delta^{13}C$ and $\delta^{18}O$ curve for CURD-9 through the Ramsay Limestone, Corrodgery Formation and the Stansbury Limestone (see Supplementary Table 1. for raw isotopic data). $\delta^{13}C$ values are weakly positive (+0.5 ‰) at the base of the Ramsay (CUR-19, 316.7 m), then trends to a negative value of -2.2 ‰ at CUR-60 (309.2 m). The curve then trends back towards +0.5 ‰ before plateauing around 0.0 ‰ (with minor deviations of 0.1 ‰) until CUR-49 (274.3 m) where values, again, become more negative with a minimum value at the top of the Ramsay Limestone of -1.6 ‰ (CUR15, 261.6 m).

This negative trend continues into the Corrodgery Formation with a nadir of -6.9 ‰ at CUR-40 (247.8 m). $\delta^{13}C$ values remain negative through to CUR-35 (-5 ‰ at 224.2 m), after which there is a 36.5 m gap in stable isotope data due to lack of carbonate lithologies. The last data point in the upper Corrodgery Formation remains negative at -3 ‰ at CUR-24 (187.7 m).

The Stansbury Limestone $\delta^{13}C$ values remain negative oscillating around -2 ‰ with minor peaks between -1.1 ‰ in CUR-21 (183.9 m) and -2.4 ‰ in CUR-5 (176.2 m). At CUR-4 (174.2 m) there is a distinctive and sharp negative spike of -5.3 ‰ before a slight positive trend to -2 ‰ (CUR-1, 169.2 m) at the top of the Stansbury Limestone. Unfortunately, there is no lithological upper boundary to this unit present in the core.

CUR D 9

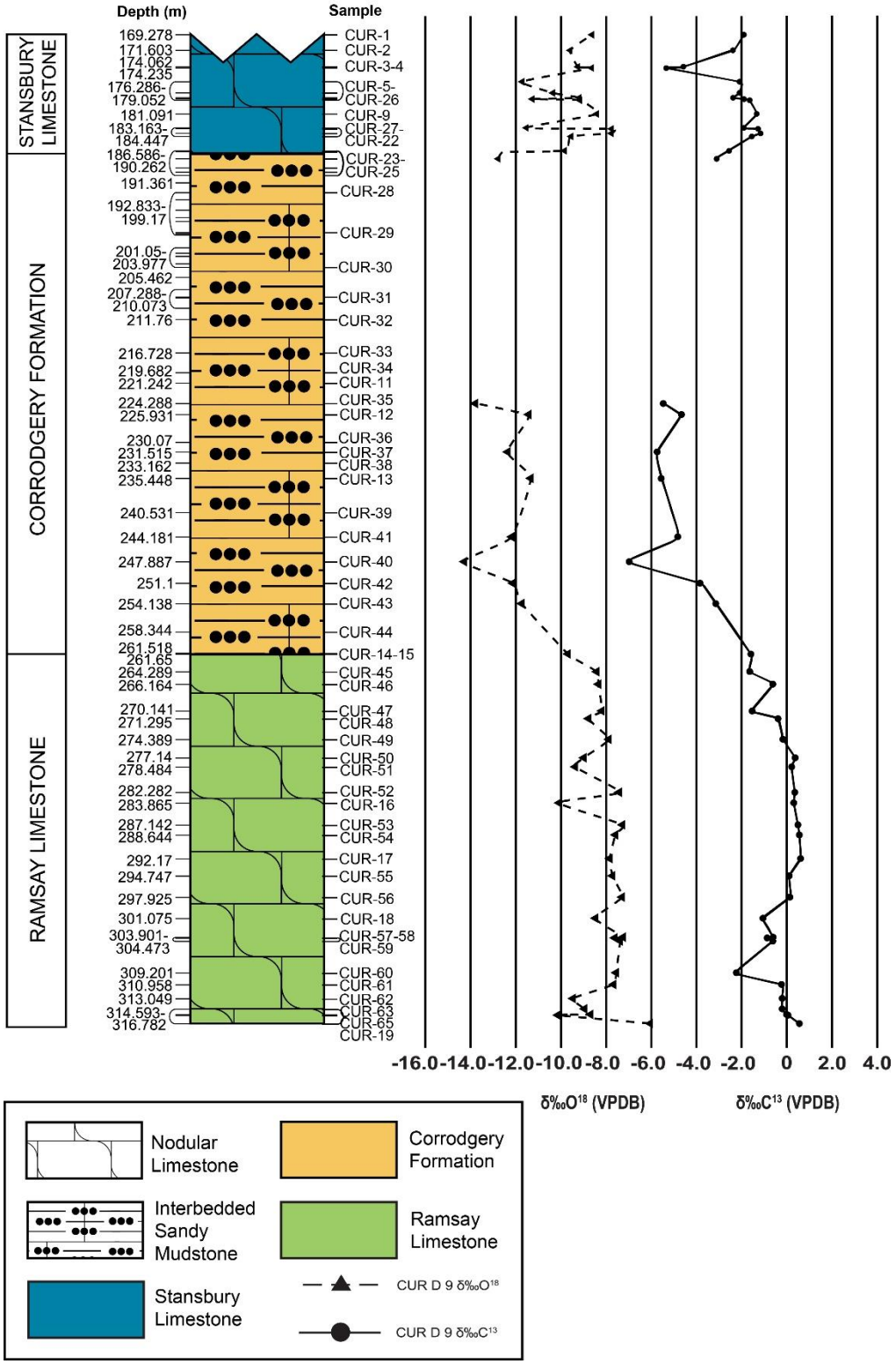

Figure 13. $\delta^{13}C$ and $\delta^{18}O$ chemostratigraphic curve for drill core CURD-9 through the Ramsay Limestone, Corrodgery Formation and Stansbury Limestone. Major negative $\delta^{13}C$ peaks include the lower Ramsay Limestone at -2.2 ‰ (CUR-60, 309.2 m), lower Corrodgery Formation at -6.98 ‰ (CUR-40, 247.8 m), and the Stansbury Limestone at -5.3 ‰ (CUR-4, 174.2 m).

6.4.2. Port Julia-1A Stable Isotope Chemostratigraphy

Figure 14. shows the $\delta^{13}C$ and $\delta^{18}O$ curve for Port Julia-1A through the Stansbury Limestone, Moonan Formation, and Coobowie Limestone (see Supplementary Table 2. for raw isotopic data). The general $\delta^{13}C$ curve for the Stansbury Limestone in Port Julia-1A displays very similar trends to the $\delta^{13}C$ curve in the Stansbury Limestone in CURD-9, albeit slightly less negative. The lower ~15 m of the Stansbury Limestone essentially plateaus at around ~0.0 ‰ from PJ1A-78 (210.073 m) to PJ1A-77 (207.288 m) with minor deviations of up to 0.1 ‰. Two weakly positive peaks occur at PJ1A-76 (202.3 m) and PJ1A-50 (186.7 m) that rise to ~ +0.9 ‰. Above PJ1A-44 (181.5 m), the $\delta^{13}C$ curve begins sharply trending toward negative values, reaching a nadir of ~ -2.7 ‰ at PJ1A-34-35 (169.9 m). The rise to -0.5 ‰ in PJ1A-16 (162.3 m) occurs at the boundary between the Stansbury Limestone and overlying Moonan Formation.

Negative $\delta^{13}C$ values continue into the Moonan Formation reaching a nadir of -5.6 ‰ at PJ1A-27 (147.06 m). All values stratigraphically above PJ1A-16 (162.3 m depth) have $\delta^{13}C$ values more negative than -2 ‰ until the lower Coobowie Limestone (PJ1A-11, 87.642 m). The Moonan Formation is largely siliciclastic (see Fig. 3F.F–I) but was sampled for $\delta^{13}C$ and $\delta^{18}O$ in the hope of retrieving enough carbonate to continue the curve above the Stansbury Limestone. In all, 22 samples were taken through this unit but only 7 samples provided enough carbonate to retrieve a carbonate signal. Cross-plot of the $\delta^{13}C$ and $\delta^{18}O$ data (Fig. 15) shows a relatively wide spread of data points that suggest potential co-variance. This, along with small number of carbonate data points recovered, indicates the isotopic data in this unit may not capture a primary signal and needs to be treated with caution.

Dolomitization is prevalent throughout the Coobowie Limestone which may have dampened the $\delta^{13}C$ signal (Weissert et al. 2008; Swart 2015). The $\delta^{13}C$ trend at the base of the Coobowie Limestone is negative and plateaus at ~ -2 ‰ until PJ1A-11 (87.642 m) at which point $\delta^{13}C$ values abruptly trend in a positive direction to -0.23 ‰. $\delta^{13}C$ values drop back to -1.4 ‰ at PJ1A-10 (85.3 m depth). The $\delta^{13}C$ curve begins to trend towards more positive values at PJ1A-9 (82.6 m depth) where values plateau at ~ +1.5 ‰ to PJ1A-3 (66.044 m). Isotope values remain positive until the top of the drill core (PJ1A-1, 60.4 m).

Port Julia-1A

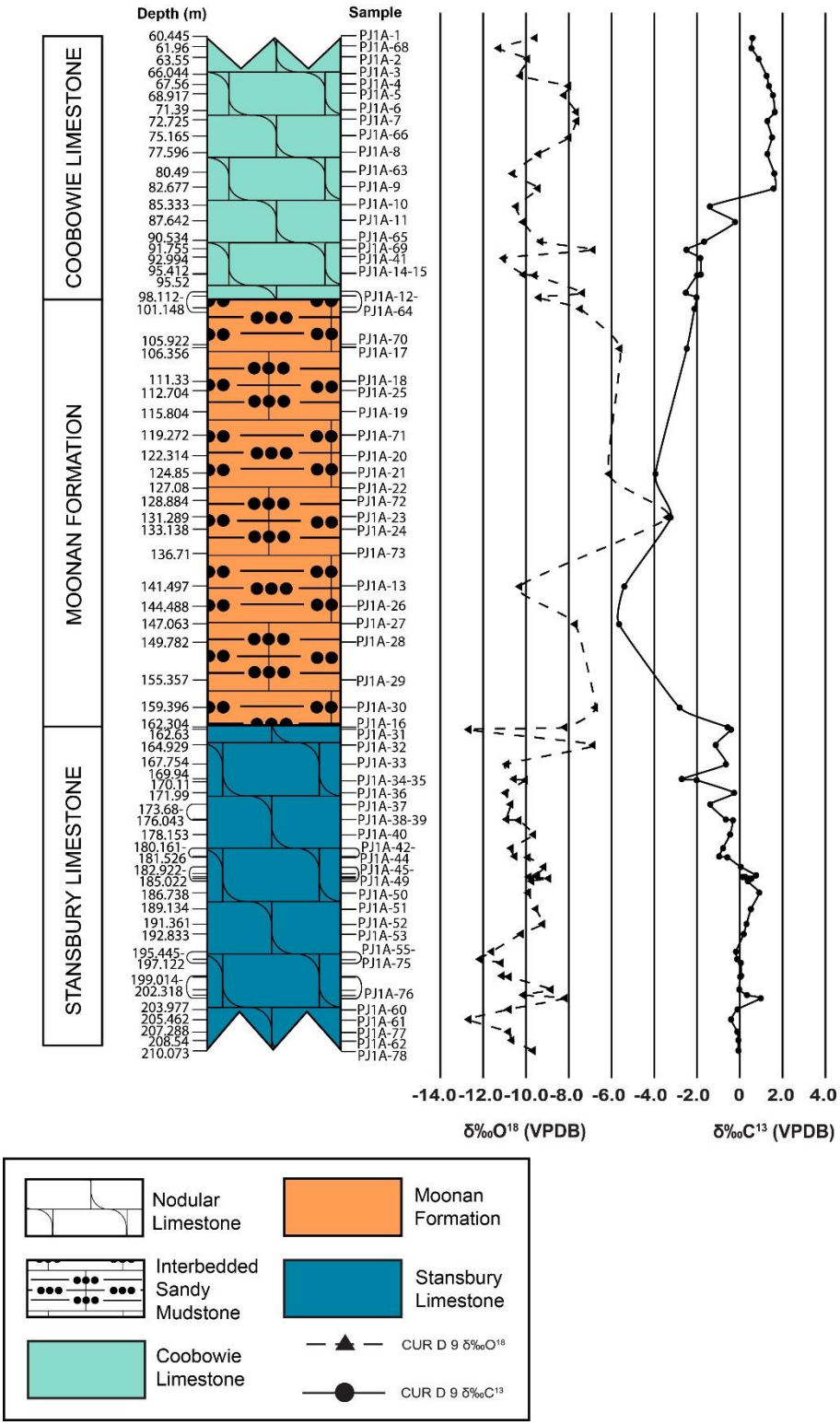

Figure 14. $\delta^{13}C$ and $\delta^{18}O$ chemostratigraphic curve for drill core Port Julia-1A through the Stansbury Limestone, Moonan Formation, and Coobowie Limestone. Major negative $\delta^{13}C$ peaks include the upper Stansbury Limestone at -2.7 ‰ (PJ1A-34-35, 169.9 m) and the lower Moonan Formation at -5.6 ‰ (PJ1A-27, 147.06 m).

6.4.3. Cross-plot for the Western Stansbury Basin

The cross-plot in Figure 15. shows tight grouping of oxygen and carbonate isotope data in the Ramsay Limestone, Stansbury Limestone (for both drill core CURD-9 and Port Julia-1A), and the Coobowie Limestone. Since the $\delta^{13}C$ and $\delta^{18}O$ values do not show a positive correlation or systematic relationship, it suggests that the data captures the primary isotopic composition in these units. On the other hand, the data from the lower Corrodgery and Moonan formations shows a weaker grouping with more spread, hinting at more co-variance or potential for diagenetic overprint, suggesting that these consistently deeply negative $\delta^{13}C$ values may reflect secondary isotopic signals and thus need to be treated with a measure of caution. The cross-plot includes data for the Yuruga Formation in Stansbury West 1 taken from Hall (2012) to compare with the data from CURD-9 and Port Julia 1. The Yuruga Formation is a thick red-brown, fine-grained sandstone and siltstone unit that has a deeply negative profile (with a maximum negative $\delta^{13}C$ value of ~ -10.8 ‰). The broad spread of data for the Yuruga Formation points to co-variance suggesting that the signal may be the product of diagenetic alteration or secondary isotopic signals from carbonate cements.

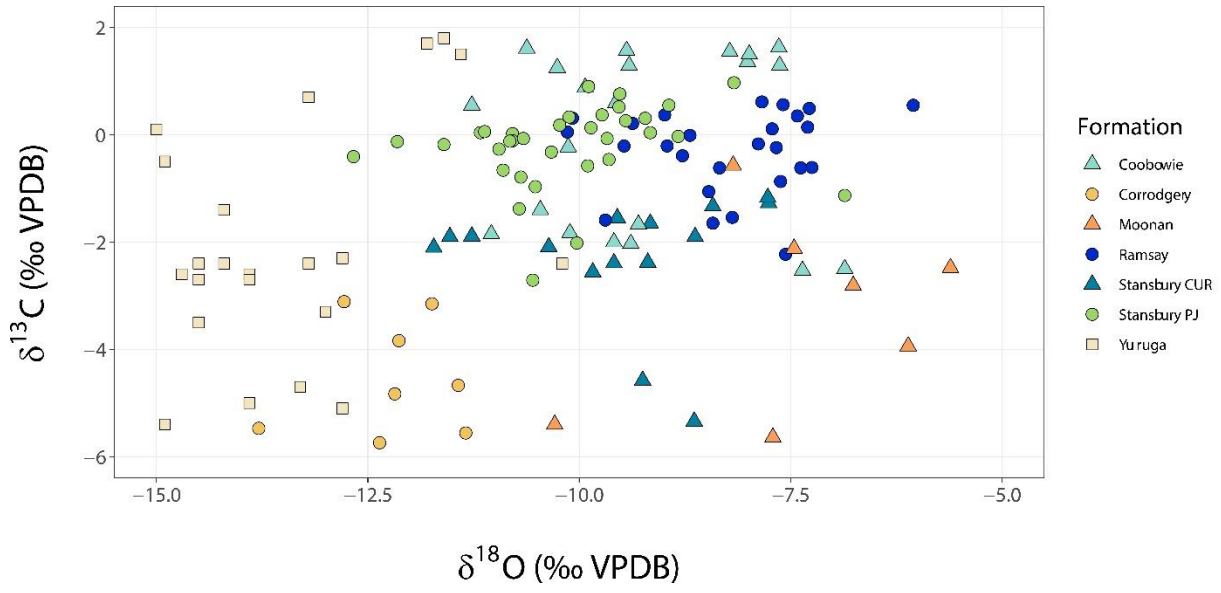

Figure 15. Plot of $\delta^{13}C$ versus $\delta^{18}O$ by stratigraphic formation from the CURD-9 and Port Julia 1A cores and data for the Yuruga Formation from Stansbury West 1 (Hall 2012).

6. DISCUSSION

7.1 Depositional Environment

The overall lithostratigraphy of drill cores CURD-9 and Port Julia-1A are consistent with previous interpretations (Gravestock & Gatehouse 1995; Gravestock et al. 2001), but detailed thin section analysis of the sedimentology reveals complexities within the depositional environment not previously identified.

The carbonate dominated units (Ramsay, Stansbury, and Coobowie limestones) share many features in common including presence of oncolites, bioclastic packstones, intervals of brecciated limestone, bioclastic grainstones, and varying abundance of terrigenous quartz. The poor sorting, fragmentary and abraded shelly material, and randomly oriented nature of skeletal allochems (Fig. 2D, 2J–K, 3B, 3D, 3K) suggest deposition within a moderate to highly agitated environment within wave base (Plumey et al. 1962). The presence of abundant isolated echinoderm plates and ossicles and individual (often broken) hexactinellid sponge spicules and chancelloriids supports an interpretation of a shallow intertidal to subtidal marine setting possibly associated with inner to mid-ramp environments (Flugel & Munnecke 2010).

The presence of distinctive oncolites throughout all limestone units also indicates relatively high energy, low intertidal to shallow subtidal environments (Flugel & Munnecke 2010). The asymmetrical nature of the outer microbial layer (except for the oncoids within the Coobowie Limestone; Fig. 3L) as well as the weak laminated meshwork of the oncoids, possibly indicate episodic periods of lower energy settings (Flugel & Munnecke 2010; Fig. 2B, 2J, 3B). Oncoids within the Coobowie Limestone are smaller, more symmetrical, and are deposited within a sparry, un-fossiliferous cement (Fig. 3L). This would suggest possible redeposition of the oncoids from a higher energy environment. The presence of terrestrial constituents (quartz grains) in combination with dark, fine-grained micritic mud matrix and nodular limestone facies suggest closer proximity to a cratonic source with deposition in a shallow marine, mid to high energy, well oxygenated, inner shelf setting (Flugel & Munnecke 2010).

The Stansbury Limestone is the only unit intersected by both cores. Notably, there are close similarities in lithologies especially in relation to the levels that capture sharp negative $\delta^{13}C$ isotopic peaks in both cores. The lithologies below the negative $\delta^{13}C$ peaks are dominated by oncolites and bioclastic packstones with fragmentary trilobite sclerites and small shelly fossils (e.g., sample CURD-9; Fig. 2K and PJ1A-76; Fig. 3B). The lithologies at horizons coincident with and above the

negative $\delta^{13}C$ peaks reveal carbonates that are possibly unfossiliferous with a nodular micritic fabric (e.g., PJ1A-34-35; Fig. 3E) suggesting a decline in diversity and abundance of fauna across this transition.

The presence of small pyrite framboids sporadically throughout the Ramsay Limestone and into the Moonan Formation highlights potential redox gradients in the environment at the time of deposition. Pyrite can form early in the process of diagenesis within sediment during transitions following anoxic settings (Wilkin et al. 1996). Therefore, pyrite is often used as a palaeoenvironmental proxy for relative oxygen conditions (anoxic, euxinic, or dysoxic) throughout the water column (Roychoudhury et al. 2003). Pyrite is abundant near the boundary between the Stansbury Limestone and Moonan Formation transition (162.25–162.65 m) in Port Julia-1A. This transition into less oxic conditions may also be associated with the lack of fossils in thin section PJ1A-34-35 (170.024–169.997 m), possibly linked to the significant negative $\delta^{13}C$ event.

The siliciclastic units (Corrodogery and Moonan formations) consist of grey and red micaceous sandstones interbedded with siltstones with soft sediment deformation in the form of minor slumps and folds; potential crossbedding (Fig. 2G, 3F), flame structures (Fig. 2F), and potential bioturbation (Fig. 2F, 3D) are also apparent. Bioturbation and flame structures indicate a moderate degree of disruption in the soft sediment by both biological and environmental means such as turbidity currents, wave action, or simply by rapid deposition of coarse sediments on top of unconsolidated fine grained sediments. Fine laminations throughout these formations indicate slow sedimentation rates associated with likely deposition in an outer shelf-slope settings (Flugel & Munnecke 2010). Lack of carbonate in these formations impacts the reliability of isotope analysis, with carbonate signals possibly representing late-stage cements or post-lithification infills producing secondary $\delta^{13}C$ signals.

A distinct transgression-regression cyclic pattern occurs in both cores (Gravestock et al. 2001). The transition from the shallow marine shelf carbonates of Ramsay Limestone to a deep-water, outer-ramp/basinal environment in the Corrodgery Formation in CURD-9 is repeated in the transition from the Stansbury Limestone to Moonan Formation in Port Julia-1A. The final shallowing cycle occurs in an inner ramp setting with the deposition of the carbonates of the Coobowie Limestone.

7.2 Chronostratigraphy of the Western Stansbury Basin and correlation in South Australia

Formal definition of the Series 2–Miaolingian boundary at the GSSP in the Kaili Formation in South China is based on the first appearance of the cosmopolitan oryctocephalid trilobite *Oryctocephalus indicus* (base of the *O. indicus* Zone) and the peak of a large negative $\delta^{13}C$ isotopic excursion (ROECE) with minimum values of -2.7 ‰ that coincides with the extinction of the widespread trilobite taxon *Redlichia* (Zhao et al. 2019). The GSSP is based largely on the description of well-preserved trilobites from outcrop representing outer slope siltstones and mudrocks which generally lack small shelly fossil assemblages. Detection of the boundary in shallow marine carbonates that lack *O. indicus* is therefore challenging since this type of biofacies, as exemplified by the Stansbury Basin, is substantially different to the GSSP.

The data presented from drill cores CURD-9 and Port Julia-1A in this study represents the most detailed systematic documentation of the fossil assemblages and chemostratigraphy for successions in the western Stansbury Basin that transect the Series 2–Miaolingian boundary (Fig. 16). The distinct faunal assemblages provide new range data for regional correlation. Biostratigraphic results reported herein confirm the faunal assemblages found previously within Port Julia-1A (Gravestock et al. 2001; Jago & Kruse 2020), as well as from other drill cores from Yorke Peninsula (Brock & Cooper 1993), but also include first discoveries and important range extensions for key taxa that straddle the Series 2–Miaolingian boundary. The new chemostratigraphic data presented herein in combination with the faunal data are interpreted to capture the globally significant AECE and ROECE events which not only allow identification of important chronostratigraphic boundaries that define the lower–middle Cambrian transition but also illustrate the importance of multiproxy methods to refine the Cambrian timescale especially in facies that lack index species.

In their broad synthesis of the Stansbury Basin, Gravestock et al. (2001) documented some of the fauna from drill core Port Julia-1A and erected the informal "*Pelagiella madianensis*" and "*Kaimenella reticulata*" zones covering the Stansbury to Coobowie limestones which they broadly assigned to an upper Stage 4 (upper Toyonian in the Siberian scheme). Unfortunately lack of detailed sampling combined with the fact that the lower and upper boundaries of these "biozones" were not formally defined makes these zones impossible to apply. Brock & Cooper (1993) noted that the two species of *Kaimenella* from the Ramsay Limestone were very rare, and this is supported herein, with only one specimen recovered from a single horizon (CUR-27, 183.12-183.19 m Fig. 6.9). Jacquet & Brock (2015) have indicated that biozones or even faunal assemblages should not be based on steinkern material of Cambrian molluscs, because identification is fraught

with difficulties. This is especially so for speciose taxa such as *Pelagiella* which range from Terreneuvian into Miaolingian deposits and are notoriously difficult to discriminate.

The first occurrence (FO) of *K. djagoran* within the Ramsay Limestone is supported by data presented in Brock & Cooper (1993) who documented *K. djagoran* (as *Hadrotreta primaevae* (Walcott)), within the upper Ramsay Limestone of drill core Stansbury West 1 (Core 5, 761.4 m). Gravestock et al. (2001) also documented *K. djagoran,* (as *Vandalotreta djagoran*) within the Coobowie Limestone in Port Julia-1A where it has a range from 92.95–77.55 m. Although Gravestock et al. (2001) did not record the presence of *C. exquisitum*, Brock & Cooper (1993) reported *C. exquisitum* within the Ramsay Limestone of drill cores Stansbury West 1 (Core 5, 761.4 m), and Stansbury Town 1 (Core 10, 981.5–984.5 m). Range data is also supported for *Kyrshabaktella* where Gravestock et al. (2001) and Jago & Kruse (2020) recovered *Kyrshabaktella* cf. *K.certa* within the Coobowie Limestone in drill core Port Julia-1A (69.15-78.40 m). Brock & Cooper (1993) also documented *?Kyrshabaktella* sp. within the Ramsay Limestone of drill core Stansbury Town 1 (Core 10, 981.5-984.5 m).

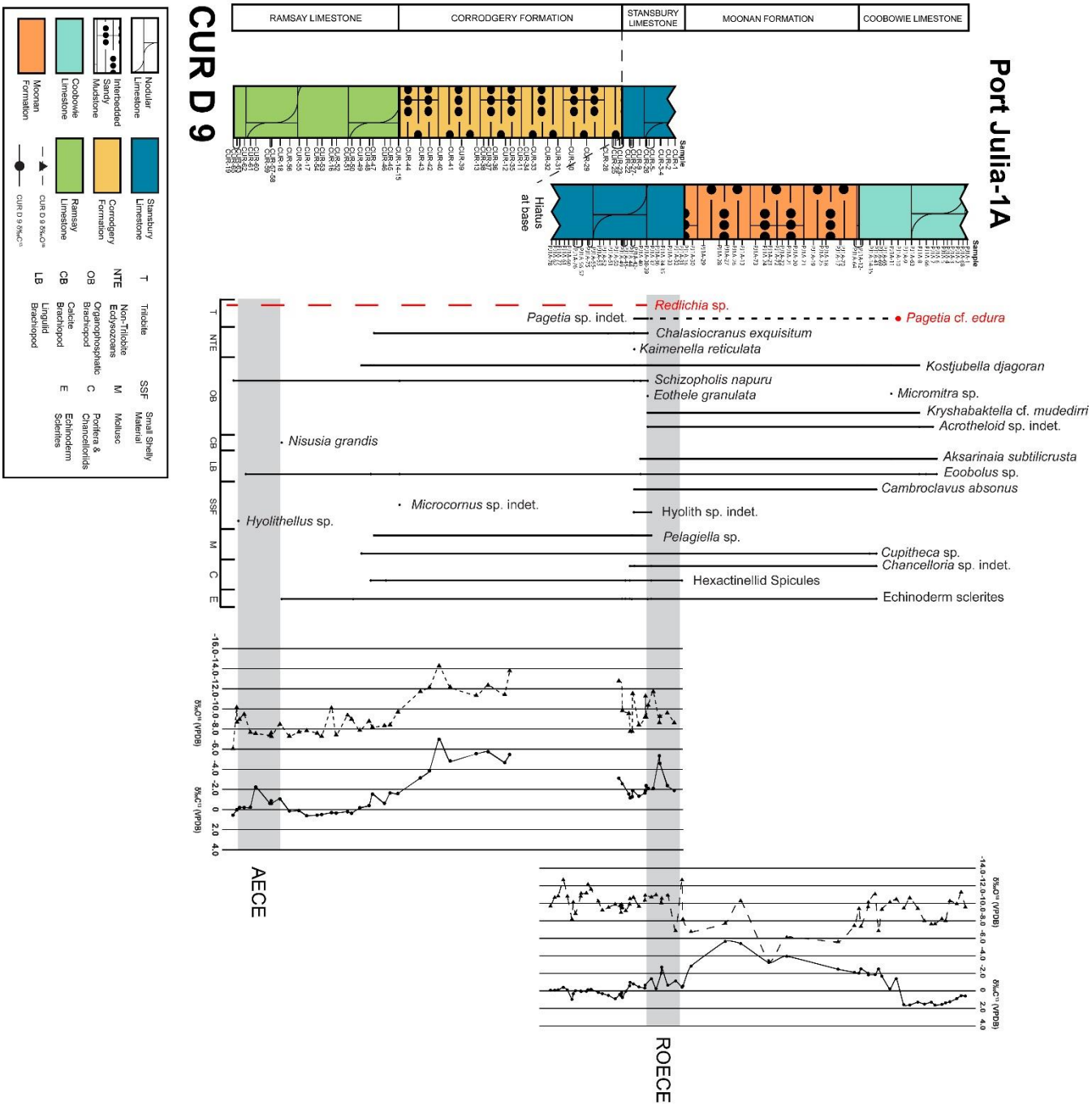

Figure 16. Composite biostratigraphy and chemostratigraphy plot showing interpreted overlap of drill cores CURD-9 and Port Julia-1A. In Port Julia-1A, the base of the Stansbury Limestone is erosional and rests disconformably on the Mesoproterozoic Oorlano Metasomatites. Dashed red line indicates extrapolated stratigraphic range of *Redlichia* sp. from outcropping Ramsay Limestone on Yorke Peninsula (Holmes et al. 2021) to lower Stansbury Limestone in Stansbury Town 1 core (Daily 1990). Red dot with dashed line (=*Pagetia* cf. *edura* from Jago & Kruse 2020) with solid line for *Pagetia* sp. indet. recovered from CURD-9 core in the current study.

7.2.1 Series 2 (Stage 4) units

Holmes et al. (2021) have recently described the full ontogeny of *Redlichia* cf. *versabunda* from outcrop of the Ramsay Limestone on Yorke Peninsula and indicated this taxon is conspecific with *Redlichia guizhouensis* previously described from the Wirrealpa and Aroona Creek Limestones in the Arrowie Basin (Paterson & Brock 2007). This regional correlation is supported by the discovery of the organophosphatic brachiopods *K. djagoran* and *S. napuru* in the Ramsay Limestone in both the CURD-9 and Port Julia-1A cores; both taxa have previously been described (as *Vandalotreta djagoran* and *Eothele napuru*) from the Ramsay and Wirrealpa limestones by Brock & Cooper (1993). This would equate with the *K. djagoran* (=*Vandalotreta djagoran)* Assemblage Zone informally erected by Brock in Jago et al. (2006) which is broadly correlated to the early–mid Ordian Stage in Australia (more commonly referred to as late Stage 4; Kruse et al. 2009). Other fauna within the Ramsay Limestone of CURD-9 supports the range data presented in Brock & Cooper (1993) including: *Kaimenella* sp. aff. *K. reticulata* in the Ramsay Limestone of drill core Stansbury Town 1 (Core 10, 981.5–984.5 m). Other taxa in common, but of little biostratigraphic importance include *Chancelloria* spp., hyolithids, including *Cupitheca* sp. and *Microcornis* sp., steinkerns of *Pelagiella* sp., and isolated echinoderm plates and ossicles.

The youngest Cambrian Archaeocyatha from South Australia are described from the Wirrealpa Limestone of the Arrowie Basin (Kruse 1991) as well as reports of Archaeocyaths from the Ramsay Limestone 6 km south of Curramulka (Daily 1990; Gravestock et al. 2001). However, no Archaeocyatha were noted from the Ramsay Limestone within CURD-9 during the current study.

The global chemostratigraphic curve (Peng et al. 2020, Fig. 19.1) records a significant negative $\delta^{13}C$ excursion event in mid–late Stage 4 called the Archaeocyathid Extinction Carbon isotope Excursion (AECE), which supposedly coincides with global extinction of archaeocyathids (Zhu et al. 2006). Recent revisions to the Cambrian chronostratigraphic scheme suggest that the AECE could be used as a potential marker for the base of the Cambrian Stage 4 (see Chang et al. 2019; Zhu et al. 2019) though currently there is no agreed faunal marker(s) to define this event (Peng et al. 2020). The occurrence of *Redlichia* cf. *versabunda* throughout the Ramsay Limestone (Daily 1990; Holmes et al. 2021) and reports of *Redlichia* sp. in the lower Stansbury Limestone (Daily 1968, 1990) in the western Stansbury basin indicate that the negative peak of $\delta^{13}C$ (-2.2 ‰ at CUR-60, 309.2 m) in the Ramsay Limestone in CURD-9 potentially represents the negative Archaeocyathid Extinction Carbon Isotope Event (AECE). Importantly, the strong faunal correlation between the Ramsay Limestone and the Wirrealpa/Aroona Creek limestones is matched by a very similar chemostratigraphic signal shown in unpublished isotopic data for the Wirrealpa Limestone sampled

in Balcoracana Creek (equivalent to the WL section in Paterson & Brock 2007) supplied via G.A. Brock (Supplementary Figure 1). The isotopic trends within the Wirrealpa Limestone are remarkably similar to those within the Ramsay Limestone. The negative peak of ~ -2‰ (60.53 m true thickness) potentially correlates with the negative peak within the Ramsay limestone in CURD-9 (-2.2 ‰ at CUR-60, 309.2 m). This would therefore mean that the negative peak within the Wirrealpa Limestone would also be equivalent to the AECE, reinforcing the interpretation that the Ramsay and Wirrealpa limestones are coeval and upper Stage 4 in age.

Fossils are essentially absent from the Corrodogery Formation. However, if the identification of *Redlichia* fragments in the overlying Stansbury Limestone are correct (Daily 1968; see Discussion below), it seems likely the Corrodgery Formation must also be late Stage 4 in age. The lower Corrodgery Formation from drill core Stansbury West 1 was described as a carbonaceous sandstone by Gravestock & Gatehouse (1995), and chemostratigraphic samples analysed as part of an unpublished PhD by Hall (2012) were thought to show a general lack of covariance suggesting a potential primary signal. However, the basal section of the Corrodgery Formation from CURD-9, consists of interbedding micaceous sandstone and siltstones (Fig. 2D-I) and the succession reveals a deep negative trend (Fig. 13; maximum nadir of -6.9‰ at CUR40, 247.8 m) in the lower part of the unit. The cross-plot of $\delta^{13}C$ versus $\delta^{18}O$ data exhibits a spread of data (similar to the younger Moonan Formation) that indicate covariance suggestive of a likely secondary signal reflecting the more siliciclastic lithology (Fig. 15; Schmid et al. 2017).

Fragments of *Redlichia* were reported (Daily 1968) in the Stansbury Limestone from drill core Stansbury West 1 (Drexel et al. 1995). These fragments have never been photographed and their whereabouts are unknown. Detailed inspection and "cracking" of the Stansbury Limestone in both CURD-9 and Port Julia-1A failed to recover any specimens of *Redlichia* to confirm its presence in this unit. Thin section analysis of the Stansbury Limestone in drill cores CURD-9 and Port Julia-1A confirm the presence of large thoracic skeletal elements of polymeroid trilobites in the lower part of the Stansbury Limestone, however, due to their fragmentary nature, identification of *Redlichia* cannot be substantiated (Fig. 2A–B, 2J–K, 3B, 3D, 3K). The presence of *Redlichia* species in the Ramsay Limestone and potentially the lower Stansbury Limestone in the western Stansbury Basin (and correlatives Wirrealpa/Aroona Creek limestones in the Arrowie Basin) would suggest the Ramsay Limestone, Corrodogery Formation, and at least the lower part of the Stansbury Limestone would correlate with a mid to late Stage 4 age.

Perhaps important for regional correlation is that the endemic (and enigmatic) taxon *Chalasiocranos exquisitum* Brock & Cooper, 1993 has a first occurrence in the upper Ramsay

Limestone (Brock & Cooper 1993), and the new data presented here extends the range into the Stansbury Limestone in both CURD-9 and Port Julia 1A. Interestingly, the last occurrence (LO) of this taxon does not extend beyond the sharp negative δ13C peaks identified as the potential ROECE event (see below) which suggests this taxon is also restricted to Stage 4.

7.2.2 The Series 2–Miaolingian Boundary and the ROECE isotopic event.

Ushatinskaya et al. (1995) discovered 10 specimens of the trilobite *Pagetia* sp., in the Coobowie Limestone at 86.15 m in Port Julia 1A core, which Jago & Kruse (2020) have recently referred to *Pagetia* cf. *edura* and which they suggest supports a Miaolingian/Wuliuan age for this unit (Jago & Kruse 2020). The new discovery of *Pagetia* sp indet. in the older Stansbury Limestone in CURD-9 (Fig. 16) presented here is thus very significant. Whilst the recovered material is poorly preserved it can be confidently identified as *Pagetia*. However, the fragmentary nature of the specimens precludes species identification. The part cranidium and pygidial axis with spine (Fig. 6.1–2) are reminiscent of *P. edura* Jell, 1975, but could be one of many species. The first appearance of *Pagetia* occurs just below the Series 2–Miaolingian boundary in the GSSP, and its presence has traditionally been used as an approximate marker for transition from Stage 4 into Wuliuan strata. Thus, this work has extended the range of this biostratigraphically significant taxon from the Coobowie Limestone down to the Stansbury Limestone.

The first occurrence of *Pagetia* sp. indet. in the CURD-9 core is at CUR-27 at 183.12–183.19 m, located ~ 9 m below a distinctive sharp $\delta^{13}C$ negative spike of -5.3 ‰ at CUR-4 (174.2 m). A very similar chemostratigraphic curve is captured in the Stansbury Limestone in Port Julia-1A though the nadir is not as negative (peak is ~ -2.7 ‰ at PJ1A-34-35, 169.9 m). *Pagetia* was not recovered from Port Julia-1A in the current study. The first occurrence (FO) of *Pagetia* sp. indet. can thus be confidently placed in the Stansbury Limestone immediately below the significant negative $\delta^{13}C$ spike recorded in CURD-9 (CUR-4, 174.2 m). This matches the known distribution of *Pagetia* in the GSSP where the FO of *P. significans* is located ~10 m below the ROECE event and therefore also the Series 2–Miaolingian boundary.

The tight clustering of $\delta^{13}C$ and $\delta^{18}O$ values in the cross-plot of isotopic data (Fig. 15) in the Ramsay Limestone, Stansbury Limestone (for both drill core CURD-9 and Port Julia-1A), and the Coobowie Limestone are interpreted to reflect primary isotopic composition in these units. The sharp negative $\delta^{13}C$ excursions in the Stansbury Limestone just above the FO of *Pagetia* sp, indet. is taken as a primary signal and the extent of the negative nadir (especially in CURD-9) is provisionally interpreted to represent the ROECE event. Whilst *O. indicus* is absent, the thin sections in both CURD-9 and Port Julia-1A reveal fossil rich packstones and grainstones (with

abundant trilobite fragments) below the ROECE in both cores. Importantly, only micritic, nodular carbonates devoid of fossils are present above the ROECE event. Whilst not definitive, this is suggestive of some type of faunal overturn at this level. Very few biostratigraphically significant taxa extend through the ROECE with only *K. djagoran* extending into the Coobowie Limestone (Fig. 16).

Interestingly, recently detailed chemostratigraphic data from South China by Zhang et al. (2022) indicates that the ROECE event is only coincident with biostratigraphic data in deeper outer shelf to slope settings (such as the GSSP). In shallow water carbonate sections, there is a disjunct between the faunal definition of the Series 2–Miaolingian boundary, consistently occurring at a higher (younger) level compared to the negative $\delta^{13}C$ nadir of the ROECE event. This disjunct in faunal and isotopic data in shallow marine carbonates needs to be verified in other Cambrian sections, but in the context of the western Stansbury Basin, available evidence suggests the ROECE is essentially equivalent to the Series 2–Miaolingian boundary The lack of *O. indicus* in Australia makes faunal definition of the boundary impossible to verify.

7.2.3 Miaolingian units

The fauna from the Coobowie Limestone is suggestive of Wuliuan age based on *Pagetia* cf *edura* (Jago & Kruse 2020) along with abundant *K. djagoran* overlapping with rarer taxa such as *A. subtilicrusta*, *Micromitra* sp., *K.* cf. *mudedirra* as well as large fragments of acrotheloid shells previously only know from Wuliuan units in northern Australia (Smith et al. 2015). The isotopic signal in the Coobowie Limestone reveals a distinctive negative to positive $\delta^{13}C$ trend that does not conform with the ROECE. Instead, the positive shift is typical of a post-ROECE signal documented in Laurentia (Montanez et al. 2000; Lin et al. 2019) and South China (Zhu et al. 2004, 2006; Guo et al. 2010; Chang et al. 2017; Zhao et al. 2019).

As noted in the results, the Moonan Formation also displays a major negative anomaly reaching a nadir of -5.6 ‰ at PJ1A-27 (147.06 m) that could also potentially represent the ROECE. However, only seven samples retrieved a carbonate signal and $\delta^{13}C$ and $\delta^{18}O$ cross-plot data (Fig. 15) reveals a large spread of data points that suggest potential co-variance. This, along with the small number of carbonate data points recovered, indicates the isotopic data in this unit may not capture a primary signal and needs to be treated with caution. As such, the preferred interpretation is that the Moonan is Miaolingian in age and post-dates the ROECE event in the Stansbury Limestone. Lack of fossils from the Moonan Formation makes it impossible to define biostraigraphically.

7.3 Regional Correlation

7.3.1 Northern Territory

Biostratigraphic and chemostratigraphic work in the Amadeus Basin of the Northern Territory is relatively well developed with faunal assemblages and isotopic trends (identified as ROECE) being consistent with the South Australian data presented here. The faunal assemblage from the Tempe Formation in the Hermannsburg 41 drill core from the Amadeus Basin is very similar to the Ramsay to Stansbury limestones (Smith et al. 2015). The co-occurrence of *Schizopholis napuru* (Kruse, 1990) and *Kostjubella djagoran* (Kruse, 1990) in the Tempe Formation provides close correlation with the Ramsay to Stansbury Limestone and likely reflects a Series 2, Stage 4 age (Smith et al. 2015). Though *K. djagoran* clearly ranges into the Wuliuan in the western Stansbury Basin based on data from Port Julia 1A. The fauna from the Giles Creek Dolostone, Ross River Gorge area, in the Amadeus Basin, includes *Aksarinaia subtilicrusta, Eothele granulata,* and *Hadrotreta* (*=K. djagoran*). But typical Stage 4 brachiopods like *S. napuru* are absent (Smith et al. 2016). This distinct faunal assemblage as well as the absence of *S. napuru* within the upper Stansbury Limestone to the Coobowie Limestone from drill cores CURD-9 and Port Julia-1A therefore potentially permits correlation to Miaolingian (Wuluian Stage) age. This would support placement of the Series 2–Miaolingian boundary within the upper Stansbury Limestone coincident with the distinct negative $\delta^{13}C$ peaks.

The ROECE has been reported by Schmid et al. (2017) within the Chandler Formation in drill cores Dingo 2 (- 2.4 ‰) and Alice 1 (- 0.8 ‰) as well as within the Tempe Formation (-10.6 ‰) in drill core East Johnny's Creek 1 (Supplementary Figure 2). However, it is important to note that the upper Tempe Formation, where the large negative carbon excursion occurs, is described as a shallow marine environment dominated by sandstone and siltstones (Bradshaw 1991; Smith et al. 2015; Schmid et al. 2017). The strong negative peak in the Tempe Formation must be treated with caution since cross-plot data presented by Schmid et al. (2017, Fig. 11) is covariant and likely the result of diagenetic alteration. As such, the Chandler Formation and Tempe Formation from the Amadeus Basin may be coeval with the Ramsay to Stansbury limestones in the western Stansbury Basin. Whilst basic faunal and chemostratigraphic data has been presented from the Amadeus Basin, none of the data provides biostratigraphic and chemostratigraphic data from the same cores. This is vital to enable accurate integration of multiproxy data to define boundaries and strengthen these correlations.

7.3.2 Daly, Wiso, and Georgina basins

The fauna from the Tindall Limestone in the Daly Basin from the Northern Territory correlates to the "early–middle" Cambrian based on faunal data. Unfortunately, no isotopic data has been presented for this formation. Kruse (1990) documented two distinct faunal assemblages based on trilobite and shelly fossil data; a *Redlichia* assemblage and a *Xystridura* assemblage (refer to Kruse 1990, Fig. 2). Smally shelly fossils including *Kyrshabaktella mudeirri, Hadrotreta djagoran* (=*K. djagoran*), and *Eothele napuru* (=*Schizopholus napuru*) range through the *Redlichia* assemblage into the *Xystridura* assemblage. Interestingly, *Micromitra nerranubawa* only occurs within the *Xystridura* assemblage (Kruse 1990). These taxa exhibit similar ranges in the Ramsay to Coobowie package from CURD-9 and Port Julia-1A. The last occurrence of *Redlichia* within the *Redlichia* assemblage in the Tindall Limestone suggests an age equivalent to Series 2, Stage 4.

Faunas in the Montejinni Limestone and Hooker Creek Formation in the Wiso Basin, and the Gum Ridge Formation in the Georgina Basin are also assumed to be equivalent to Series 2, Stage 4 based on similar faunal assemblages recovered from the Tindall Limestone (Kruse 1998). As *Redlichia* fragments were documented within the Ramsay and Stansbury Limestone (Daily 1990) and also contain *K. djagoran, Schizopholus napuru* and *Kyrshabaktella mudeirri* (within the Stansbury Limestone), it suggests that these formations (at least in part) are equivalent in age to the Tindall Limestone, Montejinni Limestone, Hooker Creek Formation, and the Gum Ridge Formation.

7.3.3 New South Wales

Faunas from Pincally Formation at Mount Arrowsmith documented by Brock & Percival (2006) show similar brachiopod faunas as the Stansbury and Coobowie limestones. Taxa in common include *Pelagiella madianensis, Eoobolus* sp., *Eothele granulata, Micromitra nerranubawu,* and Acrotheloid gen. et sp. indet. with previous interpretations correlating this formation to a Stage 4–Wuliuan age. Unfortunately, isotopic data has not been collected through this succession so the ROECE cannot be defined here.

Similarly, the brachiopod fauna documented within the Coonigan Formation on the Gnalta Shelf in far western New South Wales include *K. djagoran* (=*Hadrotreta primaeva*) and *Eothele granulata.* Although *K. djagoran* is known to occur across the Series 2–Miaoloingian boundary in the western Stansbury Basin, the presence of *E. granulata* potentially indicates an upper Stage 4–Wuliuan age for this formation (Roberts & Jell 1990). This would correlate with the Stansbury to Coobowie limestones of the western Stansbury Basin, supporting the interpretation that the Series 2–Miaolingian boundary potentially occurs within the Stansbury Limestone.

7.3.4 Queensland

Recent unpublished multiproxy data for the Thorntonia Limestone in the Georgina Basin has kindly been supplied by Dr. James Holmes and Dr Marissa Betts for comparison with the western Stansbury Basin. Trilobite faunas in the uppermost Thorntonia Limestone are much better preserved and diverse compared to the western Stansbury Basin faunas and are suggestive of a Templetonian =Miaolingian age, with fauna in the uppermost 1 m perhaps even Floran in age (J. Holmes pers. commun.). The brachiopods *S. napuru* and *K. djagoran* overlap with the Templetonian aged trilobites in the Thorntonia Limestone correlating with the upper Tindall Limestone in the Daly Basin (Kruse 1990). This Templetonian age is largely based on agnostid biozones defined by Laurie et al. (2004, 2006a, 2006b). Thus, the Series 2–Miaolingian boundary is potentially located in the lower part of the Arthur Creek Formation in the southern Georgina Basin, due to the presence of oryctocephalids and bathynotids as well as the absence of *Redlichia* that suggest taxa ranging across the Series 2-Miaolingian boundary as defined in China (Laurie et al. 2004; Zhao et al. 2019).

The upper part of the Thorntonia Limestone has a comparable faunal assemblage to CURD-9 and Port Julia-1A, consisting of brachiopods *S. napuru, K. djagoran, A. subtilicrusta* and *Micromitra* sp., suggesting a Stage 4 to Wuliuan age. As such, the Series 2–Miaolingian boundary should lie within the range of *S. napuru* and *K. djagoran* as well as within the first occurrences of *A. subtilicrusta* and potentially *Micromitra.* The boundary should also lie above the last appearance of *Redlichia*. This correlation supports the placement of the Series 2–Miaolingian boundary within the Stansbury Limestone rather than the Corrodgery Formation in the western Stansbury Basin (see Fig. 16). Hence, the supposed occurrence of *Redlichia* within the Stansbury Limestone, in combination with the occurrences of brachiopods within the faunal assemblage of the Stansbury Limestone as well as the sharp negative $\delta^{13}C$ chemostratigraphic trend in the upper Stansbury Limestone, strongly suggests close proximity to the Series 2–Miaolingian boundary.

7.4 Global Correlations

Global correlation of the shelly faunas from the western Stansbury Basin formations is very difficult due to the high level of endemicity of shelly faunas and lack of detailed description of diverse and well-preserved trilobite assemblages. Nevertheless, brief global correlations with the western Stansbury Basin are made herein.

7.4.1 Antarctica

Antarctica was once united with Australia during the Cambrian to form East Gondwana (Brock et al. 2000). This is reflected in the synonymous nature of the faunal assemblages (Debrenne & Kruse 1989; Kruse 1998; Brock et al. 2000). The presence of *K. djagoran* and *S. napuru* in allochthonous carbonate clasts in the Cape Melville Formation on King George Island in Antarctica (Holmer et al. 1996), suggest equivalence to the Wirrealpa Limestone. This would therefore suggest it is coeval with the Ramsay Limestone in the western Stansbury Basin of Series 2, Stage 4.

Faunal assemblages described by Claybourn et al. (2019) from the upper Shackleton Limestone, Holyoake Formation and Starshot Formation of the Holyoake Range, Antarctica, consist of shelly fauna typically associated with the *D. odyssei* Zone including *Schizopholus yorkensis*, *Eoobolus* sp., and *Eohadrotreta zhenbaensis*. This would perhaps suggest a lower–middle, Stage 4 age for these formations slightly older than the faunas associated with the western Stansbury Basin which have an upper Stage 4–Wuliuan age.

7.4.2 South China

In South China, biostratigraphic correlation is possible, however, due to the lack of *O. indicus* and other trilobite fauna, correlations rely on the few specimens of *Pagetia* sp. found within CURD-9 as well as chemostratigraphic trend similarities. The genus *Eoobolus* sp. has been reported from the Xihaoping Member of the Dengying Formation (Xiaoyangba section) of the *Parabadiella huoi* Zone in southern Shaanxi, South China (Zhang et al. 2021). Guo et al. (2010, 2014) developed the original chemostratigraphic curves used to ratify the GSSP of the Series 2–Miaolingian boundary (Zhao et al. 2019). These were compared to the Siberian curves developed by Montanez et al. (2000) and illustrated in Fig. 3 from Guo et al. (2010). Although the range of $\delta^{13}C$ values vary across different regions, the notable sharp negative peak is evident across all isotopic profiles. This pattern is most comparable to the -5.3 ‰ $\delta^{13}C$ negative peak at CUR-4 (174.2 m) in the Stansbury Limestone for CURD-9 (Fig. 13, 16) and the ~ -2.7 ‰ $\delta^{13}C$ negative peak at PJ1A-34 (169.9 m) in Port Julia-1A (Fig. 14, 16).

7.4.3 Laurentia

Western Laurentia biostratigraphy is predominantly based on trilobite data, hence, correlations are difficult due to the lack of *O. indicus* and other trilobite fauna found within the South Australian formations. Large discrepancies between timing of the Last Appearance Datum (LAD) of olenellids (used only in Laurentia; Faggetter et al. 2017) and redlichiids (used in Gondwana and South China; Lin et al. 2019) still exist (Sundberg et al. 2016, 2020; Zhao et al. 2019). Faggetter et al. (2017)

reported a sharp negative $\delta^{13}C$ peak of -3.5‰ interpreted as ROECE within the same horizon as the olenellid extinction in the Carrara Formation (Death Valley region in California) and the Pioche Formation (Nevada). Although no olenellid trilobite data has been found within the western Stansbury Basin, the chemostratigraphic pattern from Faggetter et al. (2017) is most comparable to the -5.3 ‰ $\delta^{13}C$ negative peak in CURD-9 (CUR-4, 174.2 m; Fig. 13, 16) and the ~ -2.7 ‰ $\delta^{13}C$ negative peak in Port Julia-1A (PJ1A-34, 169.9 m; Fig. 14, 16) within the Stansbury Limestone.

Successions from the Parahio Valley, Spiti region in the Himalayas have been described as Cambrian Stage 4–Wuliuan equivalent, based only on faunal data. Brachiopods from this unit highlight the relatively rapid evolutionary sequence of lingulides from Stage 4 to the Wuliuan. Within the Parahio Valley, brachiopods *S. napuru, Eohadrotreta haydeni* sp. nov. *Eoobolus* sp., and *Aksarinaia* sp., suggest late Stage 4, whereas the incoming of *Eothele* and *Acrothele* are interpreted to indicate transition into the Wuliuan. The occurrence of *Acrothele* sp. within the Parahio Valley also aligns with the base of trilobite *Oryctocephalus indicus* level, which defines the Series 2–Miaolingian boundary (Zhao et al. 2019). This would suggest that the Ramsay to Stansbury limestones likely correlate with late Stage 4, and the first occurrence of *E. granulata*, Acrotheloid sp. indet., and *A. subtilicrusta* indicate transition into the Wuliuan (Fig. 16).

8. CONCLUSIONS

The integrated multiproxy data in this study ($\delta^{13}C$ and $\delta^{18}O$ chemostratigraphy, small shelly fossil biostratigraphy, and lithological data) represents a new chronostratigraphic framework for formations within the upper part of subsurface packages in the western Stansbury Basin, South Australia. This research establishes the position of the Series 2–Miaolingian boundary within the Stansbury Limestone of drill cores CURD-9 and Port Julia-1A in the western Stansbury Basin. This research addressed the three main aims:

1. *Construct high resolution biostratigraphy of small shelly fossils through the Port Julia-1A and CURD-9 drill cores in the western Stansbury Basin of South Australia.*

The distinct faunal assemblages provide important range extensions for regional and global correlation to the Series 2–Miaolingian boundary. The faunal assemblage present within the Ramsay Limestone support previous correlation with the coeval Wirrealpa and Aroona Creek limestones in the Arrowie Basin, establishing an upper Stage 4 age. Last known occurrences of *Redlichia* within the lower Stansbury Limestone indicate that the Corrodgery Formation and at least the lower part of the Stansbury Limestone is also late Stage 4 in age. New range data for the

endemic *Chalasiocranos exquisitum* does not extend beyond the negative $\delta^{13}C$ peaks interpreted as potential Redlichiid–Olenellid Extinction Carbon isotope Excursion event, perhaps restricting this taxon to Stage 4. New discoveries of *Pagetia* sp indet. within the Stansbury Limestone below the interpreted Redlichiid–Olenellid Extinction Carbon isotope Excursion event conform to previous occurrences below the Series 2–Miaolingian boundary in the GSSP. Fauna present within the Coobowie Limestone is indicative of a Wuliuan age, thus, aiding the interpretation that the Series 2–Miaolingian boundary lies within the Stansbury Limestone.

2. *Utilize $\delta^{13}C$ and $\delta^{18}O$ isotopes to reveal the chemostratigraphy of Port Julia-1A and CURD-9 drill cores establishing if the global negative ROECE (Redlichiid-Olenellid Extinction Carbon isotope Excursion) event, currently used to define the Series 2-Miaolingian Cambrian boundary, is present or absent in the western Stansbury Basin.*

Chemostratigraphic analysis reveals strong primary $\delta^{13}C$ signals in the Ramsay, Stansbury, and Coobowie limestones with less reliable data in the primarily siliciclastic Corrodogery and Moonan formations. A -2.2 ‰ $\delta^{13}C$ peak in the Ramsay Limestone in CURD-9 and coeval Wirrealpa Limestone (Arrowie Basin), coincident with the youngest known Archaeocyatha in South Australia, is interpreted to represent the Archaeocyathid Extinction Carbon isotope Excursion (AECE) event. The -5.3 ‰ $\delta^{13}C$ peak in the Stansbury Limestone in CURD-9 and the ~ -2.7 ‰ $\delta^{13}C$ in Port Julia-1A are interpreted to be synchronous and are coincident with significant biofacies changes and SSF extinction. These levels are interpreted to represent the global Redlichiid–Olenellid Extinction Carbon isotope Excursion (ROECE) event.

3. *Utilize detailed thin section data to document the lithostratigraphy and original depositional environment of rock packages straddling the Series 2–Miaolingian Cambrian boundary in the western Stansbury Basin.*

Thin section analysis support previous interpretations regarding the transgression-regression cyclical deposition of sediments throughout the Ramsay to Coobowie formations. The main depositional lithologies of the Ramsay, Stansbury, and Coobowie limestones indicate a shallow-marine, inner shelf setting within wave base in comparison to the siliciclastic units which were deposited in deeper water (below wave base), outer-ramp/slope setting for the Corrodgery and Moonan formations. Similar lithologies observed within the Stansbury Limestone of CURD-9 and Port Julia-1A potentially highlight the synchronicity of the negative $\delta^{13}C$ events in both cores.

REFERENCES

Bengtson, S., Conway Morris, S., Cooper, B.J., Jell, P.A., Runnegar, B.N., 1990. Early Cambrian fossils from South Australia. Brisbane. Memoirs of the Assoc Australasian Palaeontol. 9, 1-364.

Betts, M.J., Paterson, J.R., Jago, J.B., Jacquet, S.M., Skovsted, C.B., Topper, T.P., Brock, G.A., 2016. A new lower Cambrian shelly fossil biostratigraphy for South Australia. Gondwana Res. 36, 176–208.

Betts, M.J., Paterson, J.R., Jago, J.B., Jacquet, S.M., Skovsted, C.B., Topper, T.P., Brock, G.A., 2017. Global correlation of the early Cambrian of South Australia: Shelly fauna of the *Dailyatia odyssei* Zone. Gondwana Res. 46, 240–279.

Betts, M.J., Paterson, J.R., Jacquet, S.M., Andrew, A.S., Hall, P.A., Jago, J.B., Jagodzinski, E.A., Preiss, W.V., Crowley, J.L., Brougham, T., Mathewson, C.P., García-Bellido, D.C., Topper, T.P., Skovsted, C.B., Brock, G.A., 2018. Early Cambrian chronostratigraphy and geochronology of South Australia. Earth Sci. Rev. 185, 498–543.

Betts, M., Claybourn, T., Brock, G., Jago, J., Skovsted, C., Paterson, J., 2019. Early Cambrian shelly fossils from the White Point Conglomerate, Kangaroo Island, South Australia. Memoirs of the Assoc Australasian Palaeontol. 64, 489-522.

Bradbury, H.J., Vandeginste, V., John, C.M., 2015. Diagenesis of phosphatic hardgrounds in the Monterey Formation: A perspective from bulk and clumped isotope geochemistry. Geol. Soc. of Am. Bull. 127, 1453–1463.

Bradshaw, J., 1991. Description and depositional model of the chandler formation: a lower Cambrian evaporite and carbonate sequence, Amadeus Basin, central Australia. In: Korsch, R.J., Kennard, J.M. (Eds.), Geological and Geophysical Studies in the Amadeus Basin, Central Australia. Bureau of Mineral Resources, Geology and Geophysics, Australia, Bulletin. 236, 227–244.

Brand, U., 2004. Carbon, oxygen and strontium isotopes in Paleozoic carbonate components: an evaluation of original seawater-chemistry proxies. Chem. Geol. 204, 23-44.

Brasier, M.D., Anderson, M., Corfield, R., 1992. Oxygen and carbon isotope stratigraphy of early Cambrian carbonates in southeastern Newfoundland and England. Geol. Mag. 129, 265-279.

Brasier, M., Khomentovsky, V., Corfield, R., 1993. Stable isotopic calibration of the earliest skeletal fossil assemblages in eastern Siberia (Precambrian-Cambrian boundary). Terra Nova. 5, 225-232.

Brasier, M.D., Sukhov, S.S., 1998. The falling amplitude of carbon isotopic oscillations through the Lower to Middle Cambrian: northern Siberia data. Can. J. Earth Sci. 35, 353–373.

Brock, G., Cooper, B., 1993. Shelly fossils from the Early Cambrian (Toyonian) Wirrealpa, Aroona Creek and Ramsay Limestones of South Australia. J. Paleontol. 67, 758–787.

Brock, G.A., Engelbretsen, M.J., Jago, J.B., Kruse, P.D., Laurie, J.R., Shergold, J.H., Shi, G.-R., Sorauf, J.E., 2000. Palaeobiogeographic affinities of Australian Cambrian faunas. Mem. Assoc. Australas. Palaeontol. 23, 1–61.

Brock, G.A., Percival, I.G., 2006. Cambrian stratigraphy and faunas at Mount Arrowsmith, northwestern New South Wales. Memoirs of the Assoc Australasian Palaeontol. 32, 75–101.

Butler, A., 2015. Fossil Focus: The place of small shelly fossils in the Cambrian explosion, and the origin of animals. Palaeontology. 5, 1-14.

Chang, C., Hu, W., Wang, X., Huang, K.-J., Yang, A., Zhang, X., 2019. Nitrogen isotope evidence for an oligotrophic shallow ocean during the Cambrian Stage 4. Geochim. Cosmochim. Acta. 257, 49–67.

Chang, C., Hu, W., Wang, X., Yu, H., Yang, A., Cao, J., Yao, S., 2017. Carbon isotope stratigraphy of the lower to middle Cambrian on the eastern Yangtze Platform, South China. Palaeogeogr. Palaeoclimatol. Palaeoecol. 479, 90–101.

Claybourn, T.M., Jacquet, S.M., Skovsted, C.B., Topper, T.P., Holmer, L.E., Brock, G.A., 2019. Mollusks from the upper Shackleton Limestone (Cambrian Series 2), Central Transantarctic Mountains, East Antarctica. J. Paleontol. 93, 437–459.

Claybourn, T.M., Skovsted, C.B., Holmer, L.E., Pan, B., Myrow, P.M., Topper, T.P., Brock, G.A., 2020. Brachiopods from the Byrd Group (Cambrian Series 2, Stage 4) Central Transantarctic Mountains, East Antarctica: biostratigraphy, phylogeny and systematics. Pap. Palaeontol. 6, 349–383.

Cowley, W., Conor, C., Zang, W., 2003. New and revised Proterozoic stratigraphic units on northern Yorke Peninsula, MESA Journal. 29, 46-58.

Crawford A.R., 1965. The geology of Yorke Peninsula. Bulletin of the Geological Survey of South Australia 39, 1-96.

Daily, B., 1956. The Cambrian in South Australia. In: Rodgers, J., (Ed.), El Sistema Cambrico, su paleogeografia y el problema de su base. Report 20th International Geological Congress, Mexico. 2, 91–147.

Daily B., 1968. Stansbury Town No.1 well. Subsurface stratigraphy and palaeontology of the Cambrian sequence, for Beach Petroleum N.L. South Australia Department of Mines and Energy, Open File Envelope 946, 48 (unpublished).

Daily B., 1972. The base of the Cambrian and the first Cambrian faunas. Centre for Precambrian Research, University of Adelaide, Special Paper 1, 13-41.

Daily, B., 1990. Cambrian stratigraphy of Yorke Peninsula. Geological Society of Australia, Special Publication 16, 215–229.

Debrenne F., Kruse P.D., 1989. Cambrian Antarctic archaeocyaths. In Crame, I.A., ed., Origins and Evolution of the Antarctic Biota, Geological Society of London, Special Publication 47, 15-28.

Demidenko Yu.E. 1999. Skeletnye problematichnye ostatki iz nizhnego kembriya Yuzhnoy Avstralii (Skeletal problematic remains from the Lower Cambrian of South Australia). Avtoreferat dissertat. sii ... kandidata geoLogo-mineraLogicheskikh nauk. Moscow: Moscow State University. 24 (unpublished) (in Russian).

Devaere, L., Clausen, S., Steiner, M., Álvaro, J.J., Vachard, D., 2013. Chronostratigraphic and palaeogeographic significance of an early Cambrian microfauna from the Heraultia Limestone, northern Montagne Noire, France. Palaeontol. Electron. 16, 17-91.

Devaere, L., Clausen, S., Álvaro, J.J., (Eds.). 2014. Stratigraphic overview of the Ediacaran and Cambrian from the Anti-Atlas, Morocco. University Lille 1, France.

Drexel, J.F. and Preiss, W.V. (Eds), 1995. The geology of South Australia. Vol. 2, The Phanerozoic. South Australia. Geological Survey. Bulletin, 54.

Drexel, J.F., Preiss, W.V., Parker, A.J., (Eds.), 1995. The Geology of South Australia. Vol. 2: The Phanerozoic, Bulletin / Geological Survey of South Australia. Mines and Energy, South Australia, Geological Survey of South Australia, Adelaide. 54.

Dunham, R.J., 1962. Classification of carbonate rocks according to depositional texture. – In: Ham, W.E., (ed.): Classification of carbonate rocks. A symposium. – Amer. Ass. Petrol. Geol. Mem. 1, 108-171.

Erwin, D.H., Laflamme, M., Tweedt, S.M., Sperling, E.A., Pisani, D., Peterson, K.J., 2011. The Cambrian conundrum: early divergence and later ecological success in the early history of animals. Science. 334, 1091-1097.

Erwin, DH., 2020. The origin of animal body plans: a view from fossil evidence and the regulatory genome. Development. 4, 147.

Faggetter, L.E., Wignall, P.B., Pruss, S.B., Newton, R.J., Sun, Y., Crowley, S.F., 2017. Trilobite extinctions, facies changes and the ROECE carbon isotope excursion at the Cambrian Series 2–3 boundary, Great Basin, western USA. Palaeogeogr. Palaeoclimatol. Palaeoecol. 478, 53–66.

Fan, R., Deng, S., Zhang, X., 2011. Significant carbon isotope excursions in the Cambrian and their implications for global correlations. Sci. China Earth Sci. 54, 1686–1695.

Flügel, E., Munnecke, A., 2010. Microfacies of carbonate rocks: analysis, interpretation and application, 2nd ed. (Vol. 976, p. 1-984). Berlin: Springer.

Folk, R.L., 1959. Practical classification of limestones. – Amer. Ass. Petrol. Geol. Bull., 43, 1-38.

Frimmel, H.E., 2010. On the reliability of stable carbon isotopes for Neoproterozoic chemostratigraphic correlation. Precambrian Res. 182, 239-253.

Geyer, G., 2019. A comprehensive Cambrian correlation chart. Episodes. 42, 321-332.

Gradstein, F.M., Ogg, J.G., Schmitz, M.D., Ogg, G.M., 2020. Geologic Time Scale 2020. Elsevier.

Gravestock D.I., Gatehouse C.G., 1995. Stansbury Basin. In Drexel J.F., Preiss W.V., eds. The geology of South Australia. V. 2: The Phanerozoic. MESA. 54, 5-19.

Gravestock. D.J., In. Aleksander. E.M., 2001. The Cambrian biostratigraphy of the Stansbury basin, South Australia. Izdat. Nauka, Moskva.

Guo, Q.J., Strauss, H., Liu, C.Q., Zhao, Y.L., Yang, X.L., Peng, J., Yang, H., 2010. A negative carbon isotope excursion defines the transition from Cambrian Series 2 to Cambrian Series 3 on the Yangtze Platform, South China. Palaeogeogr. Palaeoclimatol. Palaeoecol. 285, 143–151.

Guo, Q.J., Strauss, H., Zhao, Y.L., Yang, X.L., Peng, J., Yang, Y.N., Deng, Y.N., 2014. Reconstructing marine redox conditions for the transition between Cambrian Series 2 and Cambrian Series 3, Kaili area, Yangtze Platform: Evidence from biogenic sulfur and degree of pyritization. Palaeogeogr. Palaeoclimatol. Palaeoecol. 398, 144–153.

Hall, P.A., 2012. Elemental, isotopic and molecular signatures of early Cambrian marine sediments and a phantom petroleum system in South Australia 753. (PhD thesis)

Holmer, L.E., Popov, L.E., Wrona, R., 1996. Early Cambrian lingulate brachiopods from glacial erratics of King George Island (South Shetland Islands), Antarctica. In Gaidzicki A., ed., Palaeontologica Results of the Polish Antarctic Expedition. Part II, Palaeontologia Polonica 55, 37-50.

Holmes, J.D., Paterson, J.R., Jago, J.B., García-Bellido, D.C., 2021. Ontogeny of the trilobite *Redlichia* from the lower Cambrian (Series 2, Stage 4) Ramsay Limestone of South Australia. Geol. Mag. 158, 1209–1223.

Hough, M.L., Shields, G.A., Evins, L.Z., Strauss, H., Henderson, R.A., Mackenzie, S., 2006. A major sulphur isotope event at c. 510 Ma: a possible anoxia-extinction-volcanism connection during the Early-Middle Cambrian transition?: Global warming as a major determining factor in biosphere evolution. Terra Nova. 18, 257–263.

Ishikawa, T., Ueno, Y., Shu, D.-G., Li, Y., Han, J., Guo, J.-F., Yoshida, N., Maruyama, S., Komiya, T., 2014. The δ13C excursions spanning the Cambrian explosion to the Canglangpuian mass extinction in the Three Gorges area, South China. Gondwana Res. 25, 1045–1056.

Jacquet, S.M., Brock, G.A., 2015. Lower Cambrian helcionelloid macromolluscs from South Australia. Gondwana Res. 36, 333–358.

Jacquet, S.M., Brougham, T., Skovsted, C.B., Jago, J.B., Laurie, J.R., Betts, M.J., Topper, T. P., Brock, G.A., 2017. *Watsonella crosbyi* from the lower Cambrian (Terreneuvian, stage 2) Normanville group in South Australia. Geol. Mag. 154, 1088-1104.

Jago, J.B., Zang, W.-L., Sun, X., Brock, G.A., Paterson, J.R., Skovsted, C.B., 2006. A review of the Cambrian biostratigraphy of South Australia. Palaeoworld, 15, 406-423.

Jago, J.B., Gehling, J.G., Paterson, J.R., Brock, G.A., Zang, W., 2012. Cambrian stratigraphy and biostratigraphy of the Flinders Ranges and the north coast of Kangaroo Island, South Australia. Episodes. 35, 247–255.

Jago, J.B., Gehling, J.G., Betts, M.J., Brock, G.A., Dalgarno, C.R., García-Bellido, D.C., Haslett, P.G., Jacquet, S.M., Kruse, P.D., Langsford, N.R., Mount, T.J., Paterson, J.R., 2020. The Cambrian System in the Arrowie Basin, Flinders Ranges, South Australia. AJES. 67, 923–948.

Jago, J.B., Kruse, P.D., 2020. Significance of the middle Cambrian (Wuliuan) trilobite Pagetia from Yorke Peninsula, South Australia. AJES. 67, 1003–1008.

Jeppsson, L., Anehus, R., Fredholm, D., 1999. The optimal acetate buffered acetic acid technique for extracting phosphatic fossils. J. Paleontol. 73, 964-972.

Kaufman, A. J., Knoll, A.H., 1995. Neoproterozoic variations in the C-isotopic composition of seawater: stratigraphic and biogeochemical implications. Precambrian Res. 73, 27-49.

Kruse, P., Jago, J., Laurie, J., 2009. Recent developments in Australian Cambrian biostratigraphy. Journal of Stratigraphy. 33, 233–245.

Kruse P.O., 1990. Cambrian palaeontology of the Daly Basin. Northern Territory Geological Survey, Report 7. 1-58.

Kruse P.O., 1998. Cambrian palaeontology of the eastern Wiso and western Georgina basins. Northern Territory Geological Survey Report 9. 68.

Laurie, J., 2004. Early Middle Cambrian trilobite faunas from NTGS Elkedra 3 corehole, southern Georgina Basin, Northern Territory. Memoirs of the Association of Australasian Palaeontologists. 30, 221–260.

Laurie, J., 2006a. Early Middle Cambrian trilobites from the Jigaimara Formation, Arafura Basin, Northern Territory. Memoirs of the Association of Australasian Palaeontologists. 32, 103–126.

Laurie, J., 2006b. Early Middle Cambrian trilobites from Pacific Oil & Gas Baldwin No. 1 well, southern Georgina Basin, Northern Territory. Memoirs of the Association of Australasian Palaeontologists. 32, 127–204.

Laurie, J.R., 2012. Biostratigraphy of the Arthur Creek Formation and Thorntonia Limestone, Georgina Basin. 1-6 in Munson, T.J., (ed.), Central Australian Basins Symposium (CABS) III. Petroleum Exploration Society of Australia.

Lin, J.-P., Sundberg, F.A., Jiang, G., Montañez, I.P., Wotte, T., 2019. Chemostratigraphic correlations across the first major trilobite extinction and faunal turnovers between Laurentia and South China. Sci Rep. 9, 17392.

Maloof, A.C., Porter, S.M., Moore, J.L., Dudás, F.Ö., Bowring, S.A., Higgins, J.A., Fike, D.A. & Eddy, M.P. 2010. The earliest Cambrian record of animals and ocean geochemical change. GSA Bulletin. 122, 1731-1774.

Melezhik, V.A., Gorokhov, I.M., Kuznetsov, A.B., Fallick, A.E., 2001. Chemostratigraphy of Neoproterozoic carbonates: implications for “blind dating.” Terra Nova. 13, 1–11.

Montañez, I.P., Banner, J.L., 2000. Evolution of the Sr and C Isotope Composition of Cambrian Oceans. GSA TODAY. 10, 2-7.

Parkhaev, P.Yu., 2019. Cambrian Mollusks of Australia: Taxonomy, Biostratigraphy, and Paleobiogeography. Stratigr. Geol. Correl. 27, 181–206.

Paterson, J.R., Brock, G.A., 2007. Early Cambrian trilobites from Angorichina, Flinders Ranges, South Australia, with a new assemblage from the *Pararaia bunyerooensis* Zone. J. Paleontol. 81, 116–142.

Peng, S.-C., Babcock, L., Cooper, R., 2012. The Cambrian period. In: Gradstein, F.M., Ogg, J.G., Schmitz, M., Ogg, G., (Eds.), The Geologic Time Scale. Elsevier, Amsterdam. 2, 437–488.

Peng, S.-C., Babcock, L., Ahlberg, P., 2020. The Cambrian Period. In: Gradstein, F.M., Ogg, J.G., Schmitz, M., Ogg, G., (Eds.), Geological Time Scale 2020. Elsevier, Amsterdam. 1, 565-631.

Percival, I.G., Kruse, P.D., 2014. Middle Cambrian brachiopods from the Southern Georgina basin of central Australia 45, 349-402.

Plumley, W.J., Risley, G.A., Graves, R.W., Kaley, M.E., 1962. Energy index for limestone interpretation and classification. In: Ham, W.E., (ed.) Classification of carbonate rocks. American Association of Petroleum Geologists, Memoir. 1, 85-107.

Popov, L.E., Holmer, L.E., Hughes, N.C., Ghobadi Pour, M., Myrow, P.M., 2015. Himalayan Cambrian brachiopods. Pap. Palaeontol. 1, 345–399.

Richards, M.N., Lewis, P., Andrews, D.L., Gilbert, D.J., 1986. Curramulka - Pine Point. Progress and relinquishment reports from 9/7/79 to 18/6/86. South Australia. Department of Primary Industries and Resources. Open file Envelope 1986.

Ren, Y., Zhong, D., Gao, C., Liang, T., Sun, H., Wu, D., Zheng, X., 2017. High-resolution carbon isotope records and correlations of the lower Cambrian Longwangmiao formation (stage 4, Toyonian) in Chongqing, South China. Palaeogeogr. Palaeoclimatol. Palaeoecol. 485, 572–592.

Roberts. J., Jell P.A., 1990. Early Middle Cambrian (Ordian) brachiopods of the Coonigan Formation, western New South Wales. Alcheringa. 14, 257-309.

Schmid, S., 2017. Chemostratigraphy and palaeo-environmental characterisation of the Cambrian stratigraphy in the Amadeus Basin, Australia. Chem. Geol. 451, 169–182.

Skovsted, C.B., Balthasar, U., Vinther, J., Sperling, E.A., 2021. Small shelly fossils and carbon isotopes from the early Cambrian (Stages 3–4) Mural Formation of western Laurentia. Pap. Palaeontol. 7, 951–983.

Skovsted, C.B., Brock, G.A., Paterson, J.R., 2006. Bivalved arthropods from the Lower Cambrian Mernmerna Formation, Arrowie Basin, South Australia and their implications for identification of Cambrian ‘small shelly fossils’. Memoirs of the Association of Australasian Palaeontologists. 32, 7–41.

Skovsted, C., Peel, J.S., 2010. Early Cambrian Brachiopods and Other Shelly Fossils from the Basal Kinzers Formation of Pennsylvania. J. Paleontol. 84, 754-762.

Smith, P.M., Brock, G.A., Paterson, J.R., 2016. Linguliformean brachiopods from the early Templetonian (Cambrian Series 3, Stage 5) Giles Creek Dolostone, Amadeus Basin, Northern Territory. Australasian Palaeontological Memoirs. 49, 125-143.

Smith, T.E., Laurie, J.R., Edwards, D.S., 2015. Middle Cambrian Chemostratigraphy and Biostratigraphy in the Southern Georgina Basin: Correlating the Arthur Creek “Hot Shale,” in: International Conference and Exhibition, Melbourne, Australia 13-16 September 2015. Presented at the International Conference and Exhibition, Melbourne, Australia 13-16 September 2015, Society of Exploration Geophysicists and American Association of Petroleum Geologists, Melbourne, Australia. 512–512.

Steiner, M., Li, G., Qian, Y., Zhu, M., 2004. Lower Cambrian small shelly fossils of northern Sichuan and southern Shaanxi (China), and their biostratigraphic importance. Geobios. 37, 259-275.

Steiner, M., Li, G., Qian, Y., Zhu, M., Erdtmann, B.-D., 2007. Neoproterozoic to early Cambrian small shelly fossil assemblages and a revised biostratigraphic correlation of the Yangtze Platform (China). Palaeogeogr. Palaeoclimatol. Palaeoecol. 254, 67-99.

Sundberg, F.A., 2016. International correlation of the Cambrian series 2-3, stages 4-5 boundary interval. Australasian Palaeontological Memoirs. 49, 83-124.

Sundberg, F.A., Karlstrom, K.E., Geyer, G., Foster, J.R., Hagadorn, J.W., Mohr, M.T., Schmitz, M.D., Dehler, C.M., Crossey, L.J., 2020. Asynchronous trilobite extinctions at the early to middle Cambrian transition. Geology. 48, 441–445.

Swart, P. K., 2015. The geochemistry of carbonate diagenesis: The past, present and future. Sedimentology. 62, 1233-1304.

Ushatinskaya G., Zhegallo E., Esakova N., Zang W.-L., Gravestock D., 1995. Preliminary report on well Port Julia 1A. Stansbury Basin Project, Progress Report No.1. Preliminary report on well Port Julia 1A. 5, 3 (Unpublished).

Weissert, H., Joachimski, M., Sarnthein, M., 2008. Chemostratigraphy. News. Stratigr. 42, 145–179.

Wendler, I., 2013. A critical evaluation of carbon isotope stratigraphy and biostratigraphic implications for Late Cretaceous global correlation. Earth Sci. Rev. 126, 116–146.

Wray, G. A., Molecular clocks and the early evolution of metazoan nervous systems. Philos. Trans. R. Soc. B. 370, 20150046.

Yang, B., Steiner, M., Li, G.X., Keupp, H., 2014. Terreneuvian small shelly faunas of East Yunnan (South China) and their biostratigraphic implications. Palaeogeogr. Palaeoclimatol. Palaeoecol. 398, 28–58.

Zhang, P., Wang, Y., Zhang, X., Wei, Z., Wang, G., Zhang, T., Ma, H., Wei, J., He, W., Ma, X., Zhu, C., 2022. Carbon, oxygen and strontium isotopic and elemental characteristics of the Cambrian Longwangmiao Formation in South China: Paleoenvironmental significance and implications for carbon isotope excursions. Gondwana Res. 106, 174–190.

Zhang, Y., Yang, T., Hohl, S.V., Zhu, B., He, T., Pan, W., Chen, Y., Yao, X., Jiang, S., 2020. Seawater carbon and strontium isotope variations through the late Ediacaran to late Cambrian in the Tarim Basin. Precambrian Res. 345, 105769.

Zhang, Z., Zhang, Z., Ma, J., Taylor, P.D., Strotz, L.C., Jacquet, S.M., Skovsted, C.B., Chen, F., Han, J., Brock, G.A., 2021. Fossil evidence unveils an early Cambrian origin for Bryozoa. Nature. 599, 251–255.

Zhao, Y., Yuan, J., Babcock, L.E., Guo, Q., Peng, J., Yin, L., Yang, X., Peng, S., Wang, C., Gaines, R.R., Esteve, J., Tai, T., Yang, R., Wang, Y., Sun, H., Yang, Y., 2019. Global Standard Stratotype-Section and Point (GSSP) for the conterminous base of the Miaolingian Series and Wuliuan Stage (Cambrian) at Balang, Jianhe, Guizhou, China. Episodes. 42, 165–184.

Zhu, M.-Y., Babcock, L.E., Peng, S.-C., 2006. Advances in Cambrian stratigraphy and paleontology: Integrating correlation techniques, paleobiology, taphonomy and paleoenvironmental reconstruction. Palaeoworld. 15, 217–222.

Zhuravlev, A. Y., Gravestock, D., 1994. Archaeocyaths from Yorke peninsula, South Australia and archaeocyathan early Cambrian zonation. Alcheringa. 18, 1-54.

Zhuravlev, A.Yu., Wood, R.A., 2018. The two phases of the Cambrian Explosion. Sci. Rep. 8, 16656.

SUPPLEMENTARY DATA

Supplementary Table 1 – Isotopic data for CURD-9 through the Ramsay Limestone, Corrodgery Formation, and Stansbury Limestone.

Depth	Sample	δ13C	δ13C Error	δ18O	δ18O Error	Formations
169.278	CUR-1	-1.9	0.05	-8.63	0.12	Stansbury
171.603	CUR-2	-2.39	0.03	-9.59	0.05	Stansbury
174.062	CUR-3	-4.58	0.02	-9.25	0.03	Stansbury
174.235	CUR-4	-5.34	0.01	-8.64	0.04	Stansbury
176.286	CUR-5	-2.1	0.09	-11.72	0.05	Stansbury
177.958	CUR 6	-2.09	0.07	-10.36	0.1	Stansbury
178.682	CUR-7	-2.38	0.03	-9.19	0.03	Stansbury
178.872	CUR-8	-1.89	0.04	-11.27	0.02	Stansbury
179.052	CUR-26	-1.65	0.07	-9.16	0.02	Stansbury
181.091	CUR-9	-1.33	0.03	-8.42	0.02	Stansbury
183.163	CUR-27	-1.9	0.01	-11.53	0.03	Stansbury
183.318	CUR-20	-1.27	0.03	-7.76	0.05	Stansbury
183.986	CUR-21	-1.17	0.02	-7.77	0.04	Stansbury
184.447	CUR-22	-1.55	0.06	-9.55	0.09	Stansbury
186.586	CUR-23	-2.56	0.01	-9.84	0.07	Stansbury
187.785	CUR-24	-3.11	0.02	-12.78	0.04	Corrodgery
224.288	CUR-35	-5.47	0.04	-13.79	0.01	Corrodgery
225.931	CUR-12	-4.67	0.01	-11.43	0.05	Corrodgery
231.515	CUR-37	-5.74	0.02	-12.36	0.11	Corrodgery
235.448	CUR-13	-5.56	0.03	-11.34	0.03	Corrodgery
244.181	CUR-41	-4.83	0.03	-12.18	0.1	Corrodgery
247.887	CUR-40	-6.98	0.04	-14.28	0.07	Corrodgery
251.1	CUR-42	-3.84	0.08	-12.13	0.06	Corrodgery
254.138	CUR-43	-3.15	0.03	-11.74	0.06	Corrodgery
261.65	CUR-15	-1.59	0.02	-9.69	0.04	Ramsay
264.289	CUR-45	-1.65	0.05	-8.42	0.02	Ramsay
266.164	CUR-46	-0.62	0.05	-8.34	0.03	Ramsay
270.141	CUR-47	-1.54	0.05	-8.19	0.08	Ramsay
271.295	CUR-48	-0.39	0.05	-8.78	0.01	Ramsay
274.389	CUR-49	-0.17	0.07	-7.88	0.06	Ramsay
277.14	CUR-50	0.37	0.02	-8.99	0.02	Ramsay
278.484	CUR-51	0.21	0.02	-9.37	0.02	Ramsay
282.282	CUR-52	0.35	0.03	-7.42	0.02	Ramsay
283.865	CUR-16	0.31	0.05	-10.08	0.01	Ramsay
287.142	CUR-53	0.49	0.04	-7.28	0.03	Ramsay
288.644	CUR-54	0.56	0.03	-7.59	0.05	Ramsay
292.17	CUR-17	0.61	0.05	-7.84	0.08	Ramsay
294.747	CUR-55	0.11	0.02	-7.72	0.01	Ramsay
297.925	CUR-56	0.14	0.01	-7.3	0.04	Ramsay
301.075	CUR-18	-1.06	0.05	-8.47	0.06	Ramsay

303.901	CUR-58	-0.61	0.05	-7.25	0.02	Ramsay
304.008	CUR-57	-0.87	0.04	-7.62	0.06	Ramsay
304.473	CUR-59	-0.62	0.02	-7.38	0.03	Ramsay
309.201	CUR-60	-2.23	0.02	-7.56	0.01	Ramsay
310.958	CUR-61	-0.24	0.04	-7.67	0.04	Ramsay
313.049	CUR-62	-0.21	0.05	-9.47	0.04	Ramsay
314.593	CUR-63	-0.21	0.04	-8.96	0.00	Ramsay
315.43	CUR-64	-0.01	0.03	-8.69	0.02	Ramsay
315.535	CUR-65	0.05	0.04	-10.14	0.07	Ramsay
316.782	CUR-19	0.55	0.09	-6.05	0.13	Ramsay

Supplementary Table 2 - Isotopic data for Port Julia-1A through the Stansbury Limestone, Moonan Formation, and Coobowie Limestone.

Depth	Sample	δ13C	δ13C Error	δ18O	δ18O Error	Formations
60.445	PJ1A-1	0.59	0.02	-9.57	0.04	Coobowie
61.96	PJ1A-68	0.55	0.01	-11.27	0.01	Coobowie
63.55	PJ1A-2	0.88	0.03	-9.93	0.01	Coobowie
66.044	PJ1A-3	1.25	0.04	-10.26	0.03	Coobowie
67.56	PJ1A-4	1.36	0.03	-8.01	0.01	Coobowie
68.917	PJ1A-5	1.55	0.02	-8.22	0.02	Coobowie
71.39	PJ1A-6	1.63	0.07	-7.64	0.08	Coobowie
72.725	PJ1A-7	1.29	0.03	-7.63	0.03	Coobowie
75.165	PJ1A-66	1.5	0.03	-7.99	0.02	Coobowie
77.596	PJ1A-8	1.29	0.01	-9.41	0.01	Coobowie
80.49	PJ1A-63	1.61	0.02	-10.62	0.02	Coobowie
82.677	PJ1A-9	1.57	0.03	-9.44	0.07	Coobowie
85.333	PJ1A-10	-1.4	0.02	-10.46	0.02	Coobowie
87.642	PJ1A-11	-0.23	0.02	-10.13	0.03	Coobowie
90.534	PJ1A-65	-1.67	0.06	-9.3	0.01	Coobowie
91.755	PJ1A-69	-2.5	0.03	-6.86	0.03	Coobowie
92.994	PJ1A-41	-1.85	0.02	-11.04	0.03	Coobowie
95.412	PJ1A-14	-1.83	0.04	-10.11	0.06	Coobowie
95.52	PJ1A-15	-2	0.02	-9.59	0.03	Coobowie
98.112	PJ1A-12	-2.53	0.05	-7.36	0.04	Coobowie
98.793	PJ1A-79	-2.03	0.03	-9.39	0.03	Coobowie
100.479	PJ1A-67	-2.12	0.03	-7.46	0.03	Moonan
106.356	PJ1A-17	-2.48	0.06	-5.61	0.07	Moonan
124.85	PJ1A-21	-3.94	0.04	-6.11	0.09	Moonan
131.289	PJ1A-23	-3.24	0.03	-3.38	0.06	Moonan
141.497	PJ1A-13	-5.4	0.06	-10.29	0.01	Moonan
147.063	PJ1A-27	-5.64	0.11	-7.71	0.12	Moonan
159.396	PJ1A-30	-2.81	0.02	-6.76	0.05	Moonan
162.304	PJ1A-16	-0.57	0.04	-8.18	0.06	Moonan

162.63	PJ1A-31	-0.41	0.05	-12.67	0.07	Stansbury
164.929	PJ1A-32	-1.13	0.04	-6.86	0.01	Stansbury
167.754	PJ1A-33	-0.66	0.03	-10.9	0.06	Stansbury
169.94	PJ1A-34	-2.71	0.04	-10.55	0.03	Stansbury
170.11	PJ1A-35	-2.02	0.02	-10.03	0.03	Stansbury
171.99	PJ1A-36	-0.27	0.03	-10.95	0.09	Stansbury
173.68	PJ1A-37	-1.38	0.05	-10.71	0.00	Stansbury
175.904	PJ1A-38	-0.66	0.06	-10.9	0.04	Stansbury
176.043	PJ1A-39	-0.32	0.06	-10.33	0.04	Stansbury
178.153	PJ1A-40	-0.46	0.05	-9.65	0.04	Stansbury
180.161	PJ1A-42	-0.79	0.03	-10.69	0.01	Stansbury
181.361	PJ1A-43	-0.97	0.04	-10.52	0.01	Stansbury
181.526	PJ1A-44	-0.58	0.03	-9.9	0.04	Stansbury
182.922	PJ1A-45	0.04	0.04	-9.16	0.02	Stansbury
184.178	PJ1A-46	0.76	0.02	-9.52	0.06	Stansbury
184.404	PJ1A-74	0.26	0.02	-9.45	0.03	Stansbury
184.41	PJ1A-47	0.13	0.01	-9.86	0.01	Stansbury
184.636	PJ1A-48	0.55	0.04	-8.94	0.04	Stansbury
185.022	PJ1A-49	0.37	0.05	-9.73	0.05	Stansbury
186.738	PJ1A-50	0.9	0.02	-9.89	0.04	Stansbury
189.134	PJ1A-51	0.52	0.02	-9.53	0.01	Stansbury
191.361	PJ1A-52	0.31	0.06	-9.22	0.05	Stansbury
192.833	PJ1A-53	0.18	0.04	-10.23	0.05	Stansbury
195.445	PJ1A-54	-0.18	0.05	-11.6	0.03	Stansbury
196.56	PJ1A-55	-0.13	0.02	-12.15	0.03	Stansbury
197.122	PJ1A-75	0.04	0.06	-11.17	0.05	Stansbury
199.014	PJ1A-56	0.06	0.03	-11.12	0.03	Stansbury
199.17	PJ1A-57	0.02	0.02	-10.79	0.01	Stansbury
201.05	PJ1A-58	-0.03	0.07	-8.83	0.09	Stansbury
201.857	PJ1A-59	0.33	0.01	-10.12	0.06	Stansbury
202.318	PJ1A-76	0.97	0.02	-8.17	0.03	Stansbury
203.977	PJ1A-60	-0.11	0.04	-10.79	0.02	Stansbury
205.462	PJ1A-61	-0.41	0.01	-12.67	0.05	Stansbury
207.288	PJ1A-77	-0.12	0.01	-10.82	0.04	Stansbury
208.54	PJ1A-62	-0.07	0.02	-10.66	0.01	Stansbury
210.073	PJ1A-78	-0.07	0.03	-9.67	0.01	Stansbury

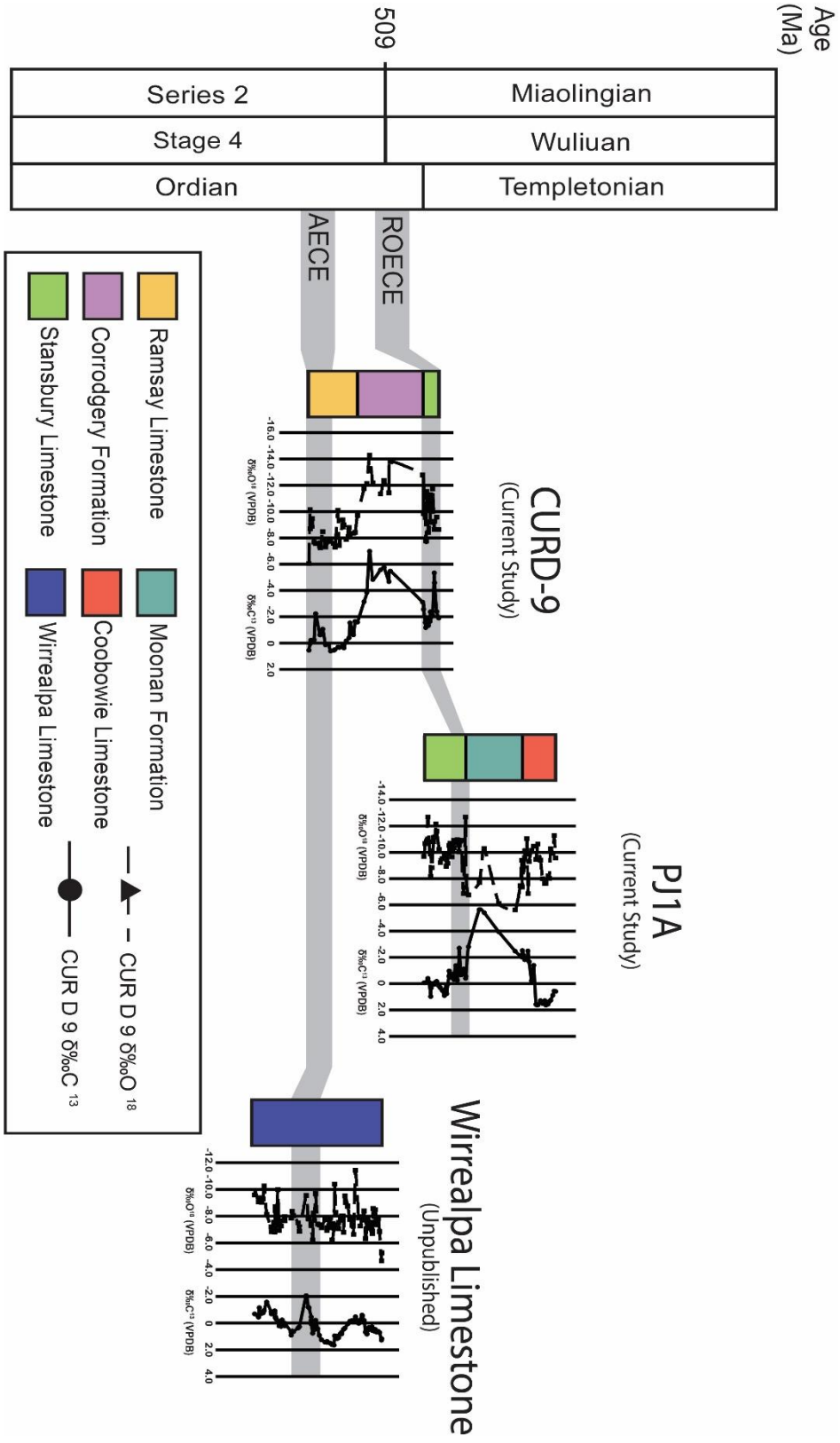

Supplementary Figure 1. Correlation of chemostratigraphic data from drill cores CURD-9 and Port Julia-1A (current study) in the western Stansbury Basin, South Australia and unpublished data from GA Brock from the Wirrealpa Limestone collected from a stratigraphic section measured in Balcoracana Creek in the Bunkers Range, Arrowie Basin, South Australia. Section is equivalent to WL section in Paterson and Brock (2007).

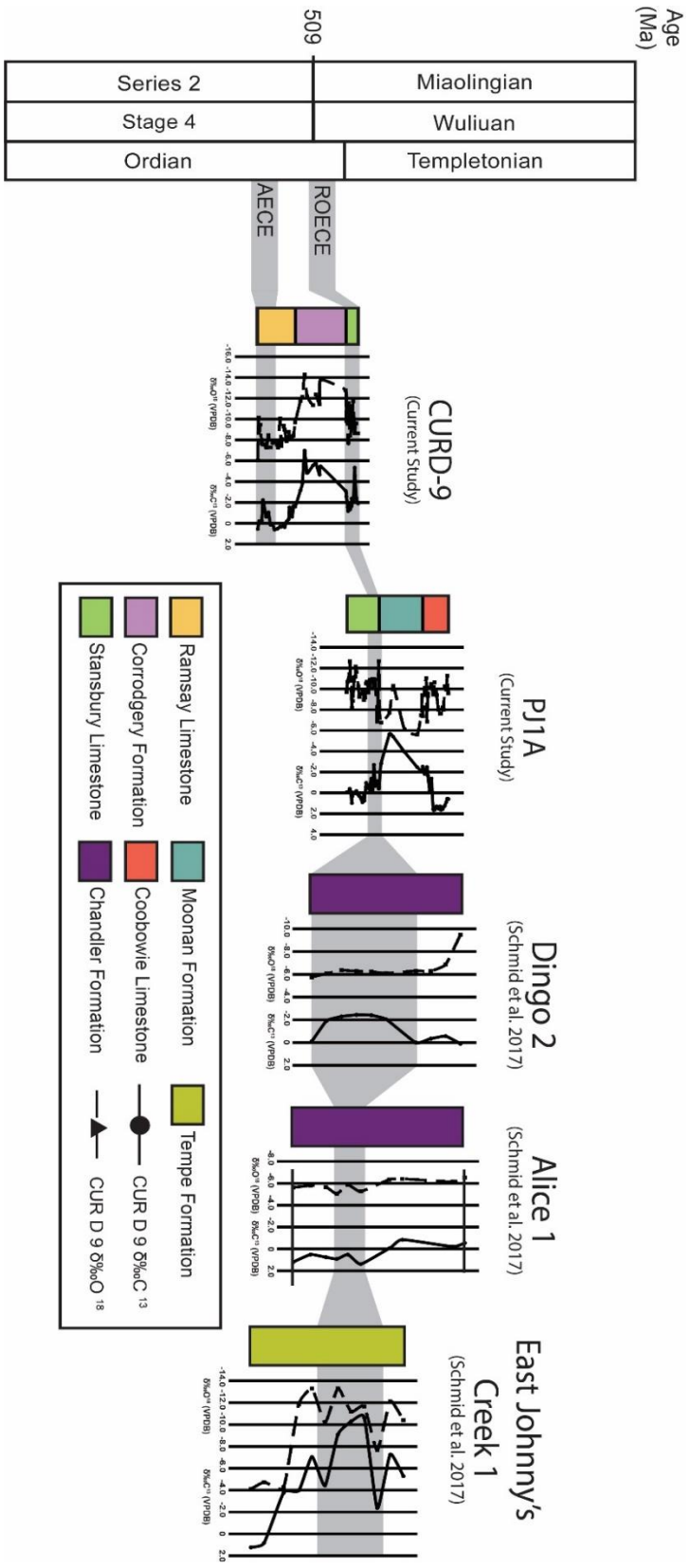

Supplementary Figure 2. Correlation of chemostratigraphic data from drill cores CURD-9 and Port Julia-1A (current study) in the western Stansbury Basin, South Australia with drill cores Dingo 2, Alice 1, and East Johnny's Creek 1 in the Amadeus Basin, Northern Territory (Schmid et al. 2017).